Development of Chatter Threshold Boundary for Milling of Metals

A thesis submitted to fulfill the requirements for the degree of
Doctor of Philosophy

Afshin Koohestani
BSME

School of Aerospace, Mechanical & Manufacturing Engineering
College of Science, Engineering and Health
RMIT University
March 2014

Declaration

I, Afshin Koohestani, declare that the PhD thesis entitled “Development of Chatter Threshold Boundary for Milling of Metals” is no more than *90,000* words in length including quotes, tables, figures, bibliography, and footnotes. I also certify the work is that of the author alone; the work has not been submitted previously, in whole or in part in order to qualify for other academic award. The content of the thesis is the result of work which has been carried out since the official commencement date of the approved research program; and, any editorial work carried out by a third party is acknowledged.

Afshin Koohestani

27 March 2014

Acknowledgements

PhD is a marathon event, and I would not have been able to complete this long and amazing journey without the support of countless people during my research program.

I wish to dedicate my deep down appreciation first to my main supervisor, Professor John Mo of the Royal Melbourne Institute of Technology (RMIT), for his invaluable help and support from the first day of this research, as well as his technical guidance, endless forbearance, and constant encouragement. I am grateful for his directness and for a well-organized research environment which led this project to success. I also wish to thank my second supervisor, Dr. Songlin Ding of the RMIT University. I am also very grateful to Dr. Sam Yang of CSIRO Material Science and Engineering Department for his scientific advice and knowledge and many insightful discussions and suggestions. He is my resource for getting my science questions answered.

I wish to thank postgraduate students of RMIT, Raja Izamshah, Adam, Vincent, Amir-Ali, Hormoz, and Amir Yadollah who are my best friends and assisted me in running of my experiments. I also wish to thank staff of Advance Manufacturing Laboratory of RMIT, Patrick and Mark, for their support and supplying necessary services and facilities for implementation of my Milling experiments.

I am most thankful to my wife, Rosita, for her love, sacrifice, continuous support and understanding during the course of this study. I also thank to my parents Parviz and Mohtaram, my sister Sima, and my brother Farshid that have instilled many admirable qualities in me and given me a good foundation with which to meet life. Finally I thank God for blessing me all these opportunities.

Table of Contents

List of Figures

List of Tables

Nomenclature

F	N	cutting force
F_t	N	tangential cutting force
F_n	N	normal cutting force
F_x	N	cutting force along cutting feed
F_y	N	cutting force along radial depth of cut
F_z	N	cutting force along axial depth of cut
V_s	*rpm*	spindle speed
V_c	*mm/min*	cutting speed
f_z	*mm/tooth*	feed rate
D	*mm*	cutting tool diameter
a_p	*mm*	axial depth of cut
a_e	*mm*	radial depth of cut
$V_{a(t)}$	V	the amplitude of acceleration in (V) acquired by sensor
$a_{b(t)}$	m/s^2	the converted acceleration
g	m/s^2	gravitational acceleration ($9.81\ m/s^2$)
L	*mm*	the length of workpiece
W	*mm*	the width of workpiece
H	*mm*	the thickness of workpiece
λ		Lyapunov's exponent

$x_{(t)}$		time series
$R_{(t)}$		the state function of n-dimensional phase space (phase space)
$F(R_{(t)})$		nonlinear function of phase space $R_{(t)}$
τ	s	time delay
$P(t)$		reconstructed phase space (or state vector)
m		embedding dimension
$C_{(k)}$		autocorrelation factor
q		delay in the number of samples of time series $x_{(t)}$
$\{X_i\}$		the intensity of the i_{th} pixel in the reference image
$\{Y_i\}$		the intensity of the i_{th} pixel in the second image
X_m, Y_m		the mean intensity of the reference and second images
r		Pearson's coefficient
j		space dimension
k		equal segments of Poincaré sections
$\boldsymbol{S_i}$		corresponding matrix to Poincaré sections
U		dependent variable
V		independent variable
α		regression coefficient
β		intercept

Abstract

Significant research effort has been carried out on the detection of chatter which is one of the main barriers preventing milling of metals. Chatter is the biggest factor affecting stability of the machining process. The phenomenon is characterized by low quality of cutting surface, cutting tool failure and noise. Chatter directly affects the productivity of the machining process. The current state of the art chatter detection techniques is unable to satisfy industry requirements in terms of in-process chatter detection.

This study reports on a new novel experimental method for the prediction of chatter based on the chaos theory. Sensor-signal driven reconstructed phase space attractor is used in the proposed method. The variation of Poincaré sections of the reconstructed phase space attractor is able to identify the transition of the machining system from a stable to an unstable condition, continuously during the milling process. Two mathematical tools are used to measure the variation of Poincaré sections they being; image correlation and a designed regression model. Image correlation uses Poincaré sections as a pattern and the computation of Pearson's coefficient assists to develop a chatter threshold boundary.

Titanium is chosen as the main material in this research, as chatter is more applicable during cutting of titanium due to its specific mechanical properties. Moreover, the method is used in detection of chatter during milling of stainless steel and aluminum in order to demonstrate that the method can detect chatter not only during cutting of titanium, but also in milling of other metals. The new method can be used to detect chatter on-line, as it is independent of the cutting parameters and dynamics of the milling process, and can be integrated in the cutting machines. The method does not need expensive equipment and complex process, so it can be easily used in normal production workshop environment.

While a regression model computes the trend of changes in the Poincaré sections and gives a numerical output value indicating the state of the system without the necessity to have an analytical relationship between the cutting parameters and the

milling dynamics. A threshold value of the trend value defines the boundary between the stable and unstable state of the milling process. These mathematical tools can be used in expert software to monitor the milling process on-line and detect the onset of chatter. The chatter detection method is validated for different materials, cutting tools, and cutting parameters.

Chapter 1

Introduction

Machining process is commonly used in production of metallic parts to produce complex shapes and geometries. The main challenge in the machining of metal products is achieving a high metal removal rate (MRR). Achieving to high values of MRR is now possible by applying advance technologies in the manufacturing of machine tool and cutting tools, and still have a reasonable tool life [1]. However, the dynamic interaction between machine tool and workpiece causes self-excited vibration, or chatter, which is the main barrier limiting the machining process.

Chatter, or self-excited vibration, is the main reason for causing tool failure and poor quality cutting surfaces. The occurrence of chatter has to be detected during the cutting process in order to stop the process before chatter harms the workpiece. Early chatter detection will increase the efficiency of production, which is the aim of this study. Chatter can occur while machining any material. Titanium, due to its material properties, is the most difficult metal to machine in regards to the chatter phenomenon. Accordingly, this study focuses on titanium machining, but with extended work on other materials such as stainless steel and aluminium.

Wide ranges of products can be manufactured by using milling and turning processes. Accordingly, a brief introduction about the dynamics of machining processes, particularly turning and milling, is outlined. The reason why chatter occurs during these machining processes is also discussed.

1.1 Machining Process

Machining is a kind of manufacturing process that produces a product from raw material by cutting it into the desired shape and size. The material removal is controlled during the machining process manually or numerically by computer (CNC- computer numerical control). Based on the characteristic of generating a certain geometry and surface the machining operation is usually classified as one of 5 types, as shown below.

- Turning,
- Milling,
- Drilling,
- Boring, and
- Grinding.

A machining process is described by a set of parameters known as the cutting parameters. Cutting speed is presented as the rate of passing raw material through the cutting tool, and is expressed in units of (*m/min*) or (*ft/min*). Spindle speed is described as the rotational movement of the spindle, which is expressed in (*rev/min*). In axial direction machining, the feed rate is the distance moved by the tool in an axial direction at each movement of the workpiece (e.g. rotation in turning and linear movement in milling). The thickness of material removed from the workpiece is defined by depth of cut. In turning processes, the depth of cut is only measured in radial direction, whereas in milling it is measured in both axial and radial directions in milling process.

The dynamics of the cutting process is directly affected by the force generated in the cutting process. The generated force provides a dynamical interaction between the workpiece and machine tool and impacts the machining quality [2]. The dynamics of two cutting processes, milling and turning, and the origin of chatter occurrence in these processes are outlined, as chatter is more common in these two machining methods comparing to other machining processes.

1.1.1 Turning

In turning, the cutting tool moves along the longitudinal axis parallel to the axis of the workpiece while the workpiece rotates. Considering cutting tool and workpiece being rigid, the cutting force (F) is applied into the cutting edge, where it resolved into normal (F_n) and tangential (F_t) components, as shown in Figure 1.1. A third vector can also be considered for the cutting force along the workpiece axis; however, it is not necessary for describing or analysing the

dynamics of the process. In an ideal turning process, Chip thickness and chip width are constant during the process [3].

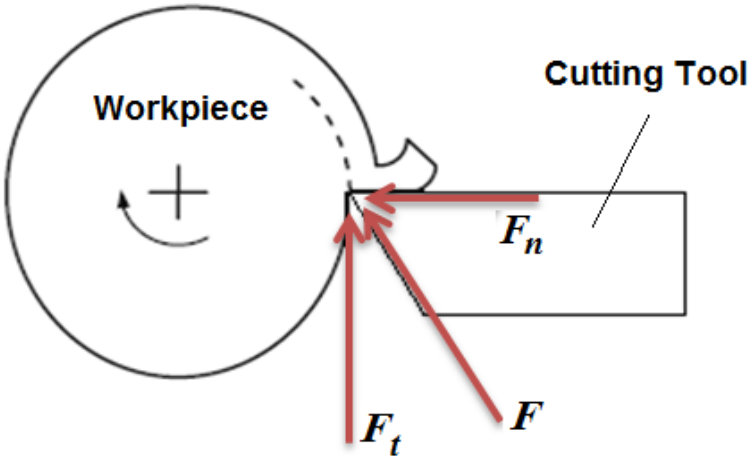

Figure 1.1: Cutting force applying from cutter during the turning process.

On the other hand and in real turning, the cutting tool is affected by the interaction between large mechanical stresses and high temperatures. Thus, edges are gradually worn down, and in extreme cases, it leads to premature destructive failure [4]. Variation in chip thickness, is caused by cutting speed and vibration frequency and this affects the dynamics of the turning process [5]. Both chip thickness variation and chip breakage create some variation in cutting forces and disturb the steady cutting forces during the process. Due to the disturbance in cutting force the machine tool structure generates a displacement between workpiece and cutting tool, which leads to variations in the cutting parameters. The interaction between the workpiece and machine tool along with the dynamics of the cutting process represents a closed loop system. Any instability in this closed loop creates a self-excited vibration in the process, which is the major constraint preventing highly productive turning processes [6].

1.1.2 Milling

The milling process is the most common form of the material removal process in order to produce goods with precision features like holes, slots, pockets, as well as 3-D surface contours. The milling process is able to provide high tolerance and excellent surface finish. The shape of the product can also be arbitrary [7]. For this purpose, a rotating cutting tool is use d to cut into a stationary workpiece by moving the workpiece linearly into the cutting tool.

Chip thickness in a milling operation is also a function of the rotation angle, whereas it is constant during a stable turning operation [8]. Cutting force (F) (Figure 1.2) is also a function of the cutting angle in the milling process. Cutting force depends on the cutting parameters such as chip thickness, the area of cut (length and width), cutting tool angle, total specific cutting energy per unit volume, and the numbers of flutes that are instantly engaged in the cutting process [9]. Therefore, the expression of cutting force is complicated due to the numerous and involved parameters.

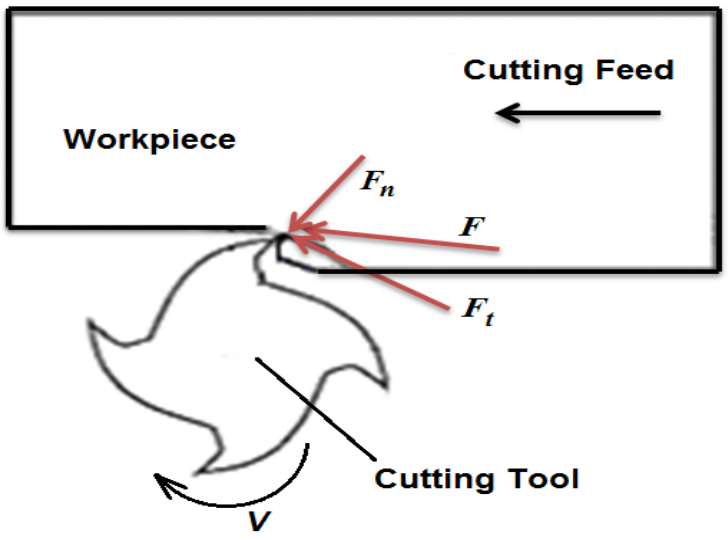

Figure 1.2: Cutting force applying from cutter during the milling process.

The cutting tool produces crescent-shaped chips as the cutting tool loses contact with the workpiece in transition between each cutting flute. Accordingly and compared to the turning process, a combination of discontinuous cutting and the rotation of the cutting edge makes milling dynamics more convoluted [10]. Chatter in the milling process is a nonlinear phenomenon that is caused by the variation in cutting force due to intermittent contact between cutting tool and workpiece.

1.1.3 High Speed Machining

Machining is efficient when MRR is maximized, while achieving a high surface quality. The machining removal rate is dependent on spindle speed, axial and radial depth of cut, and also feed rate [11]. To achieve a high MRR, Salomon [12] proposed a new machining process called high-speed-machining. Based on this method, by increasing the speed of machining five to 10 times more, chip thickness and interface temperature decreases significantly, while using a smaller cutter. This technique reduces the process time, cost, mechanical stress, workpiece temperature, and improves surface finish, while using smaller cutting tools with better dynamical stability. Consequently, the cutting force will be decreased by using this technique [13].

The appropriate range of speed for having stable process during high speed machining of different materials varies and depends on the mechanical properties and machinability of the material. Considering titanium as main material in this research, the spindle speed starts from *4000* to *10,000 rpm* for stable high speed milling [14]. Hence, the spindle speed for high speed machining of stainless steel can be started from *5000* to *10,000 rpm* [15] and from *7000* to more than *10,000 rpm* for aluminium [16].

Despite the above advantages, some drawbacks limit the application of high-speed machining. There is a vibration that may occur when the frequency of tooth passing causes of the entire system comprised of cutting tool, workpiece, and fixture to also vibrate as the same frequency [1]. This vibration mode is

called forced vibration. In this situation, cutting tool, guide ways, and spindle bearing wear quicker, which leads to higher cost [17].

1.2 Chatter

Based on the oscillating behaviour of dynamical systems such as machining, vibration is classified as one of three types, namely; free, forced, and self-excited vibration. During the machining process, self-excited vibration is the most harmful in cutting process in that it oscillates the system at its natural frequency [18]. It is characterized by creation of a mechanism in the dynamical system that guides system into vibrating at its own natural or critical frequency [19]. The vibration frequency found in forced vibration is equal to the excitation frequency, whereas it is equal to the system's natural frequency in self-excited vibration.

Self-excited vibration, which is known as chatter in machining operation, is the most important source of instability and is caused by a positive feedback mechanism leading to dynamic instability of the cutting process. Chatter affects productivity and quality of surface, and generates noise in the workplace. Chatter causes unusual tool wear, damage of tooling structure, wear of spindle bearings, and poor dimensional accuracy of the work piece [20]. Chatter can cause sudden breakage of the cutting tool during milling operations which causes workpiece surface damage. In fact, production output rate is highly affected by the extent of rejected or re-machined parts [21]. Accordingly, chatter is considered the most adverse type of vibration and is the main barrier against the effective milling of parts. It is more obvious in high speed machining.

Chatter is characterized by chaotic motions between the cutting tool and the workpiece [22]. It occurs when chip width is larger relative to the dynamic stiffness of the system [23]. Stephenson and Agapiou [18] outlined that; cutting force, dry friction, built up edge on cutting tool, metallurgical variations in workpiece material, and regenerative effects as the factors that produce chatter during machining. Dynamics of chatter is strongly dependent on cutting conditions such as workpiece material, dynamics of the machine tool, and spindle tool [24]. During

certain cutting conditions, the interactions between cutting tool and workpiece are illustrated by large amplitude vibrations, which is a drawback to achieving a high quality surface finish. The undesirable motions result in wavy surfaces on the workpiece, inaccurate dimensions, and excessive tool wear [25].

Chatter is classified further as primary and secondary chatter [11]. Primary chatter is usually caused by the cutting process [26]. The frictional, mode coupling, and thermo-mechanical chatters are dependent on the cutting process, consequently they are considered as a kind of primary chatter [27]. Primary chatter is important especially in peripheral milling operations such as thin-wall milling processes where the radial immersion of the cutting process is a small percentage of the cutter radius. A small radial immersion rate may result in non-continuous contact between cutting tool and workpiece, and this cutting process is a nonlinear dynamic system [28]. Furthermore, self-excited vibration sometimes occurs due to the regeneration waviness of the workpiece surface, which is called secondary chatter [29]. Regenerative chatter occurs when the cutting tool passes through the waves remained on the surface of the workpiece from previous cutting run, and previous surface history is reintroduced to the cutting edge [30].

1.2.1 Chatter in Machining of Titanium

Industries always desire to use materials with the ability to produce cost effective and high performance products. Accordingly, titanium is increasingly in demand, particularly in the aerospace, automotive, sport, and biomedical industries.

Titanium and its alloys are non-ferrous metals with excellent corrosion resistance, fatigue properties, high strength-to-weight ratios [31], and good ductility [13]. Moreover, titanium represents good durability in harsh environments [32]. The specific weight of titanium is approximately two thirds of steel and higher than aluminium with similar strength as steel [33]. This physical property assist manufacturers to reduce the weight of products without loss of strength [34]. Furthermore, less fuel consumption would be the result of reduction of weight in vehicles with titanium parts [35].

On the other hand, the mechanical and physical characteristics of titanium such as low thermal conductivity, low young modulus, as well as high chemical dependency to the cutting tool material induce some difficulties in cutting of titanium [36]. During machining of titanium, the low Young's modulus and high yield stress ratio of titanium cause small plastic deformations in the workpiece. The workpiece keeps springing back against the cutting force and causes rubbing between the cutting edges and enhances friction. Friction increases temperature at the cutting area and the segmented chips that occur further increases the fluctuation of cutting forces [33, 37]. As mentioned above, a high cutting force created between workpiece and cutting tool produces self-excited vibration or chatter [13]. The forces that are induced by chatter also cause tool failure [38].

1.2.2 Chatter in Machining of Stainless Steel

Stainless steel has a broad range of engineering applications due to its excellent properties of corrosion resistant, formability and strength. The high corrosion resistant allows stainless steel to be used in severe environments [39]. Its resistance to heat in demonstrated by low scaling and ability to retain strength at high temperatures [40]. It has a non-porous surface coupled with the easy cleaning ability making it the primary choice for applications which require strict hygiene control. Its strength to weight advantage that allows it to be used with a reduced material thickness compared to other materials, often generates cost savings [41]. The ease of fabrication due to the use of modern steel manufacturing techniques allows stainless steel to be cut, machined, fabricated, welded, and formed as readily as traditional steels [42].

However, stainless steels have common weakness of chatter occurrence during machining, similar to titanium [43]. Low quality surface finish and short cutting tool life are common issues encountered during machining of stainless steel [44]. So due to the wide usage of stainless steel in industry, especially in food and chemical industry, it is chosen as one of the materials for investigation of the applicability of the proposed method to predict the onset of chatter.

1.2.3 Chatter in Machining of Aluminium

Today in industry, aluminium is the second most useable metal after steel. Comparing to other non-ferrous metals, aluminium is produced far more than all other metals. light weight, corrosion resistance, formability, appearance, and recyclability are properties that make aluminium and its alloys most economical and attractive for a wide range of applications [45]. Aluminium has a density of about one-third of steel [46], which it assists to reduce weight of product in applications need low to medium strength.

Similar to titanium and stainless steel, chatter is the main barrier encountered during machining of aluminium parts, too [47]. Accordingly, it is useful to detect chatter during aluminium machining processes. Its detection assists in developing cost effective production processes. To determine the boundary of chatter onset, similar to titanium and stainless steel, a set of experiments have been undertaken on aluminium workpieces with different cutting tools and cutting parameters.

1.3 Goals of the Thesis

Chatter, especially during machining of titanium, is the main barrier encountered in developing effective machining processes, noting that it is important to detect chatter before it occurs. Accordingly, chatter detection is a much discussed topic in the manufacturing field. Despite extensive research, there is still not a reliable detection method for industrial applications. This research aims to develop a new method to detect chatter on-line during milling processes, especially for titanium. Therefore, the aim and main contribution of this study are:

1. A critical literature review of current chatter detection methods demonstrates that they are usually analytical or experimental methods to determine a boundary for choosing cutting parameters. Still industry suffers from lack of on-line chatter detection methods. Accordingly in this thesis, it

is aimed to develop a novel technique to predict chatter rather than detecting after almost happening, which will be applicable to industry.

2. Current methods can only detect chatter when it has significantly developed and damaged the part. Therefore, it is noted the actual computation time of the chatter detection process plays an important role in proposing effective method of chatter detection. It means that a complex method, with a long computation time, is not desirable for industrial applications. Accordingly, this study aims to develop a simple method with a reasonably short computation time, so that it can be used to detect chatter on-line.
3. The method aims to experimentally determine a boundary between stable and unstable milling processes, Therefore, a set of experiments was carried out to explore the criteria for detecting chatter prior to its occurrence.
4. Titanium was the main metal used to develop the detection method. This material was chosen as the occurrence of chatter is more prevalent during machining of titanium. However, other materials, particularly stainless steel and aluminium were used to verify the criteria for other materials.
5. Some production workshops employ highly skilled professional operators in order to prevent chatter, but these operators are not always available. Hence the possibility of human error must be considered when using these operators. The detection method should work simply and with readily accessible non-expensive equipment.

1.4 Outline

In chapter two, a literature review is presented. In this chapter, chatter detection techniques are classified under 5 different categories and are introduced and discussed. Furthermore, since most chatter detection methods use stability lobe diagrams to present their results, this aspect is introduced and discussed separately in chapter two.

Chapter three represents the experimental setup that is required to acquire consistent data from milling processes. The main factor in the design of the experiment is to acquire the pure vibration that occurs between the workpiece and the cutting tool. Hence, the milling process must be designed in a way that it runs in stable condition and continuously moves into the unstable condition.

In chapter four, the methodology is explained. Phase space attractor Poincaré sections of the milling process are illustrated in different time intervals during the processing time.

In chapter five and six, image correlation and linear regression are used to create the required numeric indicator by measuring the variation between the Poincaré sections.

Chapter seven demonstrates the data analysis and results for milling of titanium, aluminium, and stainless steel under various milling conditions.

In chapter eight, the conclusion and recommendations for future research are presented.

Chapter 2

Chatter Detection Methods - A Review

2.1 Introduction

In the first chapter, chatter was introduced as a phenomenon that occurs during machining processes due to interactions between workpiece and cutting tool. It is also the main barrier preventing development of highly productive machining processes, especially for machining of titanium. Much research has been done to understand the scientific nature of chatter through mathematical modelling of the cutting dynamics. Despite these research efforts on the detection, prevention, reduction and suppression, chatter still occurs during many machining processes.

This chapter reviews in chatter detection techniques and their drawbacks and limitations. The review focuses on the ability of these techniques when they are applied in practice in a production workshop environment. The literature review forms the basis of establishing a new theoretical framework and methodological focus of the research.

2.2 Chatter Detection Techniques

In 1907, Taylor [48] introduced the term “chatter” for the first time. He introduced it as a kind of machining vibration, which causes poor machining process productivity. However, no significant research was done until middle of 1940’s, when Arnold [49] theoretically explained chatter generation as being negative damping. Afterwards, more studies were done in order to explain chatter, as well as detect it. Tobias and Fishwick [50] created a theoretical stability chart based on the process dynamics and the machine tool structure. Tlusty and Polacek [51] observed that the varying chip thickness in a lathe turning processes can dynamically affect cutting force, which in return vibration amplitudes will be increased. Olgac and Hosek [52] modelled the machining process as a root locus plot analysis of time delayed systems and proposed an active vibration suppression method.

Detection of chatter assists in improving production efficiency of machining processes. Usually in workshop environments, highly experienced machining

operators are able to detect chatter by listening to the generated noise. However, it does have high rate of human error. Accordingly, many methods including analytical, numerical, and experimental have been proposed in order to better detect chatter. The methods focus on providing more machining productivity, and reducing human error. They are classified under five main categories.

2.2.1 Time Domain

Time domain methods use time-domain simulation of the machining process in order to assess the stability of the system. In these techniques, time behaviour of the machining process is evaluated by analysing mathematical functions or physical signals with respect to time [20]. For this purpose, the combination of cutting parameters and milling process vibration is numerically simulated by discretising the delayed differential equation (DDE) [53]. Insperger and Stepan [54] analysed the stability of the machining process by using the semi-discretization method (SDM). In this method, time is discretised into equal time intervals.

In the last few decades several methods have been proposed based on analysing time-domain of the machining process. In 1960's, Tlusty [55] and Tobias [56] began the study of chatter with respect to the time domain with establishment of the basis of the regenerative chatter theory. Sridhar *et al.* [57] firstly introduced the time-varying directional cutting force coefficients in modelling the stability of the milling process. Budah and Ozlu [58] used a multidimensional model with precise process geometry to predict chatter in turning and boring operations by simulation. Fu et al [59] used a cantilever tool with extended length to investigate the effect of tool vibration on chatter occurrence. They were successful in developing a chatter suppression method using an adaptive pressure clamping interface.

In several studies, physical or mechanical properties of the machining process are recorded and used to analyse the stability of the dynamical system. The sampling is usually based on the sampling rate of once per tooth or once per

revolution [60]. Nair *et al.* [61] detected the onset of chatter from recorded sound signals from turning processes by using permutation entropy. Schmitz *et al.* [62] and Bayly *et al.* [63] tried to detect chatter during milling processes by using the statistical variance in the once-per-revolution sampled audio signal. Time domain simulation was done in order to determine the variance in the once-per-cutting tool revolution sampling rate. However in order to have enough data points for variance calculations, larger numbers of simulated cutting tool revolutions are required.

The influence of chip thickness variation has been considered in many time domain based studies. During machining process, chip thickness varies and this leads to variations in the cutting force. Accordingly, the cutting force variation causes vibration, which further leads to the occurrence of chatter, if the cutting parameter combination is unfavourable [64]. In these methods, the simulation of milling process is involved to detect chatter, rather than using sampling technique. Zhongqun and Qiang [65] modelled the instantaneous chip thickness caused by tool vibrations by using a set of force equations. They were able to deduce those cutting conditions which avoided chattering. Wan and Zhang [66] calculated instantaneous uncut chip thickness and cutting force by instantaneous incorporation of the cutting tool and workpiece deflections, as well as immersion angle variation. The cutting force model was used as the basis for chatter detection.

Another time domain based method simulates machining process by simulating Peak-to peak force. The peak-to peak force value is used to identify the limits of the stability during milling [67, 68]. In these studies, peak-to-peak force amplitude values are provided over a range of cutting conditions.

The self-excited damping ratio is also a numeric value that is considered in time domain simulating methods in order to determine the boundary of stability in milling [69, 70]. Machine tool structure is a continuous, time-variant, nonlinear elastic structure. By definition of the damping ratio at when self-excited vibration happens, the response of the machine tool structure can be determined [60].

Time domain methods have some advantages but processing issues prevent them being used effectively in the workshop environment. Time domain techniques can model the kinematics of milling and nonlinear effects such as the loss of contact between cutting tooth and workpiece [71], which is unavailable in linear stability analyses [72]. This provides a realistic simulation of milling and its instability, reducing the need to make a large number of assumptions [73]. In summary, time domain simulation methods can model kinematic and nonlinear effects of the milling process.

Unfortunately, time-domain numerical simulation methods and experimental approaches are computationally time intensive and cannot be widely used in industries [74]. It is more useful when the methods are used to predict the chatter threshold boundary, and to do this a large number of simulation runs are required under different milling conditions. Each simulation has to run in a reasonably short time in order to effectively detect chatter [69]. Because they are successful, time domain methods are often used as a reference for other methods.

2.2.2 Frequency Domain

Frequency domain chatter detection methods analyse signal or mathematical functions related to the cutting process with respect to frequency [75]. They are based on the fact that the frequency of the forced and self-excited vibrations are unequal during the cutting process [60]. Altintas and Budak [76] were the pioneer researchers who used frequency domain to effectively detect the occurrence of chatter. They used Fourier series expansions of the periodic matrices truncated at the zeroth-order constant terms. The method was efficient and fast, however it was not able to predict the existence of the additional stability regions in the case of low radial depth cut for milling operation. Merdol and Altinas [10] did overcome this limitation by adding higher harmonics to the former method. This method was named multi-frequency solution.

Fast Fourier Transform (FFT) is the simplest method for frequency domain detection of chatter during milling. In this method, the energy of chatter vibration

is reflected in the power spectrum diagram. From the power spectrum, it is possible to extract the tool passing frequency and its harmonic frequencies in terms of signal power. Harmonic frequencies are identified as multiplies of the tooth passing frequency. When chatter occurs, a frequency which is not a multiple of the tooth passing frequency can be identified as the chatter frequency [77]. This technique has been used to detect chatter in several studies. Toh [78] used FFT to analyse vibration of the cutting path orientations during rough and finish milling processes. For this purpose, he used the cutting force acquired during the milling process with new and worn cutters. Independent of the cutting tool condition, FFT analysis demonstrated minimum vibrations in the vertical upward orientation. Ding *et al.* [79] managed to transform the cutting force into the frequency domain by applying FFT. They identified chatter frequency by comparing its power spectrum with a predefined threshold. Schmitz *et al.* [80] proposed that the statistical variance in the once-per-revolution sampled audio signal be used as a chatter indicator. They evaluated their method by using a FFT chatter detection method

Some frequency domain methods use cross-coherence to examine the relationship between two signals or data sets, and thereby to detect the chatter vibration. Dong *et al.* [81] suggested a chatter prediction method independent of cutting conditions using coherence analysis in the frequency domain. Li *et al.* [82] proposed cross coherence of two perpendicular acceleration signals in order to detect wear and chatter. Zaghbani *et al.* [83] used cross coherence to analyse the stability in robotic high speed machining of aluminium alloys.

Several studies proposed using the entropy of the system as a tool to demonstrate the change of cutting dynamics caused by the onset of chatter [84]. Nair *et al.* [61] analysed the variation of permutation entropy (PE) using sound signal recorded with a microphone to detect the onset of chatter. Pérez-Canales *et al.* [85] used approximate entropy (AE) to monitor chatter. This method works based on the fact that unstable vibration is related to the emergence of random dynamics; hence stable vibration is dominated by regular periodic dynamics. Gradišek *et al.* [86] proposed using two entropy and coarse-grained information

rate to detect chatter automatically during grinding process. They calculated entropy from the power spectrum; and thereafter the coarse-grained information rate was calculated from fluctuations of a recorded signal.

The spectrogram is other tool used in the frequency domain method to assist detecting the onset of chatter. This tool is a visual demonstration of the spectrum of frequencies in sound or other signals that usually vary with time [87]. As an example, Messaoud *et al.* [88] used time series analysis and multivariate control charts in order to monitor drilling processes. They showed by using a spectrogram how a system moves from a stable to a chatter state.

Frequency domain techniques have many advantages for detection of chatter. Compared to time domain methods, they are reasonably fast and accurate except at very low radial immersions [63]. Of the frequency domain techniques available, FFT is the most used by researchers. The method provides good information about frequency of machining processes and in particular chatter frequency. But, it cannot provide information about prediction of chatter occurrence [89]. The frequency domain techniques indicate the chatter frequency is usually smaller than the tooth passing and harmonic frequencies. Accordingly, the outline chatter frequency cannot be used as a numeric indicator to predict chatter. Normally in frequency domain techniques, a large range of sampling rates is necessary to define the occurrence of chatter, although time domain techniques need only one sample per spindle revolution to define chatter [62]. Moreover, for frequency domain techniques, some approximations are needed to formulate the system [73].

2.2.3 Wavelet Transform

As mentioned above, the main shortcoming of frequency domain chatter detection methods is that the lack of related time information. To overcome this, time-frequency domain or Wavelet-based methods were proposed [90], which are able to provide significant resolution in both time and frequency domains [91].

Wavelet transforms were first applied to signal processing by Mallart in the middle of the 1980's [92]. The application of wavelet transform has since then been rapidly developed and used in much engineering research such as [93, 94], in the field of signal processing [95], image processing [96], computer science, and mathematics [97]. It was also used to detect chatter during machining processes in many studies [98, 99].

Wavelet transform uses wavelet basic functions to analyse signals. To analyse signals in both frequency and time domains, the original signal is separated into two signals, which are named as the "detail" and "approximation" signals, and this procedure is called "wavelet decomposition". The procedure is repeated at different levels. The wavelet basic function is then applied to analyse the signals formed in the levels [89].

From the literature, chatter research has been mostly analysed by using one of four methods; continuous wavelet transform (CWT), discrete wavelet transform (DWT), the maximum likelihood method and biorthogonal method. Khraisheh *et al.* [100] particularly used continuous wavelet transform to analyse chatter signals observed during CNC lathe processes. It was an experimental technique which used cutting force and vibration signals in order to detect chatter. Bickraj *et al.* [101] also used continuous wavelet transformation to develop chatter analysis during milling operation of a plate. Abu-Zhara and Lange [102] presented an application of CWT to monitor chatter by analysing the ultrasound waves observed in turning. Using ultrasound sensor helps to easily monitor parameters such as the first contact of the cutting tool, tool chipping and tool flank wear. However, the sources of noise in the workshop environment can affect the accuracy of the proposed technique.

Wang *et al.* [103] proposed to detect chatter based on discrete wavelet transform (DWT). Their method was a statistical analysis of Wavelet Transform Modulus Maxima (WTMM). This method describes the points that the wavelet transform of the signal is locally maximal at a corresponding time location. In this technique, noise must be removed before signal transformation. Besides this study, Huang *et al.* [104] analysed cutting force signals that are observed during

milling of titanium by using time domain, frequency domain, and time–frequency domain techniques. In the time-frequency domain analysis, they used DWT to determine the value of cutting speed at the onset of chatter. Ji *et al.* [105] proposed a combination of the discrete wavelet transform with statistical estimations of the signal energy distribution in order to monitor drill wear, which occurs due to chaotic and unsteady characteristics during drilling. Fang *et al.* [106] used DWT to process vibration signals and thereby measure cutting vibrations. They demonstrated the effect of tool edge wear on the cutting vibrations during high speed milling of titanium.

Maximum likelihood estimation is a statistical method that combination of maximum likelihood and wavelet transform provides a parameter estimation algorithm. This algorithm is appropriate in prediction, control or diagnosis of the state of a dynamic system [107]. As an example, Choi and Shin [108] used wavelet transform and maximum likelihood in order to detect chatter during both turning and milling processes.

If wavelet transform is invertible not orthogonal, then a biorthogonal wavelet is applied in order to provide more degrees of freedom [109]. Berger *et al.* [110] identified stable and chatter states during turning processes by analysing bi-orthogonal wavelet decomposition of the cutting force measurement. Cao *et al.* [111] detected tool breakage in end milling process using acoustic emission signals. They proposed a method based on the lifting scheme and the mahalanobis for the sample point evaluation. In this technique, they constructed a biorthogonal wavelet with an impact property.

From the literature review it appears that wavelet transform is an effective tool for detecting chatter. The method can assist operator in early detection of chatter during the process [89]. It also provides more significant time and frequency resolution from the machining process, specifically in the low frequency band. Unfortunately, it cannot provide appropriate resolution in the high frequency band.

Definition of the number of levels of decomposition and the specific level is always a challenge in wavelet based methods, particularly when the chatter frequency is unknown. Detection of chatter is sensitive to the number of levels, accordingly the proposed methods cannot effectively detect occurrence of chatter when cutting condition changes [90]. Apart from being computationally time consuming, wavelet-based methods are also sensitive to signal shift and have poor directionality [112].

2.2.4 Stability Lobe Diagrams

Illustrating the stability lobe diagram (SLD) is an effective tool which demonstrates the relationship between spindle speed and axial depth of cut in machining processes. SLD assists an operator to select spindle speed and axial depth of cut in a way that the machining process remains stable (as shown in Figure 1.3) [113]. The boundary between stable and unstable cutting regions is demonstrated with a set of lobes in diagrams.

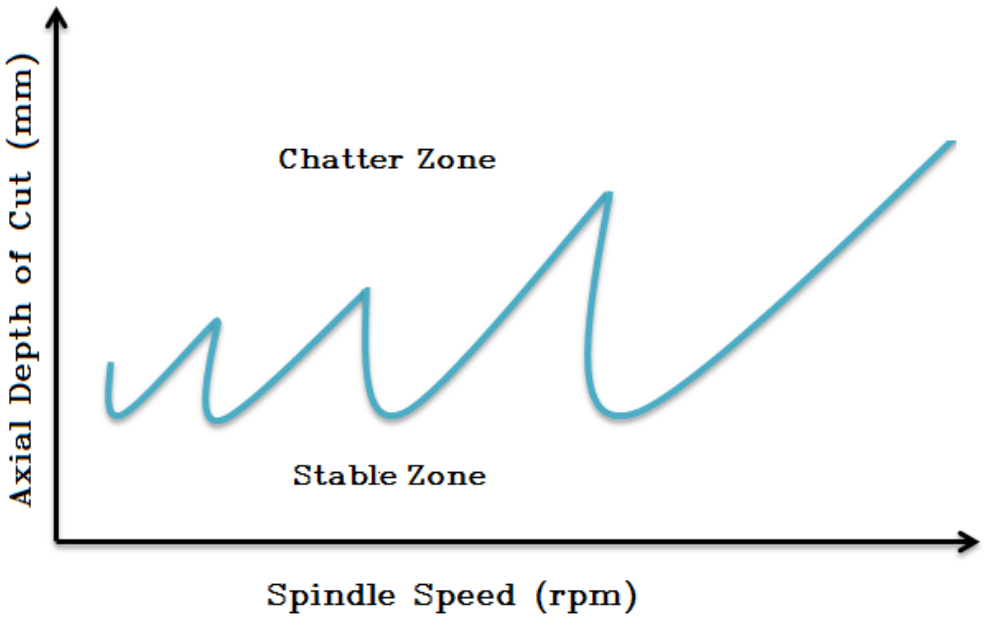

Figure 2.1: A typical stability lobes diagram.

Illustration of stability lobe diagrams were first introduced in the 1950s by Tobias [114], and Tlusty and Polacek [51]. They introduced the factor of regenerative chatter in an orthogonal cutting process and developed a set of diagrams to determine the stability region of the process. To generate stability lobes diagrams, a set of various experimental and analytical techniques are used. These methods are numerous and include the use of time domain, frequency domain, and time-frequency domain [76, 115, 116]. Pal Pandian *et al.* [117] used an analytical method to develop stability lobe diagram for machining of thin ribs. In the method, the frequency response function of the process was predicted along with real and imaginary parts. Thevenot *et al.* [118] developed 3D stability lobe diagrams for thin-walled structure milling in order to determine the stability regions.

Stability lobe diagrams assist operators in choosing the most appropriate cutting parameters before running the machining operation. Successful milling depends very much on the process parameters used and hence accurate prediction of chatter, such that use of incomplete or inaccurate parameters may run the milling process into undesired chatter condition.

2.2.5 Soft Computing

Simulation of decision making capabilities similar to the human mind is the concept of soft computing methods such as Fuzzy Logic (FL), Artificial Neural Networks (ANN), evolutionary computation, etc. [119]. Zadeh [120] introduced the concept of soft computing as the fusion of methodologies designed to demonstrate solutions for problems that are not normally modelled mathematically. It has then been applied in different areas of science, particularly in engineering applications, such as [121-124]. Soft computing techniques have also been applied to detecting the state of systems during machining processes. For this purpose, fuzzy logic and neural networks techniques are widely used.

Using normal binary logic, propositions can have a value of true or false; however fuzzy logic works based on degrees of true and not exactly true or false.

In fuzzy logic, the propositions are presented as a variable that can have the answer of true or false. The propositional variables are related to each other by connectives, hence the combination of connectives are described by fuzzy function [125]. The concept of fuzzy logic has been used to detect the stability of machining processes. Xu [126] developed a fuzzy logic control approach to suppress the occurrence of chatter by using a coherence function value associated with the vibration energy level. Sims *et al.* [127] investigated the chatter stability of milling processes using a fuzzy logic algorithm. They showed their method is able to solve process design problems with robustness, even given the uncertainty of the parameters. Kim and Jeon [128] designed a fuzzy-logic controller which could adjust feed rate automatically during milling. In this case, the cutting force would be regulated by adjusting the feed rate and therefore control chatter occurrence.

Artificial neural networks are a kind of computational models that are worked in a similar way that a human's brain would performs a particular function. They replicate a system of interconnected "neurons", which are able to compute values from inputs by feeding information through the network [129]. Neural networks have been used to predict the state of dynamic systems. Tansel *et al.* [130] used two trained neural networks in order to identify the harmonic acceleration signals and their frequency during cylindrical turning of long slender bars. This method predicted the occurrence of chatter. Lamraoui *et al.* [131] developed a methodology using neural networks to detect chatter during CNC milling. Pontes *et al.* [132] applied a radial base function neural network to predict roughness average for turning processes, which is an important factor for chatter detection.

In general, soft computing models are close to how the human mind works, with the advantages of them being linguistic, reasonably simple, comprehensible, fast in computation, and effective in practice [133]. Soft computing models are characterized as being knowledge representational and data acquisitional. Comparing the two main techniques in soft computing, fuzzy logic and neural network, both are applicable for nonlinear representation between inputs and outputs. However, fuzzy logic designs a process in order to define the

parameters, whereas in neural networks the process is developed by learning. Consequently, an operator can operate fuzzy systems easily compared to neural network models. On the other hand, the nonlinear function developed by neural networks is smooth, while the obtained function from fuzzy logic is rough [134]. Neural networks and fuzzy logic differ in the number of inputs they can have. There is no limitation for the inputs in neural networks, while fuzzy logic systems are limited to two or three inputs.

Neural network models sometimes fail to explain the cause and result logically in the excitation response relationships, which affects the accuracy of the model [135]. Fuzzy systems also may miss adaptation capabilities for a long time [136]. In addition to these drawbacks, a large number of chattering experiments is required to train neural networks and much fine tuning and simulation is required for fuzzy systems in order for them to detect chatter. This limits the application of soft computing techniques for detecting chatter. Both fuzzy logic and neural networks can provide a chatter control system for milling operations [137, 138], but these cannot respond quickly to control cutting forces [91].

2.2.6 Topography

The topography is a method which focuses on the cutting surface in order to detect chatter marks. In this technique, a profilometer is usually used in order to investigate the cutting surface. Demonstrating the application of profilometer in definition of chatter, Seguy *et al.* [139] used this method along with spindle speed variation in high speed milling processes to detect chatter. A 3-D Profilometer was used by them to measure the surface roughness. Surface roughness can be considered a parameter that has a direct effect on chatter occurrence. Accordingly, Nurul Amin *et al.* [140] minimized surface roughness by using cutter with uncoated WC-Co (tungsten carbon-cobalt) inserts. In this case, end milling of mild-carbon steel was carried out in a magnetic field which was provided by permanent magnets. They used a Profilometer to measure surface roughness during experiments.

The literature review demonstrates that a profilometer is usually used to detect chatter marks at the end of cutting processes [141, 142]. The proposed methods cannot predict chatter online during the machining process. Profilometer are generally used for approving or validating other chatter detection methods.

2.3 The Application of Poincaré section in Definition of Stability

Phase space attractor Poincaré section is another technique which is precisely explained in chapter 4. Its application in defining the state of machining processes is reviewed in this section.

Phase space attractor Poincaré section is a tool that is able to determine the transition of a dynamic system from a stable state to an unstable condition. It has been applied to different dynamic systems such as machining processes. One of the first pioneers in using phase space attractor Poincaré section were Nayfeh and Balachandran [143]. They proposed this technique to show the stability of a nonlinear dynamic system by the variations that occur between sections.

Rusinek et al [144] analysed the effect of nonlinearity on the stability of the regenerative model of machining processes by using the time delay technique and plotting the Poincaré sections. They examined the effect of cubic nonlinearity on the stability of chatter. Wiercigroch and Krivtsov [145] examined frictional dynamic models of milling with chatter occurring and used phase space analysis techniques to analyse orthogonal machining. They observed some unusual chaotic behaviour, the study of which could be used to improve machine tool design. Davies et al [146] measured tool deflections of high length-to-diameter ratio end mills and used Poincaré sectioning to identify chatter. In general, the method predicted the stability of high immersion cuts but was inconsistent in partial or low immersion cuts. Therefore, Schmitz et al [80] proposed using the audio signal variance as a chatter indicator. They extended the work of Davies et al [146] by including once-per-revolution sampling of the milling audio signal and statistical evaluation of the results. However, the results can be compromised if the

microphone used has limitations in bandwidth and if there is too much environmental noise.

Zhao and Balachandran [147] studied the dynamics and stability of range of milling operations numerically and by experiment. They were able to identify chatter using Poincaré sections on the data stream. Liu et al [148] developed a simultaneous time-frequency control theory to determine the various nonlinear dynamic instabilities including tool chatter and tool resonance which can be displayed by a multi-dimensional, time-delayed micro-milling model. The unstable states were investigated using Poincaré section and instantaneous frequency. Under this time-frequency control scheme, stable cutting was able to be achieved.

Johnson and Moon [149] used the combination of Poincaré sections and false nearest neighbours to define the stability of the system during turning processes. The effect of loss of contact during milling has not been investigated because of the difference between the dynamics of milling and turning processes. The chip thickness is constant during turning process, while it is function of the rotation angle in milling processes [150]. Accordingly and as mentioned in the introduction, dynamic modelling in milling process is more complicated than turning, as the cutting forces change the direction of excitation and contact is lost continuously during the process [151].

The above state of the art demonstrates that phase Poincaré section has been previously used in machining process in combining with other techniques to provide stability lobe diagrams, or to confirm the applicability of other chatter detection methods. It has not been used to directly define the occurrence of chatter on-line.

2.4 Summary

The state of the art review shows that numerous analytical and experimental studies have been done so far in order to provide an appropriate method for detection of chatter before it occurs. However, none of the methods researched so far can

effectively predict chatter occurring while the cutting process is progressing and cannot be used for online detection. The methods need expensive equipment or highly qualified professional employees. The methods are applicable in off-line or in laboratory conditions to provide stability lobes diagram. In the other hand, some methods are slow and time consuming. As a result, industry still suffers from the damages done by the chattering phenomenon.

The Poincare section method seems to match what is required for predicting the behaviour of non-linear systems like the cutting process but there has been no record of exploiting this idea to chatter detection. Accordingly in order to overcome the limitations in the existing chatter detection methods, a novel method based on the analysis of non-linear systems and a more direct indicator for industry use is required. The method must be computationally fast and provide definite and clear criteria to detect the onset of chatter prior to its occurrence.

Chapter 3

Experiment Design

3.1 Introduction

In this study, a new method for determining chatter threshold during milling processes is proposed. For this purpose, the vibration between the cutting tool and workpiece has to be acquired in the form of a signal. Accordingly, it is required to design a set of experiments in a way to ensure that the acquired signals are with the minimum amount of noise with no faults.

This chapter discusses the most appropriate parameters and the sensors needed for acquiring the vibration between the cutting tool and workpiece during milling operation. The design of the experiment apparatus is also explained in detail. The signals will be analysed to determine the onset of chatter for different materials. The cutting processes are designed to run with normal speed as normal milling operation is general and run in most general production workshops.

3.2 Research Methodology

Before demonstration of experimental design, an overview of the research methodology is represented by a flow diagram to provide better understanding of the research aims. The flow diagram, which is shown in Figure 3.1, illustrates the overall organization of this research. It will improve the objective of the research and. also assist to understand research methodology clearly.

3.3 Parameters Required

For this study, two physical parameters must be acquired. In the early stage, the vibration between the cutting tool and workpiece has to be recorded, and this will be acquired by measuring acceleration. In addition the cutting force must be recorded in order to be used in the Fast Fourier Transform (FFT) method approving the proposed method of chatter detection. The methods of measuring these two parameters plus the required instruments are explained.

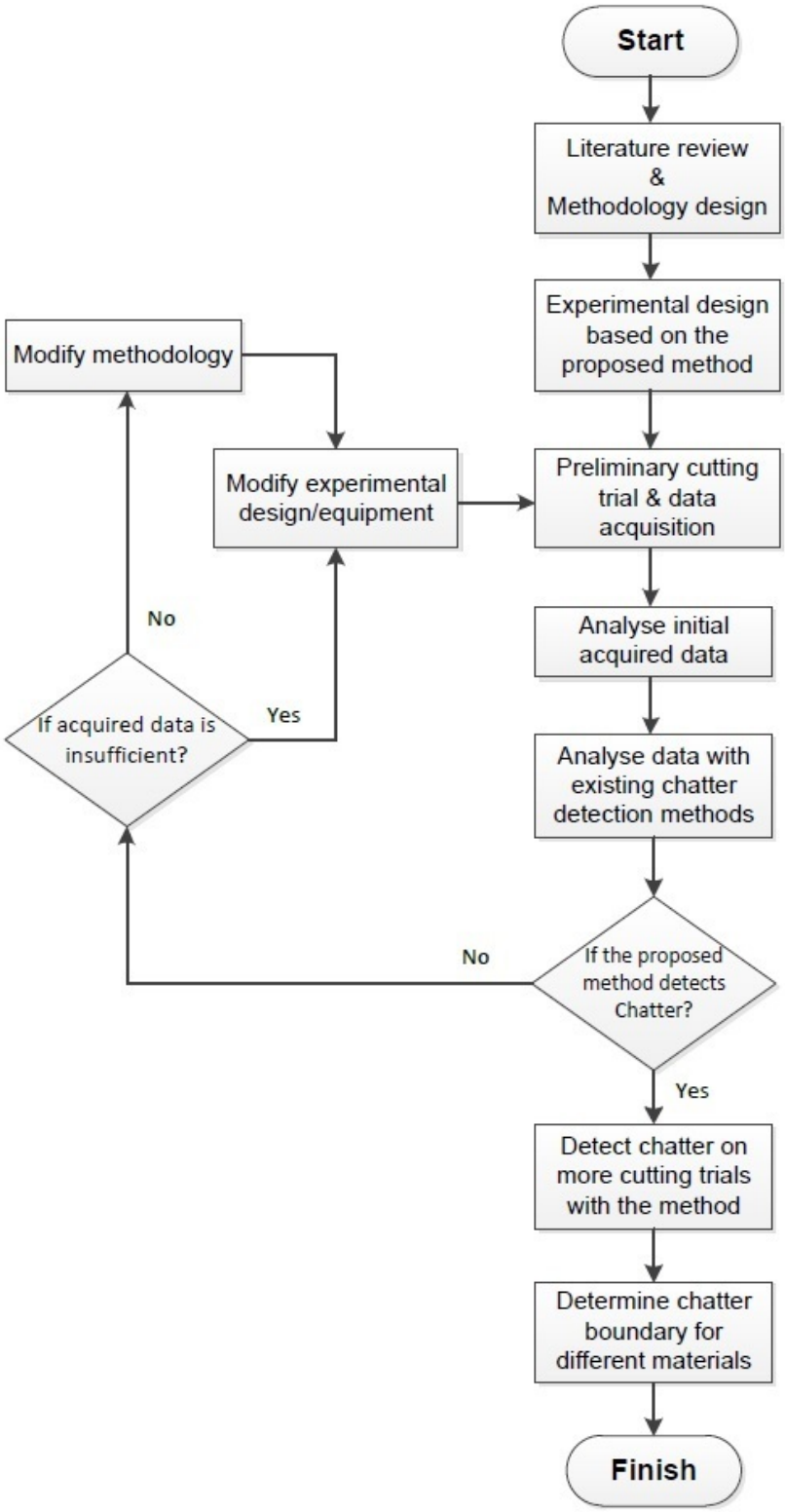

Figure 3.1: Overal research methodology flow-diagram

3.3.1 Acceleration

To investigate chatter behaviour, displacement [152], velocity [153], sound, and acceleration [154] are usually acquired in order to measure the generated vibration between the cutting tool and workpiece. These parameters are recorded during the machining process, consequently they are analysed by different methods in order to detect chatter. Acceleration is the most useful one and from which can be determined both low and high frequencies during the process [155]. Comparing to other parameters such as displacement and velocity, the acceleration signal is not so easily affected by instrument noise at high frequencies, which makes acceleration one of the better vibration characteristics that can be measured.

Accelerometer sensors are widely used to measure acceleration. They are tiny and provide a link between vibrating structures and electronic measurement equipment. They are installed on the surface or within the vibrating object. They contain a tiny mass that is suspended by flexible components that operate like springs. The movement of the accelerometer will cause the small mass to deflect proportionally to the rate of acceleration. Accelerometers can provide acceleration information in one or more axes.

The accelerometer sensor (Figure 3.2) is chosen in this research to record vibration between the cutting tool and workpiece, due to:

- they are robust, compact, and self-generating,
- they have a large dynamic and wide frequency range,
- they are relatively cheap,
- they are easy to calibrate and use, hence they are relatively insensitive to environmental changes,
- they are very reliable with long term stability, and
- they can be used in any orientation to measure acceleration along the axes.

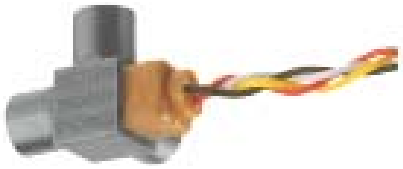

Acceleration Rate:	±500g
Sensitivity:	(±5%) 4 mV/g
Freq. Response:	10-20000 Hz
Connector:	4-pin neg. int.
Mass:	2.5 gr
Random Vibration, max:	± 2000grms

Figure 3.2: A tri-axial accelerometer Kistler 8694.

Acceleration signal acquired by accelerometer is periodic during the milling process [156]. Hence, signal is time based and is able to indicate the vibration level in order to identify any problem during the milling process [157]. Signal can be illustrated in the form of time series $x_{(t)}$ as shown in Equation (3.1). $x_{(t)}$ is the output voltage of the accelerometer at time i with unit millivolts (mV).

$$x_{(t)} = \{x_1, x_2, x_3, \dots, x_t\} \tag{3.1}$$

3.3.2 Cutting Force

Before discussing the other equipment and devices required, the method of acquiring the cutting force will be outlined. In chapter 5, the Fast Fourier Transform method is applied to determine whether the proposed chatter threshold boundary is approved with Fast Fourier Transform. For this purpose, the FFT power spectrum of cutting force signal must be plotted to detect whether chatter occurs in the milling process, as well as establishing the definition of chatter frequency. Accordingly and in addition to the acceleration signal, the cutting force has to be acquired during the milling trial. The cutting forces along with the acceleration signal will assist in determining which direction is most appropriate for detection of chatter.

Considering Figure 3.3, the force produced along cutting feed direction is named cutting feed force and is displayed by (F_x). Consequently, cutting force along

radial depth of cut is named radial cutting force (F_y) and cutting force along axial depth of cut is named axial cutting force (F_z). The literature review and observation from the acquired cutting force during the milling process indicate that the axial cutting force (F_z) is much smaller than other forces, cutting feed force and radial cutting force. Therefore, it cannot contribute to the chatter [158]. On the other hand, cutting feed force is larger than radial cutting force, when the chatter occurs [159].

Similar observation has been gained from examining the acceleration signals in three cutting directions. Accordingly, chatter appears to be mainly affected by the acceleration signal along cutting feed. This signal is therefore considered in the analysing methodology.

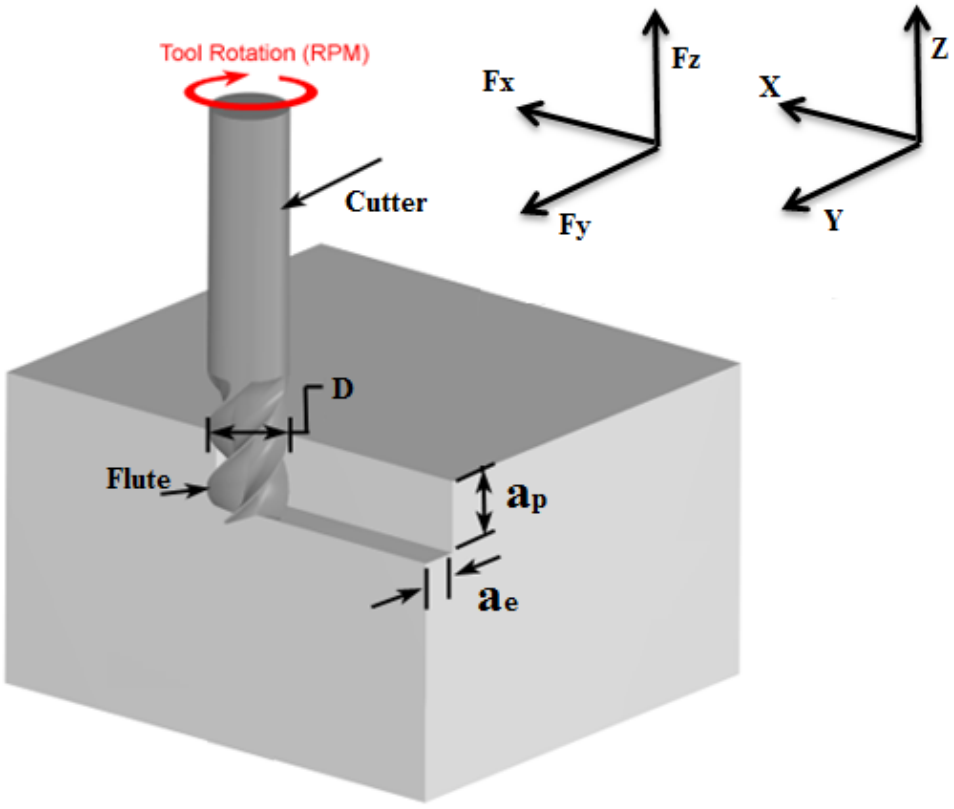

Figure 3.3: The schematic milling process demonstrating the cutting forces.

3.4 Experimental Hardware Arrangement

Milling trials are performed using a HAAS 4-axis Milling Machine (Figure 3.4) in the advanced manufacturing laboratory located at Royal Melbourne Institute of Technology (RMIT), Melbourne, Australia. The machine is made in the USA. Besides the milling machine, a data acquisition card, amplifier, and software are required to successfully record high quality signals from the accelerometer. The schematic arrangement of experimental hardware is shown in Figure 3.5.

Mach. Contl:	HAAS 32 Bit CNC
Table Size:	26" x 14"
Mach. Travel: (X/Y/Z):	20" x 16" x 20"
Table Capacity:	3000 Lbs
Spindle Speed:	0-9900 rpm
Transmission:	2-Speed Geared Head
Drive System:	Inline Direct-Drive
Max. Cutting Feed Rate:	500IPM
Tool Changer:	Carousel
Max Tool Diameter:	89 mm

Figure 3.4: 4-axes milling machine used to perform the experiment.

3.4.1 Equipment & Instrument Devices

In this section, the equipment and devices that are used to acquire the signals are introduced. As shown in Figure 3.5, the dynamometer and accelerometer acquire the vibration and cutting force during the milling process. Consequently, the amplifiers excite sensors, condition the signal and display directly the measured values. Lab-View is the program developed by the National Instruments Company. This program is used for programming computer-controlled instruments, as well as measuring and recording sensor readings.

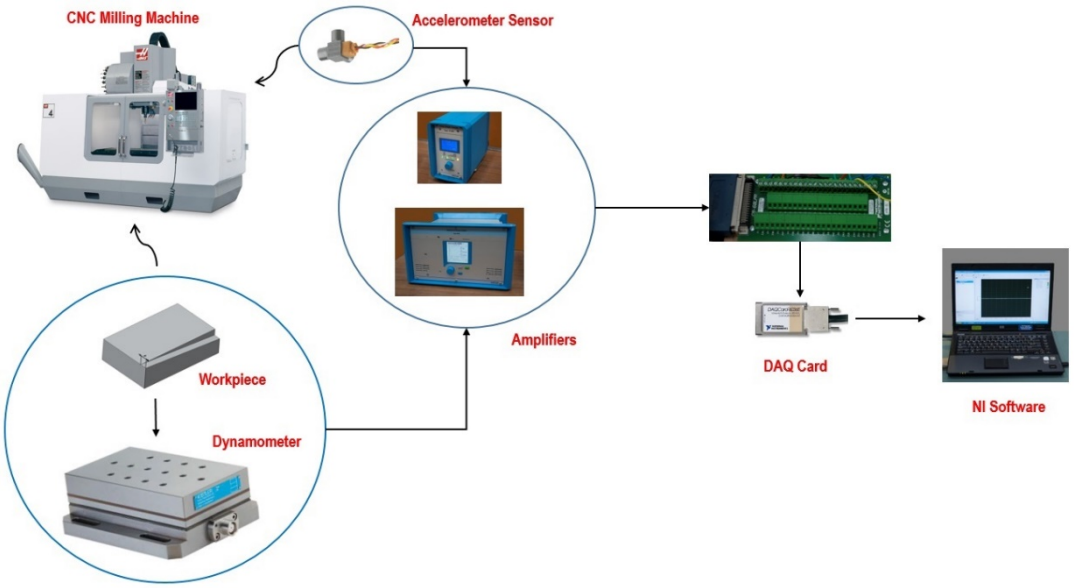

Figure 3.5: The experiment hardware arrangement.

3.4.1.1 Accelerometer Sensor

A tri-axial piezoelectric miniature accelerometer sensor, model 8694 M with ±500 g of range manufactured by Kistler (Figure 3.2), with wide frequency response and voltage mode is used to record the amplitude of vibrations along milling process.

The accelerometer includes three individual piezoelectric sensors which are mounted orthogonal to record signals in three directions *X*, *Y*, and *Z*. This model of sensor has a low impedance voltage mode, quartz sensing element, high resonant frequency, as well as it being small and light. Consequently, this model of accelerometer is suitable for very light test objects, modal testing, ability to record dynamic changes in mechanical variables, as well as it is able to measure vibrations on thin-walled structures[1].

[1] The technical information is presented from the manufacturer catalogue.

The signal acquired by the accelerometer is in the form of a voltage proportional to the actual acceleration. To convert voltage (*V*) to acceleration (m/s^2), the sensitivity of the accelerometer is needed. Every accelerometer has its own sensitivity, which is determined by the manufacturer. The data sheet for this model states the sensitivity of the output *0.004 V/g*. Accordingly, the Equation 3.2 can be used to convert the recorded voltage (*V*) from sensor to acceleration (m/s^2).

$$a_b(t) = V_a(t).\frac{g}{0.004} \quad (3.2)$$

Where:

$V_a(t)$ is the amplitude of acceleration recorded by sensor in the form of voltage and is function of process time.

$a_b(t)$ is the converted acceleration.

g is the acceleration due to the gravity and its value is equal to $9.81\ m/s^2$.

3.4.1.2 Dynamometer

As mentioned earlier, cutting force along milling process is needed to be acquired. For this purpose, a dynamometer type 9257B manufactured by Kistler is used (Figure 3.6). This quartz three-component dynamometer can measure cutting forces in three orthogonal directions. The dynamometer has a great rigidity and consequently a high natural frequency. Its high resolution enables the smallest dynamic changes in large forces to be measured.

Number of Axes:	3
Measuring Mode:	Direct
Measuring Range (Fx/Fy):	-5.00 – 5.00 KN
Measuring Range (Fz):	-5.00 – 10.00 KN
Sensitivity:	7.5 pC/N (Fx.Fy) 3.7pC/N (Fz)
Natural Freq.	3.5 KHz
Capacitance:	220 pF
Size (L/W/H):	170/100/60 mm
Degree of protection:	67 IP

Figure 3.6: dynamometer Kistler type 9257B.

3.4.1.3 Data Acquisition (DAQ) Card

DAQ card-6036E (Figure 3.7) is used in order to acquire data from the sensor. It is recommended by accelerometer and dynamometer sensor suppliers. It has a 16-bit multifunction I/O card with *16* analogue inputs and two outputs. This card is able to do continuous data logging up to *200 kS/s*, as well as being capable of triggered data acquisition. Hence, it uses dithering reduced quantization error method in order to improve resolution of data acquisition. The effective input resolution of the card is a minimum of *18* bits.

Analog Input:	16 SE/B DI
Input Resolution:	16 bits
Max. Sampling Rate:	200 kS/s
Input Range:	±5 - ±10 V
Analog Output:	2
Output Resolution:	16 bits
Output Rate:	1 kS/s
Output Range:	± 10 V
Digital I/O:	8

Figure 3.7: DAQ Card 6036E used in experimental setup.

3.4.1.4 Amplifiers:

Two amplifiers, one Kistler type 5070A for dynamometer and one Kistler type 5134B for accelerometer, are used. The amplifiers are recommended by the dynamometer and accelerometer sensor suppliers. The dynamometer produces an electric charge which varies in direct proportion with the load acting on the sensor. The amplifier type 5070A (Figure 3.8(a)) converts the electric charge into a proportional voltage.

Amplifier type 5134B (Figure 3.8(b)) is a flexible and simple to use signal conditioner that provides excitation power, signal processing and acts as an interface between the voltage mode piezoelectric accelerometer and the measuring instruments.

No. of channel:	4	Supply:	230/115 VAC
Connector at Input end:	BNC neg.	No. of channel:	4
Measuring Range:	200 – 200000 pC	Connector at Input end:	BNC neg.
Output Signal:	-10 – 10 V	No. of Signal Output:	4
Freq. Response:	0 – 45 KHz		

Figure 3.8: a) Multichannel Charge Amplifier 5070A. b). Piezotron coupler 5134B.

3.5 Experiment Design

Having both stable and unstable states in the same milling process is the most desirable condition for investigation of chatter behaviour using concept of chaos theory. For the experiment it is important to minimize variation in the parameters like process hardware, laboratory environment, workpiece material, and cutting tool geometry as these will all affect the state to change from stable and an unstable state. This will then affect the chatter threshold boundary. Accordingly, cutting path, cutting parameters, hardware, and sensor location must be designed in a way to achieve the objective of capturing the change in state from stable to unstable.

3.5.1 Cutting Path Design

For the cutting path parameter, it is important the direction of cutting path does not change during the milling trials. Since the accelerometer can acquire signals along three axes *X* (cutting feed), *Y* (radial depth of cut), and *Z* (axial depth of cut), then any variation in direction of cutting path makes it necessary to switch between acceleration signals for the different cutting feed directions. The data processing then becomes complex. To avoid this issue, a straight type of cutting path is chosen and the workpiece is cut in the form of a slot.

Stability lobe diagrams are usually plotted by axial depth of cut (a_p) versus spindle speed (V_s). Accordingly to have a stable condition at the start of milling process and continuously transform the process into the chatter, the cutting path can be designed in a way that axial depth of cut or spindle speed changes can be made continuously during the process. For this purpose, two kinds of cutting path are designed, which are discussed in continue.

3.5.1.1 End-mill Cutting Path

The first solution to force a milling process from a stable condition to chatter is to increase cutting speed (V_c) continuously. In this model of cutting process, axial depth of cut (a_p) does not change. Accordingly, cutting path will be in the form of normal cutting slot, as shown in Figure 3.9.

To cut workpiece in the slot form, CNC codes must be written in a way that spindle speed increases (V_s) continuously up to the desired value. To cut slot with constant axial depth of cut (a_p), end-mill cutting tool is used. Accordingly, the designed milling process is named end-milling operation, and hence the cutting path is named end-mill cutting path.

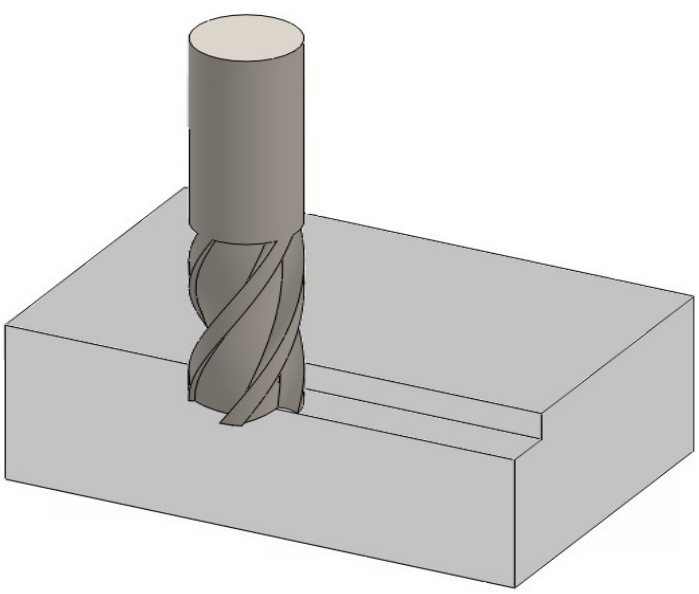

Figure 3.9: End-mill cutting path.

3.5.1.2 Ball-nose Cutting Path

The next solution to force a milling process from a stable condition to chatter is continuously increasing the axial depth of cut (a_p). For this purpose, the workpiece should be cut at an angle as shown in Figure 3.10. Accordingly, CNC codes are written in a way to have axial depth of cut (a_p) equal to zero at the beginning of the cutting process. It is continuously increased up to desired axial depth of cut at the end of the cutting process.

Slot drill end mill cutting tools are generally used when rotate on axis vertical to the cutting path, and they are weak to cut a path with an angle. When cutting tool axis is not vertical to cutting path, cutting force is more critical in end-mill cutter and causes to cutter breaks easily. Slot drill ball-nose cutters overcome this problem. A ball nose cutter has a semi-sphere at the tool end

and is most suitable for cutting path with complex shape, and also in the form of slope. Therefore to cut this form of slot, a ball-nose type of cutting tool has to be used. The designed milling process is therefore named ball-nose milling operation, and hence the cutting path is named ball-nose cutting path.

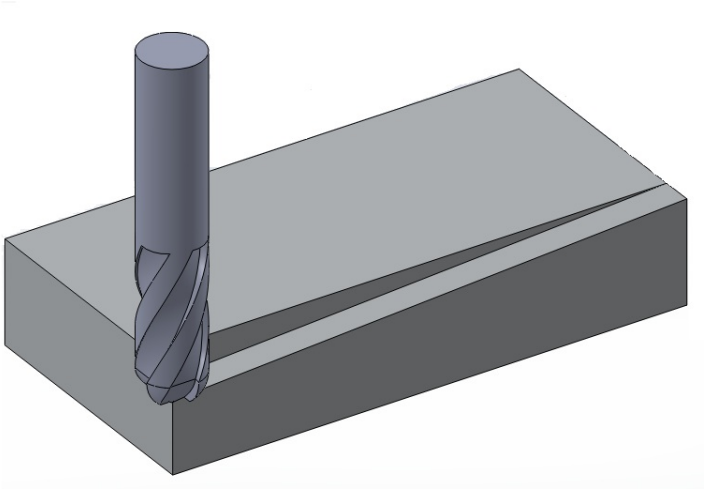

Figure 3.10: Ball-nose cutting path.

3.5.2 Workpiece Material

The objective of this research is to design a chatter threshold boundary mainly for titanium milling processes. However to verify the applicability of the method for other materials, two materials, namely an stainless steel and aluminium, are used and the proposed method is applied to the acquired signal during cutting of these materials. These materials are considered due to their demand for industrial purposes.

Titanium alloy 6Al-4V is accessible alloy of titanium that is widely used by industry. Accordingly, a block of titanium with dimension $150 \times 100 \times 30$ *mm* ($L \times W \times H$) is used as workpiece (Figure 3.11). The length of the workpiece is long enough to ensure the machining process reaches chatter. A similar geometry is used for the other two materials, aluminium alloy 6061, and stainless steel grade 316.

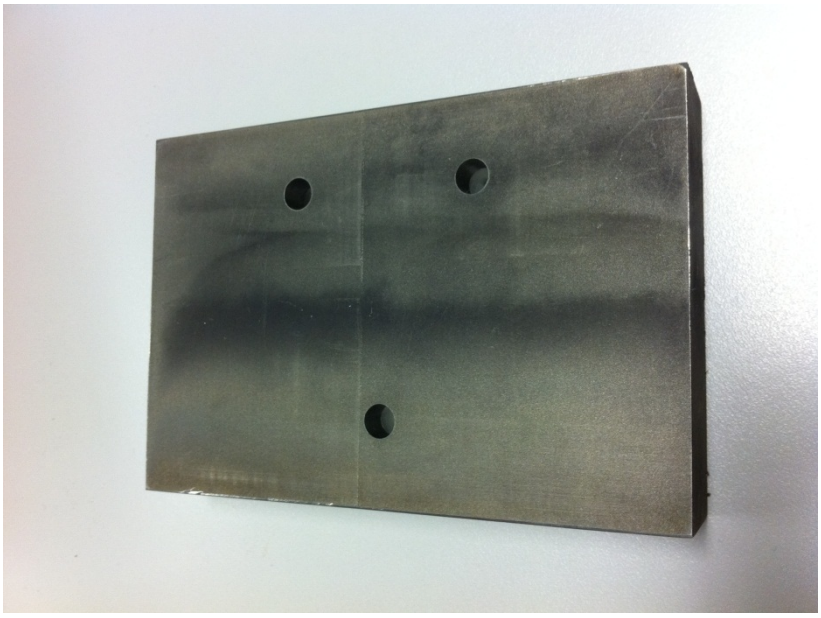

Figure 3.11: Workpiece material.

3.5.3 Cutting Tool

Based on the designed cutting path, two different kinds of cutting tools, end-mill and ball-nose cutter, are required in order to cut the material (Figure 3.12). The cutters also vary in diameter and the number of flutes. Based on their geometry, a series of experimental milling cuts are designed. In this study, milling trials are done using two different diameters, *4 mm* and *6 mm*. Hence, they have different numbers of flute, two and four, respectively.

Besides geometry of the cutter, its material is important, too. Cutting tools with HSS (high speed steel) and carbide material are most usable in industry. HSS cutters have better strength to withstand cutting force, as well as being low cost. However, carbide cutting tools have many advantages such as:

- Carbide tools are more efficient and more cost effective,
- Carbide tools have a longer working life due to have higher resistance to wear,

Figure 3.12: a). End-mill cutter with 4 flutes. b). Ball-nose cutter with 2 flutes.

- Carbide tools are more durable, and
- Achieve to better surface finish quality.

Accordingly and for this research, cutting tools manufactured by carbide are supplied and used during milling trials.

3.5.4 Cutting Parameters

Cutting parameters have to be chosen for each milling trial in a way that the process moves into chatter. Accordingly, it is required to determine the range of cutting parameters for each material, for which chatter is most possible to occur. For this purpose, the range is indicated by combination of using machining handbook [160], technical handbook of the cutting tool supplier[2], and also with a number of preliminary cutting processes for each cutting material. The range of cutting parameters shown in Tables 3.1 is selected for milling trials using a 6-mm cutting tool. For milling trials with a 4-mm cutter, the ranges of cutting parameters are indicated as shown in Table 3.2.

[2] Sutton Tools, Technical Information Guide. p.p. 352-368. www.sutton.com.au

Table 3.1: Cutting parameters that chatter occurs for a 6-mm cutter.

Cutting Parameters	Range of cutting parameters per materials		
	Titanium	Stainless Steel	Aluminium
Spindle Speed (V_s) (rpm)	4500 - 5000	5000 - 5500	8500 - 9000
Cutting Speed (V_c) (mm/min)	225-250	500-550	1000-1125
Axial Depth of Cut (a_p)(mm)	1	1	1
Radial Depth of Cut (a_e)(mm)	0.25D - 0.75D	0.25 D - 0.75 D	0.25 D - 0.75 D

Table 3.2: Cutting parameters that chatter occurs for a 4-mm cutter.

Cutting Parameters	Range of cutting parameters per materials		
	Titanium	Stainless Steel	Aluminium
Spindle Speed (V_s) (rpm)	3500-4000	5000 - 5500	8500 - 9000
Cutting Speed (V_c) (mm/min)	175-200	500-550	850-900
Axial Depth of Cut (a_p)(mm)	0.5	1	1.5
Radial Depth of Cut (a_e)(mm)	0.25D - 0.75D	0.25 D - 0.75 D	- 0.75 D

3.5.4.1 Ball-nose Milling Process

The experiments are designed based on the indicated cutting parameters by using the Taguchi method. The Taguchi method employs specific partial factorial arrangements to optimize the number of physical experiments required to detect process change [161]. The Taguchi approach is a form of experiment design with special application principles, which makes uniform the experiment design technique. It has a number of advantages. It employs specific partial factorial arrangements, orthogonal arrays and balanced factorial combinations, in order to determine the optimum design. The product development cycle time can therefore be significantly reduced because a lower number of experimental runs is needed.

To apply the Taguchi method, three main cutting parameters are considered in three levels, as shown in Table 3.3. The axial depth of cut is changed in this cutting model. Accordingly, its value is constant in each set of milling processes designed by the Taguchi method. Using Taguchi, the cutting trials are designed in a way that is shown in Table 3.4. This set of experiments can be similarly designed for each cutting tool.

Table 3.3: Cutting parameters and levels for ball-nose milling process.

Cutting Parameters	**Level 1**	**Level 2**	**Level 3**
Spindle Speed (V_s)	1	2	3
Cutting Speed (V_c)	1	2	3
Radial depth of cut (a_e)	1	2	3

Table 3.4: Experimental design of ball-nose milling process based on the Taguchi method.

Test No.	V_s	V_c	a_e
1	1	1	1
2	1	2	2
3	1	3	3
4	2	1	3
5	2	2	1
6	2	3	2
7	3	1	2
8	3	2	3
9	3	3	1

3.5.4.2 End-milling Process

In the end-milling process design, spindle speed changes continuously. Accordingly, feed rate changes are based on the spindle speed. Using the Taguchi model, cutting parameters are designed as shown in Table 3.5.

Table 3.5: Experimental design of end-milling process.

Cutting Parameters	Trial 1	Trial 2	Trial 3
Spindle Speed (V_s)	V_{s1} *to* V_{s2}	V_{s1} *to* V_{s2}	V_{s1} *to* V_{s2}
Cutting Speed (V_c)	V_{c1} *to* V_{c2}	V_{c1} *to* V_{c2}	V_{c1} *to* V_{c2}
Axial depth of cut (a_p)	*Constant*	*Constant*	*Constant*
Radial depth of cut (a_e)	*0.25D*	*0.5D*	*0.75D*

3.5.5 Accelerometer Sensor Location

The literature review demonstrates that acquired signals from different locations of milling machine have been analysed in order to investigate the occurrence of chatter. Chen J and Chen WL [162] located accelerometer on the milling table. Sekiya *et al.* [163] mounted an accelerometer below the spindle head. Matuszak *et al.* [164] fixed accelerometer on the machine body close to the spindle. However, none of these places can acquire the pure vibration between the cutting tool and workpiece.

Therefore to acquire the vibration between the cutting tool and workpiece, only two locations can be considered suitable for mounting the accelerometer sensor, the spindle and the workpiece. However, the workpiece is mounted on the machine table which can transfer vibrations to the sensor. There is a high level of risk at this location, because the sensor may break down during the milling process. Thus, the spindle is the most interesting place for sensor to be placed in order to achieve high quality vibration signal from the milling operation (Figure 3.13).

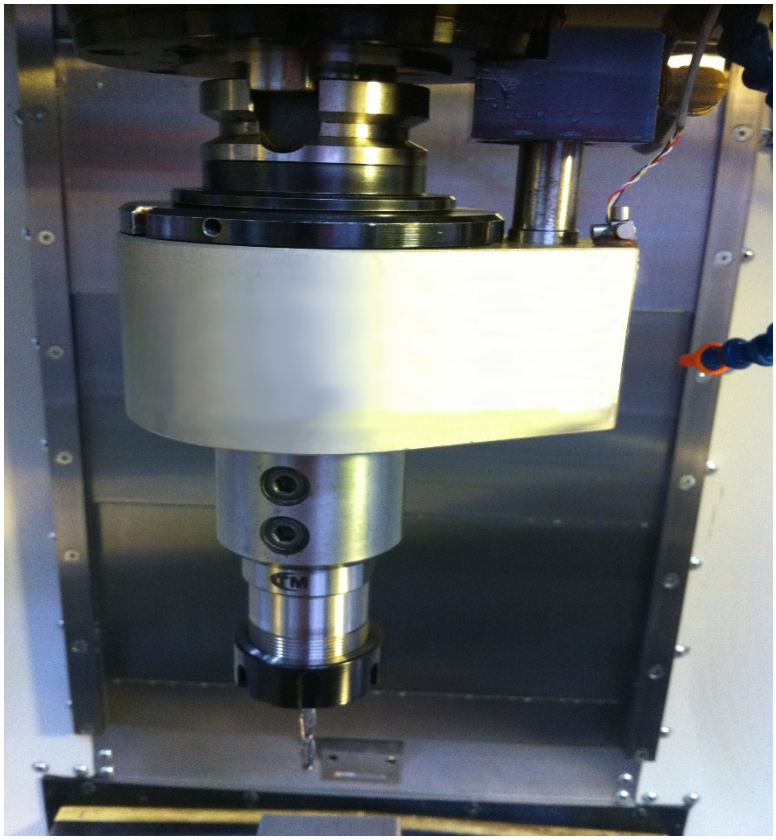

Figure 3.13: The mounted accelerometer on the spindle.

As spindle rotates during the milling process, the sensor cannot be directly mounted on the spindle. To solve this issue, the cutting tool can be located on an adaptor, which is installed on the spindle (Figure 3.14). The body of adaptor is the closest place to the cutting tool.

For this purpose during the milling process, a BT45 rotary coolant adaptor tool holder manufactured by Kennametal Co. is used (Figure 3.14). The accelerometer is mounted on its body to acquire vibrations directly from the milling process.

Figure 3.14: A Kennametal rotary coolant adaptor installed on the spindle.

3.6 Conclusion

Three parameters are used to measure the vibration between the cutting tool and workpiece. In this chapter, the advantages of acceleration in compared with the other measurable parameters, velocity and distance, is discussed.

Two cutting path models, ball-nose and end-mill cutting paths, are designed in order to have stable condition at the beginning of the milling process, and then to continuously moves into the chatter condition. Furthermore, cutting parameters are designed by using the Taguchi method. The most appropriate devices are chosen in order to record high quality signals during the milling trials. The devices are introduced, as well.

To acquire high quality vibration between cutting tool and workpiece, the place of accelerometer is important. Spindle was determined as the most suitable location for placing sensor. For this purpose, an adaptor is supplied to mount sensor on its body, as sensor cannot be placed directly on the rotating spindle.

In the next chapter, the methodology of the proposed chatter detection method will be discussed in details. The method can then be verified by analysing the acquired acceleration signals from the milling trials.

Chapter 4

The Application of Phase Space Attractor in Determining Chatter Occurrence

4.1 Introduction

The state of the art cited in the chapter 2 referenced the limitation of existing chatter detection methods in detection of chatter during cutting of metals, particularly on-line and in the production workshop. The early detection of chatter during cutting process is still an important research topic of industrial and academic interests in the manufacturing sector.

The milling process is a nonlinear and quasi-periodic motion. The state of the art research on the stability of such dynamic systems shows the chaos theory can predict the state of the system. As a part of this concept, phase space attractor demonstrates the state of system and is able to determine whether the dynamic system is in a stable state or it has moved into instability. Phase space has an incomparable attractor that represents each state of the system, which is normal cutting and chatter. Reconstruction of the phase space attractor and its cross sections in different moments of the milling process can then be shown as regular patterns which alter depending on the state of system.

In this chapter, the method of the signal-data-driven reconstruction of phase space will be discussed and illustrated. The phase space of milling processes is investigated by illustration of the cross sections of the phase space attractor as they change during time. The outline patterns are able to indicate the state of the milling process and hence be able to predict the stability of the process on-line and in the work shop environment.

4.2 Chaos Theory

In milling processes, chatter is a complex dynamic phenomenon of nonlinearity which involves different types of bifurcations. Hence, chatter is quasi-periodic and has chaotic behavior [85]. Initial models of chatter occurrence were previously described by use of a linear model. However, the stability analysis based on linear dynamics is not able to predict some phenomena in the milling process [165]. Thus

recently stability analysis and determination of chatter has been considered as a system with non-linear dynamic behaviour. Consequently, chatter occurrence can be considered as a nonlinear, quasi-periodic dynamic system with chaotic behavior.

Chaos theory works from the principle that small causes in a system might produce large effects in dynamic systems. The first scientist who established this principle was J.C. Maxwell [166]. He demonstrated that the collision between molecules of gas provides progressive amplification of small changes and yielded microscopic randomness. After Maxwell, several scientists such as H. Poincaré, B. Van der Pol, and etc. discovered similar phenomenon in different dynamic systems. However in 1962, E. Lorenz experimented with very small undesirable changes in the initial inputs of dynamic systems and modelled the system with two different initial conditions from one similar pattern [167]. He discovered that the end result of his model differed significantly from the original. Later on, others studying iterated maps with sensitive dependency on initial condition became popular, particularly by R. May's discussion in 1970's [166]. This phenomenon is known today as chaos theory [168]. Based on this theory, a small change in the initial conditions can drastically change the long-term behavior of a system.

Sensitivity to initial conditions is not the only pre-condition of a dynamic system to be chaotic. A chaotic dynamic system must also have two more conditions to be classified as a chaotic system. Chaotic dynamic systems usually evolve over time, thus any given region of their phase space will overlap with another region. This specification is known as topologically mixing [169]. In these systems an infinite number of unstable periodic orbits are embedded in the underlying chaotic set [170]. Dynamic systems that are topologically mixing with a high density of unstable periodic orbits are not necessarily sensitive to initial conditions [171]. So, they might not be a chaotic system.

Chaos is translated as the science of finding underlying order in apparently random data, which helps to predict the state of dynamic systems. Even though, complexity and irregularity are always identical with unpredictability [172]. Consequently, chaotic behavior has been detected in several natural systems or in the laboratory, such systems as electrical circuits, lasers, oscillating chemical reactions, fluid

dynamics, mechanical and magneto-mechanical devices, and also computer models of chaotic processes. Chaotic behavior can be explained through analyzing chaotic mathematical models or through analytical techniques such as recurrence plots, phase space plots, and Poincaré maps [173].

Three specifications of a chaotic dynamic system was introduced above. However, it is necessary to determine a method to define whether these conditions occur in the dynamic system and if it is chaotic. Several mathematical solutions have been proposed in order to define chaos, however the most common ones are computation of fractal dimensions and Lyapunov Exponents [174].

In a dynamic system with chaotic behaviour, the trajectories are exhibited in the phase space of the system. These trajectories converge to strange attractors. The fractal dimension of these strange attractors gives the effective number of degrees of freedom in the system, and also quantifies the complexity of the system that explains the chaotic behaviour of dynamic system [175]. For a chaotic dynamic system, the fractal dimension is a non-integer [176].

The computation of the Lyapunov Exponent is also a reliable solution to determine whether a dynamic system is chaotic. In a chaotic dynamic system, sample points in the neighbourhood of a trajectory converge toward the same orbit, which causes the attractor to change to a fixed point or a limit cycle. Hence in a chaotic system with strange attractors, every pairs of trajectories that are close to each other will move far away and exponentially from each other during time [177]. Lyapunov's Exponent explains the sensitivity to initial condition of the chaotic dynamic system. This phenomenon is described by the Equation 4.1.

$$\left\|\delta.x_{(t)}\right\| \approx e^{\lambda t}\|\delta.x_0\| \tag{4.1}$$

In the above equation λ is Lyapunov's exponent, the mean rate of separation of trajectories of the chaotic system. A positive value of λ indicates the sensitivity to initial condition in the system, or if the dynamic system is chaotic. For practical applications, it is most important to know the largest Lyapunov exponent. If the

largest value in the spectrum of Lyapunov exponents is positive, it means that the system is chaotic [178].

4.3 Phase Space

Phase space, also known as state space, is categorized as partly physics and mathematical. Phase space was introduced first by French mathematician Joseph Liouville in 1838 [179]. However, the first explicit use of the term "phase-space" were initiated by Arthur Rosenthal and Michel Plancheral in two separate papers [180]. Phase space was introduced as a tool to investigate the state of deterministic dynamic systems and detect whether a system is chaotic [181]. Besides the simple nature of phase space, it can provide an overview of all possible trajectories of a dynamic system. Hence by using phase space, time can be eliminated from the dynamics of a system, which has the benefit of reducing the number of trajectories to static curves [167].

Based on classical mechanics, phase space is an *n*-dimensional space, which can be demonstrated in the form of Equation (4.2), which all states of a system exhibit. In this space, each axis represents one parameter of the dynamic system. Axes can also belong to the degrees of freedom [182].

$$R_{(t)} = \left|r_{1(t)}, r_{2(t)}, \dots, r_{n(t)}\right| \tag{4.2}$$

Where:

t is the index for time series and $R_{(t)}$ is the state function of *n*-dimensional phase space. As an example, one single particle moving in only one direction has a two-dimensional Phase space, which is called a phase plane. Phase plane displays a relationship between variables; position ($r_{1(t)}$) and momentum ($r_{2(t)}$), during movement of the particle. Both variables have a role in determining the future behaviour of the system [182].

Considering a dynamic system with *n* degrees of freedom (or *n* parameters), each instantaneous dynamic state of a system with respect to the time is exhibited by a point in its corresponding *n*-dimensional phase space. The result of linking these points up to each other is a geometric shape, which is recognized as a phase space attractor of the dynamic system. A phase space attractor does not change while the state of the system does not change. Any change in the state of system leads to a change in the geometric shape of the attractor. The attractor acts as an abstract representation of the underlying dynamic system [183-185].

4.3.1 Application of Phase Space Attractor in Dynamic Systems

Based on the above rule, researchers have used phase space attractors to determine the transition of dynamic systems from a stable state. In engineering systems, the complexity and influence have been increased, which create potential counterintuitive and catastrophic accidents. Owens [186] illustrated the number of phase space attractors required in order to evaluate these dynamic systems. Besides this research, phase space has been used in different applications such as medicine, mathematics, computer science, and etc. Ayala *et al.* [181] analysed the mechanical vibrations through speckle interferometry by using phase space. Accurate classification of arrhythmias is a crucial task for cardiologists. Therefore, Roopaei *et al.* [187] suggested chaotic based reconstructed phase space features for detecting Ventricular Fibrillation (a kind of arrhythmias). Xia *et al.* [188] determined the corrosion types from electrochemical noise. They used phase space reconstruction theory. Sethi and Roy-Chowdhury [182] built a Multi-resolution phase space descriptor, to represent complex activities in multiple domains directly from tracks without having different heuristics.

4.4 Phase Space Reconstruction

In a dynamic system, a phase space attractor illustrates the variation of the system. If a time series describes a dynamic system, then a phase space attractor can be

used to predict the state of time series by having defined a segment of phase space [179]. However, part of the dynamic system information is sometimes lost while a phase space attractor is being illustrated. To retrieve the information, the phase space has to be reconstructed.

The basic concept of phase space reconstruction results from the fact that any observed data from a dynamic system contains all the information of unobserved state variables of data which can be recovered from time delayed copies and used to predict the present state [189]. In the other word, the state of a system is specified at time *t* by embedded dimension and time delay data [190].

The phase space can be reconstructed by re-writing the equation of the dynamic system as a system of differential equations that are first-order in time and by introducing new variables at embedded times. Considering phase space $R_{(t)}$ (Equation (4.2)), a nonlinear function $F(R_{(t)})$, can be used to explain the transition of R(t) in time, as well as determining the value of system at t-τ (where τ is time delay), as shown in Equation (4.3).

$$R_{(t)} \rightarrow F\left(R_{(t)}\right) = R_{(t-\tau)} \tag{4.3}$$

The original variables at time *t* and new variables at time t-τ form a vector in the phase space. The solution becomes a curve in the phase space which is parameterized by time [167]. This method is known as the time delay embedding theory that is introduced by Takens [191]. This theory is commonly practiced in various studies to reconstruct phase space attractors in a multi-dimensional phase space [149, 191, 192].

Time delay embedding theory is also applicable in time series. By applying time delay embedding theory, then time series are converted to state vectors. To convert time series into the state vector, an attractor related to the logged time series $x_{(t)}$ (Equation (4.4)) must be reconstructed by plotting delayed coordinate vectors [190]. $P(t)$ (Equation (4.5)) demonstrates the delayed coordinate vectors that can be plotted in a multi-dimensional orthogonal coordinate.

$$x_{(t)} = \{x_1, x_2, x_3, \dots, x_t\} \quad (4.4)$$

$$P_{(t)} = \{x_{(t)}, x_{(t-\tau)}, x_{(t-2\tau)}, \cdots, x_{(t-(m-1)\tau)}\} \quad (4.5)$$

Where:

m is embedding dimension, and τ is the length of the delay.

4.4.1 Embedding Dimension

In Taken's theorem, the embedding dimension is sufficient to recover the object without distorting any of its topological properties. Based on the theorem, if m is large enough, the reconstructed attractors have similar mathematical properties as the original system and provides an image similar to the original system [191].

Many methods are proposed to determine the embedding dimension. Based on Shang et. al, [193] the optimal embedding dimension of m can be estimated by the nearest false neighbours in the phase space. Based on this method, by moving from embedding dimension m_0 to m_{0+1}, the number of false neighbours is equal to zero for the point in the phase space of dimension m_{0+1}. Hence for the same point in the phase space with embedding dimension m_0, the number of false neighbours is not equal to zero.

4.4.2 Time Delay

Many methods such as mutual information, autocorrelation, approximate period, and etc. are used to define time delay [194, 195]. However, the autocorrelation function is used by many researchers such as [28] and [196] to determine time delay in reconstruction of phase space attractors, as well as state vectors. The first zero-crossing of the autocorrelation function (Equation (4.6)) is normally considered as the time delay. It is the most appropriate time delay because $x_{(t-\tau)}$ is completely de-correlated from $x_{(t)}$ at this time [197]. Autocorrelation function is computationally efficient and works well with noisy data in determination of the time delay.

$$C_{(k)} = \frac{\sum_{i=1}^{n}\sum_{q=0}^{n-1}(X_i-\bar{X})(X_{i+q}-\bar{X})}{\sum_{i=1}^{n}(X_i-\bar{X})^2} \quad (4.6)$$

Where: q is the delay in the number of samples for time series $x_{(t)}$.

4.5 Poincaré Section

In nonlinear dynamic systems with many parameters, the illustration of phase space attractors is usually complex and difficult. So instead of plotting the phase space attractor, a similar image can be generated by using each pair of vectors of the reconstructed state vector $P_{(t)}$ (Equation (4.5)). It provides one cross section of the phase space attractor, which is also known as the Poincaré section. To plot phase space attractor Poincaré section, the vector $x_{(t-(m-1)\tau)}$ must be plotted versus vector $x_{(t)}$ in an orthogonal coordinate [183]. This concept has been used in many studies which apply to different dynamic systems and help define the stability of the system.

4.5.1 The Poincaré Section Deviation during Milling

Considering the use of time series $x_{(t)}$, the acquired vibration between the cutting tool and workpiece, can be obtained by dividing phase space into equal intervals, from which phase-space attractor Poincaré sections are extracted from the attractor. These Poincaré sections demonstrate the shape of phase space attractor at each time interval. The variation between Poincaré sections expresses the variation in the shape of phase-space attractor in a series of 2D representations. The variation can be used to trace the transition of system from a stable state to an unstable state.

A typical signal acquired during the cutting process is demonstrated in Figure 4.1 (a). This signal is divided into equal time intervals with overlapping sections. The overlapping section maintains consistency and continuity. To describe the attractor variation during the milling process, the corresponding Poincaré section for each time segment is plotted. For this purpose and from Equation (4.5), the

Poincaré section at time segment i can be illustrated by plotting vector $x_{i(t-(m-1)\tau)}$ versus vector $x_{i(t)}$ in an orthogonal coordinate, as shown in Figure 4.1 (b) to (d).

In dynamic systems such as milling processes, the embedding dimension m is always more than 2, so it is not necessary to estimate the value of m at this stage. The cross section of the phase space attractor, which is plotted by $x_{i(t-\tau)}$ and $x_{i(t)}$, can be used to investigate the behaviour of the phase space attractor in time segment i. Similarly, the Poincaré section can be plotted for all time segments.

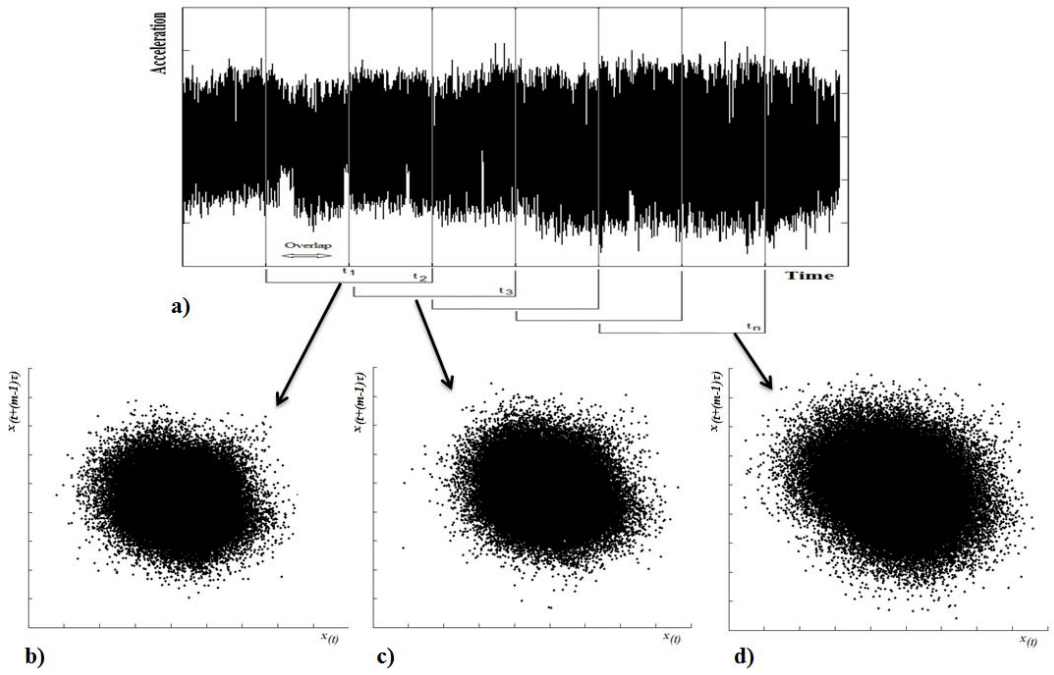

Figure 4.1: (a) Acceleration signal acquired along milling process. (b). Poincaré sections in time interval t_1. (c) Poincaré sections in time interval t_3. (d) Poincaré sections in time interval t_n.

The experimental evidence is demonstrated to exhibit the above theory, and hence display the difference in the phase space attractor Poincaré section in stable milling process and unstable or the chatter condition. For this purpose, two sets of data are acquired during the milling process, one stable process and one unstable process, have been chosen in order to plot the corresponding phase

space attractor Poincaré sections during the entire process. The variation in the shape of attractors has been applied for both stable and unstable milling process.

4.5.1.1 Chatter Condition

A milling trial was run at cutting speed of *4000 rpm* to cut a slot with *25%* immersion rate. The axial depth of cut changed continuously from *0* to *2 mm*; hence, the radial depth of cut is *1.5 mm*. A tri-axial accelerometer was located on spindle speed to acquire vibration between workpiece and cutting tool. The signal along cutting feed (*X* axis) is demonstrated in Figure 4.2. Chatter was detected at 9 s after running the process. Therefore, the onset of chatter is observed in the 4th time interval. The unstable condition is continuously extended until the end of process. The acquired signal is divided into the equal time segments, with overlap.

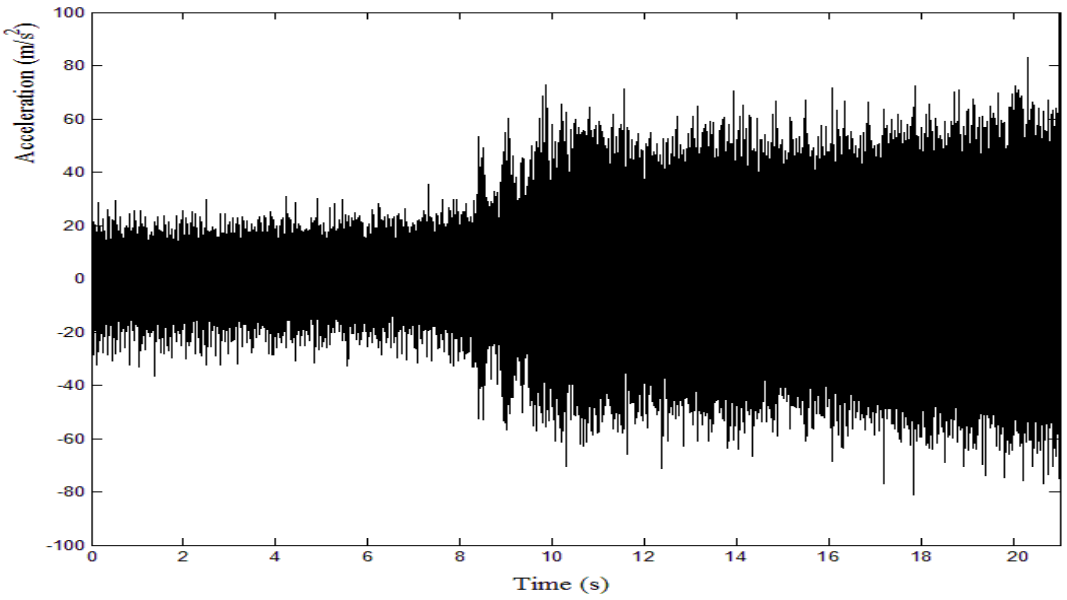

Figure 4.2: Acceleration acquired during cutting of titanium. Spindle speed: *4000 rpm*, Cutting speed: *320mm/min*, a_p: *0-2 mm*, a_e: *1.5 mm*.

To plot the Poincaré section, $x_{i(t)}$ and $x_{i(t-\tau)}$ are the considered vectors in the form of time series at time segment *i*, as shown in Equations (4.7) and (4.8).

$$x_{i(t)} = \{x_1, x_2, x_3, \dots, x_n\} \tag{4.7}$$

$$x_{i(t-\tau)} = \{x_{1-\tau}, x_{2-\tau}, x_{3-\tau}, \dots, x_{n-\tau}\} \qquad n \geq \tau \tag{4.8}$$

The Poincaré section of phase space attractor is formed by n-τ ordered pairs (x_l, $x_{l-\tau}$) (where l is an integer and $1 \leq l\text{-}n \leq n$), as shown in Figure 4.3.

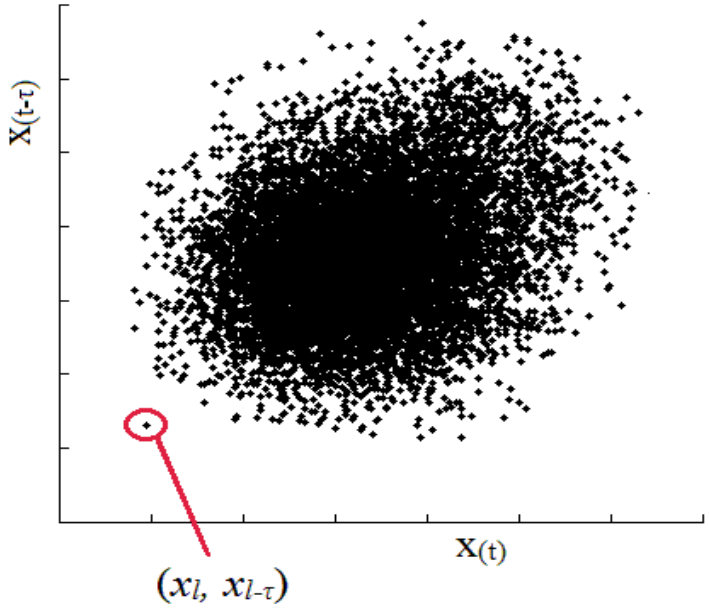

Figure 4.3: A typical Poincaré section at time segment *i*.

Corresponding Poincaré sections for every time interval are shown in Figure 4.4 for the milling trial. The illuminated phase space attractors obtained during the milling process has a circular shape. It does not have noticeable fluctuation while the system is stable (first three Poincaré sections). As soon as cutting process transfers to unstable state (from the 4th section), the phase space attractor does change size significantly. The attractor grows up to nine times larger than the attractor at stable state during the cutting trial.

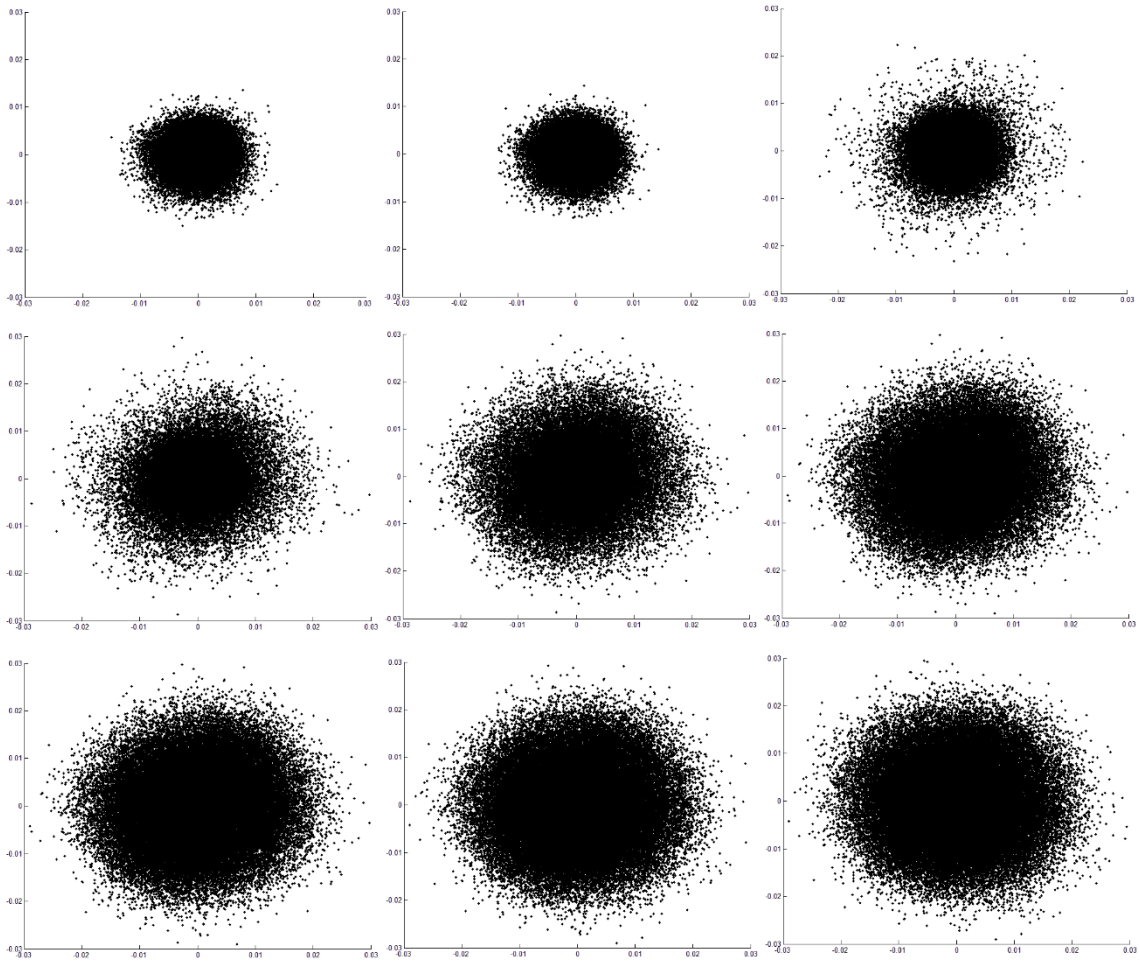

Figure 4.4: Phase space attractor variation during unstable cutting process.

4.5.1.2 Stable Condition

A stable milling process was tried and vibration between workpiece and cutting tool was acquired in the form of a time series. The milling trial was run with a cutting speed of *3500 rpm* to cut a slot with *50%* immersion rate. Similar to the previous trial, axial depth of cut changed continuously from *0* to *2 mm*; hence, radial depth of cut is *3 mm*. The acquired signal is demonstrated in Figure 4.5. This cutting process was run reasonably stable and chatter was not occurred during the process.

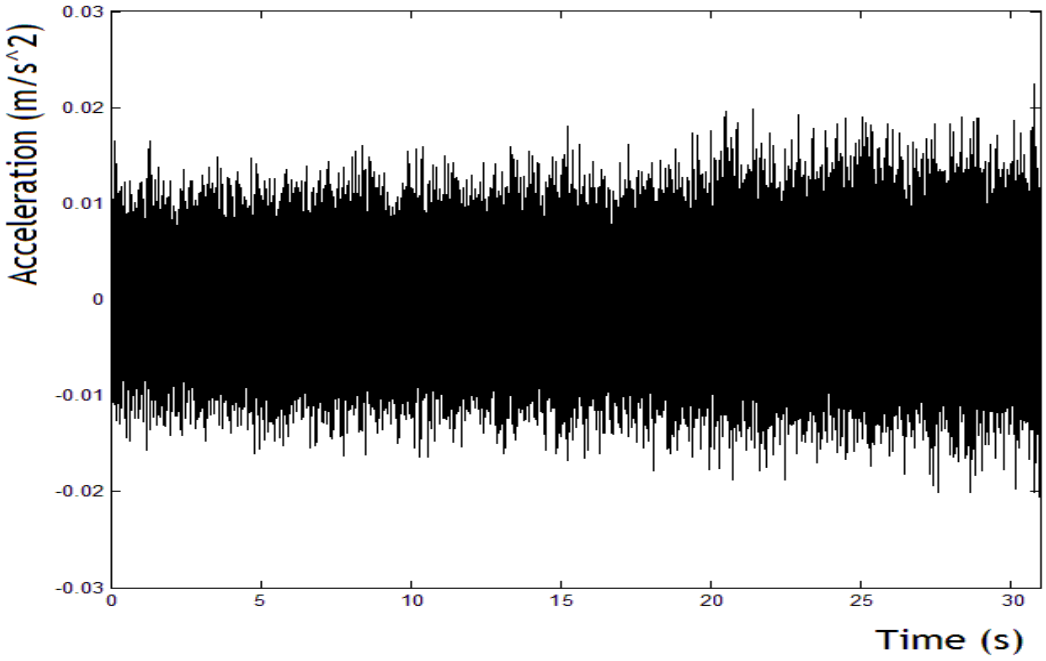

Figure 4.5: Acquired signal during milling trial; Spindle speed: *3500 rpm*, Cutting speed: *280 mm/min*, a_p: *0-2 mm*, a_e: *3 mm*.

Similar to the previous section, acquired signal was divided into the equal time intervals with overlap; hence it was reconstructed in the form of a state vector. The corresponding Poincaré sections are plotted for every time segment, as it was done for unstable milling trial in the previous section.

Corresponding Poincaré sections for each time interval are shown in Figure 4.6. As shown, phase space attractor is still a circular shape, similar to the attractor in the previous unstable trial. However, the shape does not change size significantly along the milling process. Hence, the size of attractor is almost constant and it has not grown up during the process.

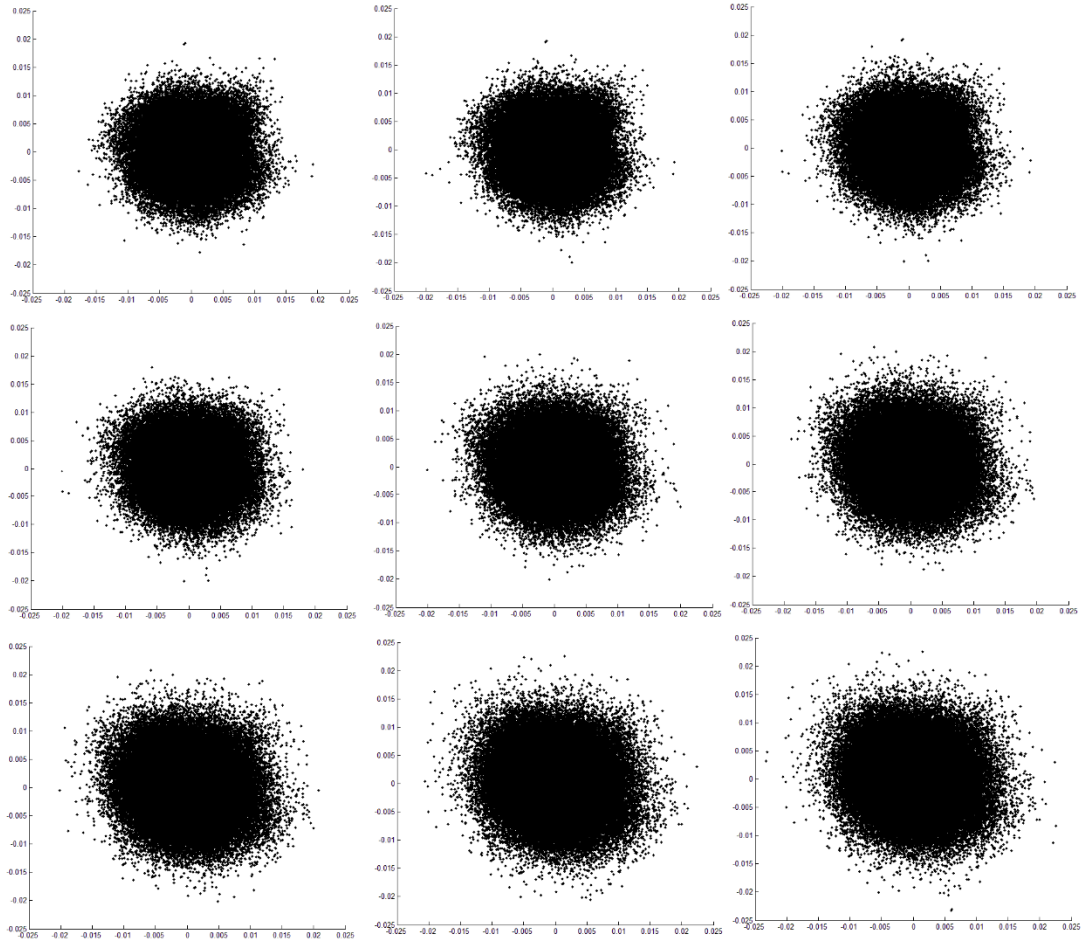

Figure 4.6: Phase space attractor variation during stable cutting process.

4.6 Discussion

When the cutting system chatters, it becomes nonlinear and should be analyzed as a quasi-periodic dynamical system that potentially has chaotic behavior. Consequently, chaos theory is introduced in this chapter to understand the changes in the cutting process and to form the basic theory for designing a method to detect chatter, both online and during the milling process.

This chapter illustrates with some preliminary laboratory investigations that phase space attractors demonstrate the state of dynamical system in time. Variations in the shape and size of attractor (which has been created from time signals captured in

experiments) represent a variation in the state of the system. The preliminary investigation on two stable and unstable signals indicates the variation that can occur in phase space attractor Poincaré sections along the milling process can also indicate the transition of milling process from stable state to the chatter condition.

To visualize the implications of the signals on the recognition of chatter and trying to look for clues that indicate chatter threshold, the time domain signals should be divided into the equal intervals with overlap and reconstructed in the form of state vectors. The outline phase space attractor Poincaré sections corresponding to the intervals are developed as shown in this chapter and provide some visual hints of the onset of chatter in the cutting process. Accordingly, the measurement of deviation in the phase space attractor along the process should be able to provide an indication of the boundary for chatter threshold. To use the deviation of phase space attractor during the milling process, a computational technique is required to parameterize the deviation of attractor so that the method can be executed automatically online.

Chapter 5

Image Correlation

5.1 Introduction

It has been established that chatter is considered to be a type of chaotic behaviour. Understanding chaotic behavior can be done through analysis of a mathematical model, or through analytical techniques such as recurrence plots and phase space plots. The evolution of a dynamic system is often described in its phase space attractor, which coordinates all the variables that enter the mathematical formulation of the system. The variation in the shape of the phase space attractor can demonstrate variation in the state of the dynamic system. Consequently, the transition of milling process from stable cutting to chatter condition can be indicated by investigation of the deviation in the shape of the phase space attractor.

In this chapter, the possibility of using image correlation to indicate the variation of the phase space attractor is investigated. In chapter 4, a scientific study on the application of phase space attractor as representing the state of dynamical systems was introduced. The milling process is regarded as one such non-linear dynamic system. The phase space attractor for the system of the milling process was reconstructed using acquired vibration signals between the cutting tool and workpiece. The reconstructed phase space attractor is in the form of a state vector with an embedded time delay dimension. Poincaré section of the reconstructed state vector corresponds to a cross section of phase space attractor at a point in time. The variation in Poincaré sections during milling processes indicates the state and transition from one state to another of the system.

2D images are difficult to interpret by the production workshop floor. It is better to have a representative linear numerical indicator to show the variation of the 2D images over time. Furthermore, it is also desirable that the numerical indicator can be defined within the boundary between stable and unstable states. Image correlation is a powerful technique to interpret the variation of 2D images. This technique represents the variation between two or more 2D images by Pearson's coefficient.

5.2 Image Correlation

Image correlation is a form of image processing to compare photographs, contours, figures, etc. so that a set of parameters describing the image transformation can be evaluated.

A correlation coefficient is used in statistics to measure the degree of relationship between two variables [198]. A number is formed as the ratio between the products of the deviation of each of the two variables from their respective means, to the product of their variances. The similarity between the two sets of variables is presented by Pearson's coefficient, which was first developed by Pearson in 1895. Due to its simplicity, it is widely used in statistical analysis, pattern recognition, and relationship assessment. The Pearson's coefficient is also known as correlation coefficient. When this technique is applied to analyse an image, where the pixels of the image constitute the population of a variable, it is commonly known as image correlation.

5.2.1 Applications of Correlation Coefficients to Images

Image correlation refers to a class of non-contact methods that acquire images of an object and perform image analysis to extract full-field shapes, deformation and/or motion measurements. Image processing has been performed with many types of object-based patterns, including lines, grids, dots and random arrays. One of the most commonly used approaches employs random patterns and compares sub-regions throughout the image to obtain a full-field of measurements. Image correlation is recognised as a superior method for measuring motion, deformation, and any variation in the image [199]. It has become popular and powerful during the last few decades as it is fast and it is easy to access the required hardware [200].

Image processing is combined with the correlation coefficient technique to provide general parameters which indicate the similarity of the patterns. Greenhalgh et al [201] presented an improved pixel by pixel analysis based on

Pearson's coefficient over the entire area of two images. The result revealed both nonlinear signals as well as highlighting the structures that are generated by only one of the nonlinear signals. In an application used by autonomous robots, Pearson's correlation coefficient was used to select regions of interest in consecutive frames [21]. The autonomous system demonstrated the ability of obstacle avoidance by vehicles in an experimental environment.

An image is characterised by numerical values in each pixel of the image. The pixels are represented as a sequence of numbers $\{X_i\}$. When two images are available (second image is represented by $\{Y_i\}$), the Pearson's coefficient can be computed by Equation (5.1):

$$r = \frac{\sum_{i=1}^{n}(X_i - X_m).(Y_i - Y_m)}{\sqrt{\sum_{i=1}^{n}(X_i - X_m)^2}.\sqrt{\sum_{i=1}^{n}(Y_i - Y_m)^2}} \tag{5.1}$$

Where:

X_i is the intensity of the i^{th} pixel in the reference image,

Y_i is the intensity of the i^{th} pixel in the second image, and

X_m and Y_m are the mean intensity of the images.

Pearson's Coefficient measures the linear dependency between two patterns or variables [202]. It condenses the comparison of two 2D images to a single scalar quantity. Hence, the Pearson coefficient is invariant to linear transformations of {X} or {Y} [203].

The value of Pearson's coefficient varies between ± 1. If the similarity between patterns is high, the value of r is close to $+1$. At the extreme, if the images are identical, $\{X_i\} = \{Y_i\}$, the Pearson's coefficient is:

$$r_{identical} = \frac{\sum_{i=1}^{n}(X_i - X_m).(Y_i - Y_m)}{\sqrt{\sum_{i=1}^{n}(X_i - X_m)^2}.\sqrt{\sum_{i=1}^{n}(Y_i - Y_m)^2}} = 1 \tag{5.2}$$

On the other hand, negative correlation indicates opposite behaviour among the variables [204]. At the extreme, if the images are directly opposite (inverse), $\{X_i\} = \{-Y_i\}$, the Pearson's coefficient is:

$$r_{inverse} = \frac{\sum_{i=1}^{n}(X_i - X_m).(Y_i - Y_m)}{\sqrt{\sum_{i=1}^{n}(X_i - X_m)^2}.\sqrt{\sum_{i=1}^{n}(Y_i - Y_m)^2}} = -1 \quad (5.3)$$

5.2.2 Image Correlation Applied to Phase Space Recognition

The basic principle of applying the image correlation technique to phase space attractors is tracking the corresponding pixels in two images (patterns). Figure 5.1 shows two images that have some minor complimentary differences. The first image, which is the reference image, is the image of a system in a recognized condition. The next image can be any image that is required to compare with the reference image to define variation over time in the system. The patterns might be acquired during a mechanical test to define the variation in the mechanical and physical properties of the part, or from a medical test, or a security camera, and etc. The patterns can also be drawn from acquired time series via a sensor system. The similarity of two images in different time periods can be compared to define the amount of variation in the system. As shown schematically in Figure 5.1, the patterns are segmented and the corresponding pixels are compared with each other [205] on the basis that if one variable changes, the other correlated variable changes in a predictable way [206].

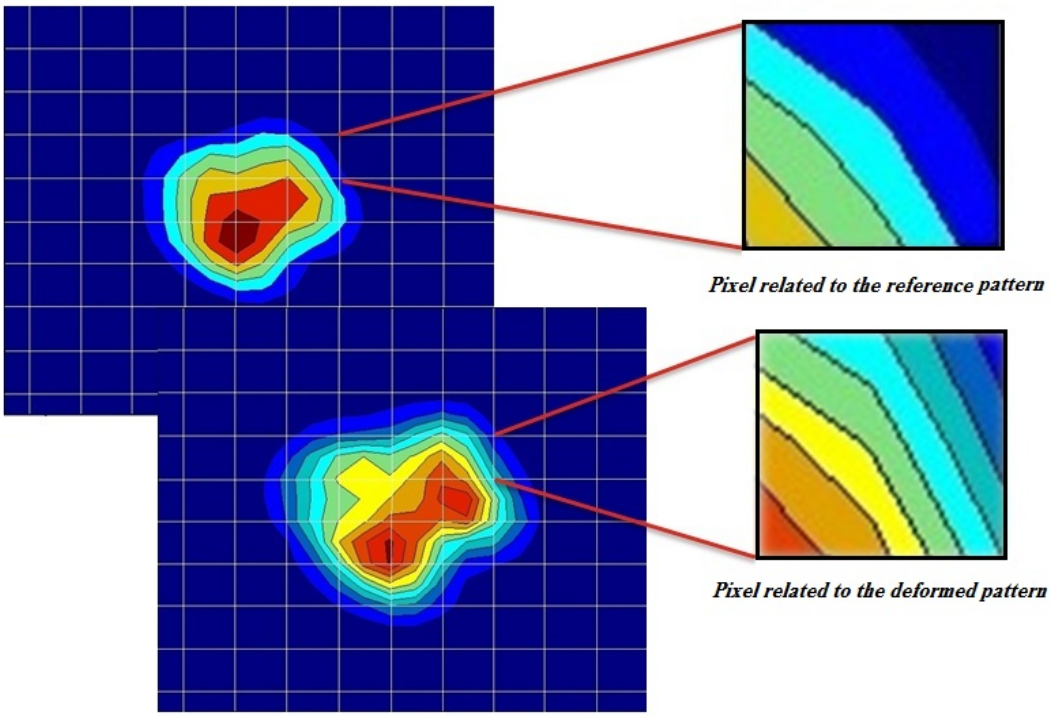

Figure 5.1: The relationship between two Poincaré sections of the phase space attractor

When a phase space attractor is cut to sections to be revealed as Poincaré sections, a series of images is formed. Obviously these images change over time because the sections are cut at different times of the phase space attractor. An image correlation method is required to detect sequential changes over the sampling time.

5.3 Methodology

The vibration between a cutting tool and a workpiece is acquired in the form of time series data. The acquired time series data can be reconstructed into state vectors by using a time delay embedding theorem. The Poincaré sections of reconstructed state vectors can then be plotted for every time segment by $x_{(t-j\tau)}$ versus $x_{(t)}$. Every value of j demonstrates one cross section of the phase space attractor in its j^{th} space dimension.

The image in Figure 5.2 (a) is the Poincaré section at time segment t_i, which is during the stable period of milling. Figure 5.2 (b) is Poincaré section at time segment t_{i+n} (n is an integer), which is an unknown state of milling process. The correlation (Pearson's) coefficient compares two patterns and represents the variation of phase space attractor from t_i to t_{i+n}. Extending this concept, during any milling period, when the state is unknown, can be correlated with the reference pattern. The change of Pearson's coefficient over time will indicate the state of the milling process, including the trend of the process moving into chatter. Pearson's coefficient then parameterizes the variation of the phase space attractor during the milling process.

Poincaré sections must be converted into an appropriate form in order to be used for image correlation analysis. Accordingly, Poincaré sections are plotted in the form of contours.

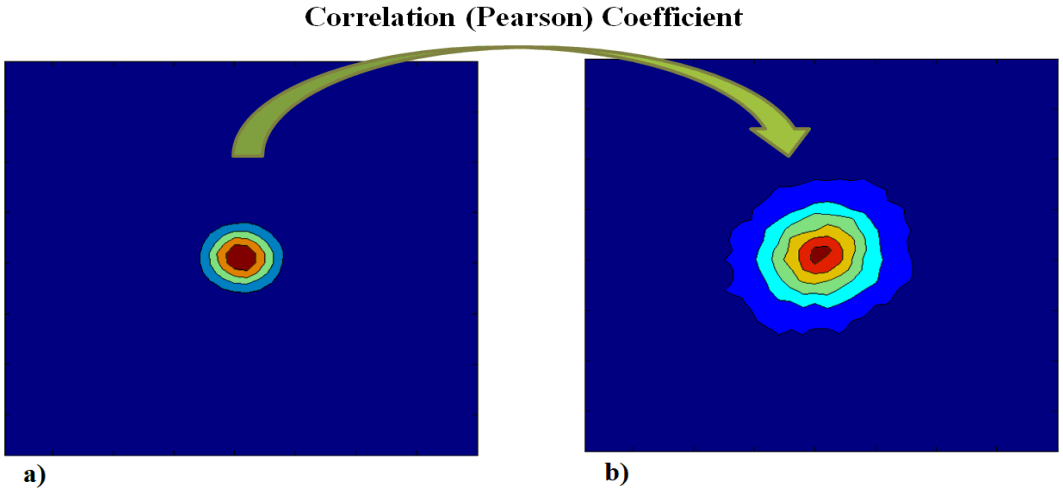

Figure 5.2: a) Poincaré section (Reference) at time t_i. b) Poincaré section at time t_{i+n}.

Effectively, Pearson's coefficient will change over time due to the sliding computation of Poincaré sections if the state of the system changes. At the early stage of the milling process, the system is in a stable condition. Hence, consecutive images, while the system is stable, will have very good correlation. The Pearson's

coefficient at the start of the image will be close to one, by reasoning of Equation (5.2). When chatter occurs, consecutive images will differ greatly. The Pearson's coefficient value will move away from one, i.e. the Pearson's coefficient will decrease from the initial value close to one as the system becomes unstable.

In each milling job, the operator will start the cutting process in a stable condition. Continuously the cutting parameters are changed in order to move to the chatter condition. Consequently, the first Poincaré section can play the role of reference pattern. The future Poincaré sections are compared with the reference pattern. The similarity between phase space attractor Poincaré sections can be parameterized by computation of Pearson's coefficient.

Let us represent the images at period j by $\{X_{ij}\}$ where i is the indexing within the variable $\boldsymbol{X_j}$ at image segment j. To determine if there are changes of the phase space attractor over time, the Poincaré sections are compared to the reference Poincaré section $\{X_{i1}\}$ by computing their Pearson's coefficient:

$$r_j = \frac{\sum_{i=1}^{n}(X_{ij}-X_{mj})(X_{i1}-X_{m1})}{\sqrt{\sum_{i=1}^{n}(X_{ij}-X_{mj})^2}.\sqrt{\sum_{i=1}^{n}(X_{i1}-X_{m1})^2}} \tag{5.4}$$

Where:

$\{X_{i1}\}$ is the image at time t_1.

From the nature of the milling process, the Pearson's coefficient will be reducing while the new Poincaré sections matching the reference section $\{X_{i1}\}$ deteriorate.

The question remains: what Pearson's coefficient value should be taken as the threshold value for stopping the process before chatter. An independent assessment of the onset of chatter in the signal structure is required.

5.4 Experimental Test

In order to test the idea of using Pearson's coefficient to detect changes, and to determine the value of Pearson's coefficient that indicates start of a chatter condition, an experiment has been set up and the data obtained will be analysed using Equation (5.4). This section describes how the acquired data is analysed to verify whether the theory is representative to detect the onset of chatter.

5.4.1 Cutting Parameters

For this purpose, a set of cutting trials have been run and vibration between the cutting tool and workpiece was acquired by an accelerometer. The experimental setup was explained in Chapter 3. Titanium has been cut with a *6 mm* ball-nose carbide cutter having four flutes. The cutting parameters are also expressed in Table 5.1. The radial depth of cut is various between *0.25D* to *0.75D*, which allows investigating the effect of loss of contact between cutting tool and workpiece in the result. The axial depth of cut is continuously changed from *0* to *2 mm* along the milled section.

Table 5.1: Cutting parameters.

Test No.	V_R *(rpm)*	F_m *(mm/min)*	f_z *(mm/tooth)*	a_p *(mm)*	a_e *(mm)*
1	3000	240	0.08	0-2	0.25 D
2	3000	240	0.08	0-2	0.50 D
3	3000	240	0.08	0-2	0.75 D
4	3500	280	0.08	0-2	0.25 D
5	3500	280	0.08	0-2	0.50 D
6	3500	280	0.08	0-2	0.75 D
7	4000	320	0.08	0-2	0.25 D
8	4000	320	0.08	0-2	0.50 D
9	4000	320	0.08	0-2	0.75 D

5.4.2 Observation of Chatter Condition

Chatter was detected during trial no. 7 (Table 5.1), so the acquired vibration between workpiece and cutting tool is chosen to analyse this trial. Firstly, the acquired vibration in the form of time series is divided into equal time segments, each *6 s* (11 time segments in total) with *4.5 s* overlap, as shown in Figure 5.3. The optimum length of time interval is determined based on total length of milled section and sample rate. Continuously and to reconstruct the time series state vector, the time delay is computed by calculating the first zero cross value of autocorrelation of the $x_{(t)}$. The value of time delay is then equal to 10.

As is obvious from acquired signal (Figure 5.3), a severe vibration signal occurs *9s* after starting milling. Inspection of the cutting surface after the process shows that this point is the onset of chatter during the operation. Therefore, the onset of chatter can be seen in the 4th time segment. The unstable condition continues until the end of milling.

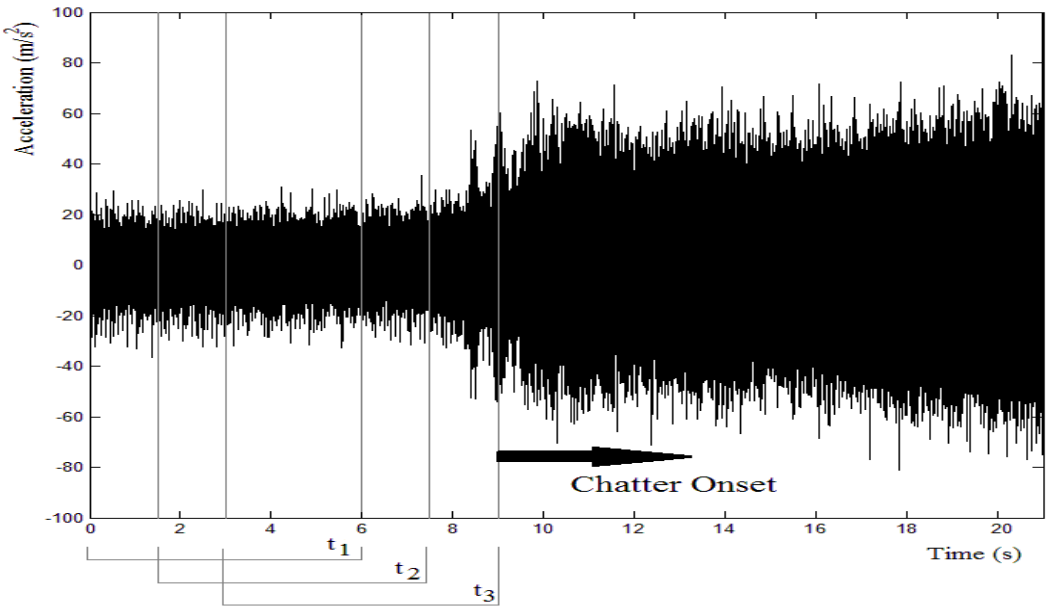

Figure 5.3: Acceleration acquired during cutting of titanium. Spindle speed: *4000 rpm*, Cutting speed: *320 mm/min*, a_p: *0-2 mm*, a_e: *1.5 mm* (*0.25D*).

5.4.3 Formation of Poincaré Sections

The Poincaré sections of Figure 5.3 data are plotted in Figure 5.4. As shown in Figure 5.4, the phase space attractor has a circular shape. It does not have any noticeable fluctuation while the system is stable. As soon as milling enters the unstable state, the attractor changes significantly.

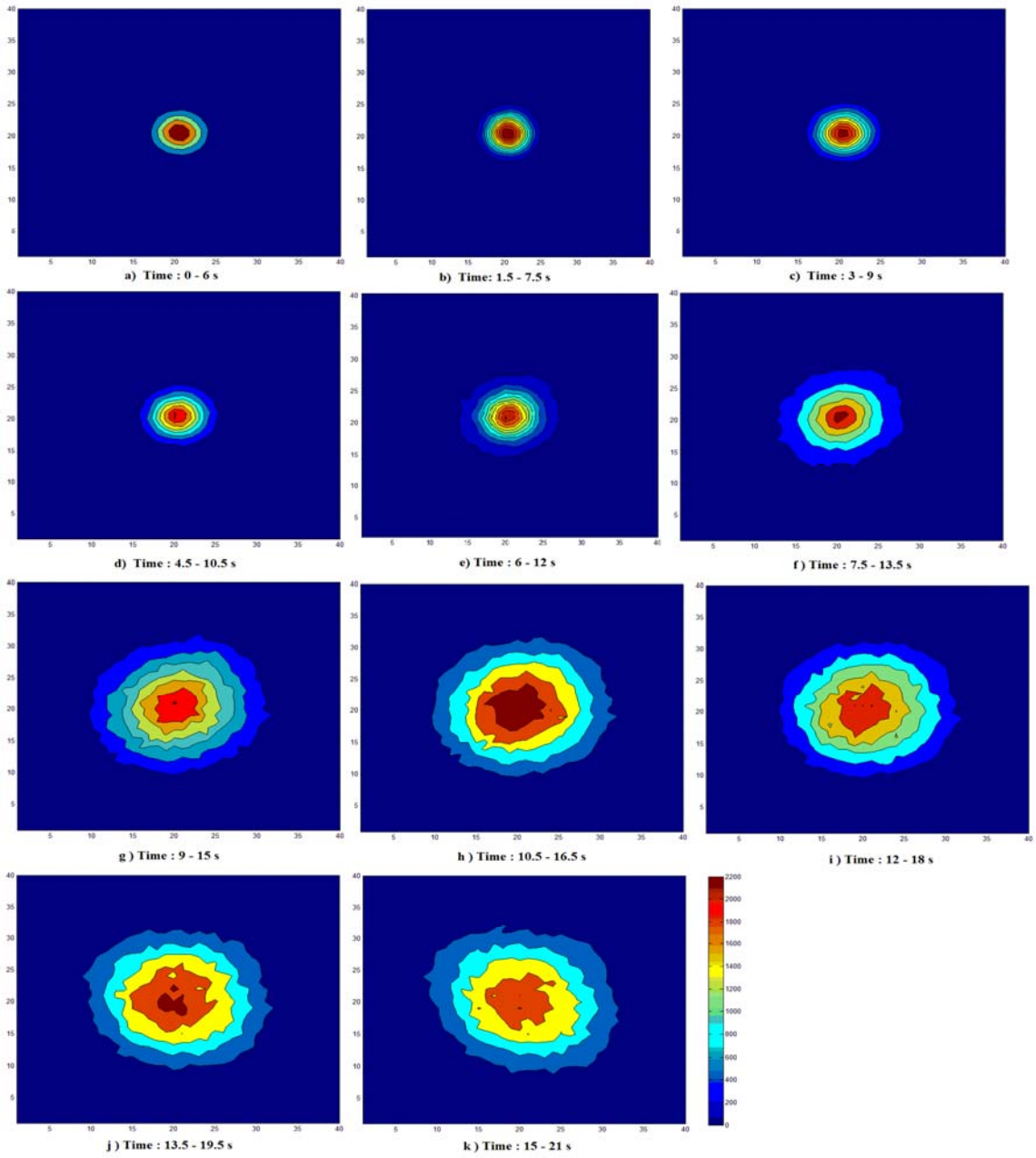

Figure 5.4: Poincaré sections along milling process. Spindle speed: *4000 rpm*, Cutting Speed: *320 mm/min*, a_p: *0-2 mm*, a_e: *1.5 mm* (*0.25D*).

5.4.4 Computation of Pearson's Coefficient

The Pearson's coefficient is computed. The correlation between the 1st Poincaré section and itself provides Pearson's coefficient equal to 1 (*100%* similarity). The Pearson's coefficient value between the phase space attractor pattern at time segment 2 and reference pattern is *0.999* (*99%*), when system runs stable to *0.52* (*52%*), chattering is happening. The result is demonstrated in Figure 5.5.

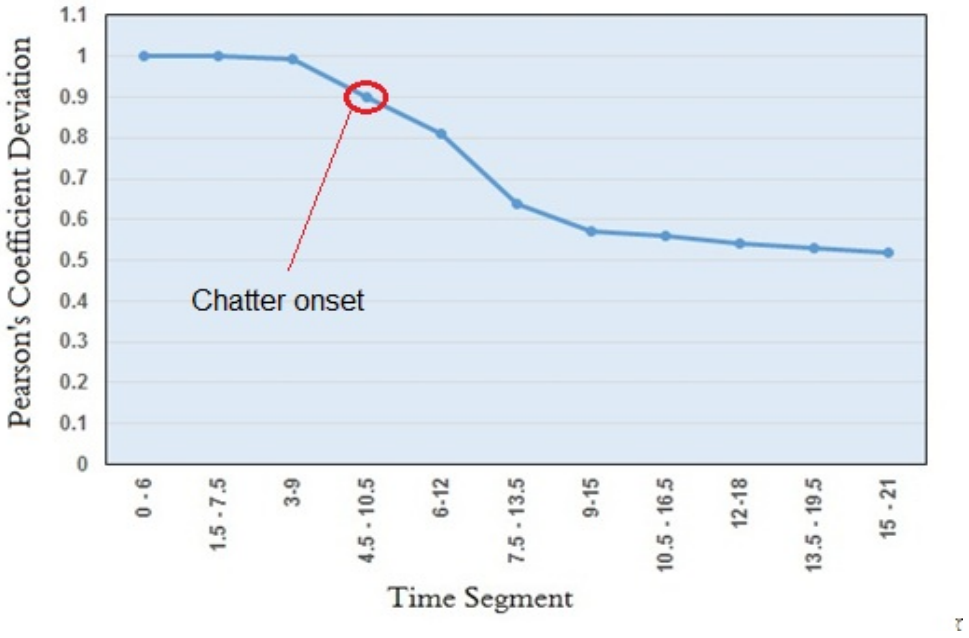

Figure 5.5: Pearson's coefficient deviation along trial no. 7. The deviation is suddenly indreased after time segment (*3-9 s*) due to the chatter occurrence. Chatter onsets at time segment (*4.5-10.5 s*).

5.4.5 Phase Space Attractor Variation during Stable Milling

Similar to trial no. 7, the vibration between workpiece and cutting tool was acquired during trial no. 5 in the form of a time series. Milling was reasonably stable and chatter was not occurring (Figure 5.6). It is obvious the system is stable from the acquired signal, as well as there are no chatter marks observed in the cutting surface.

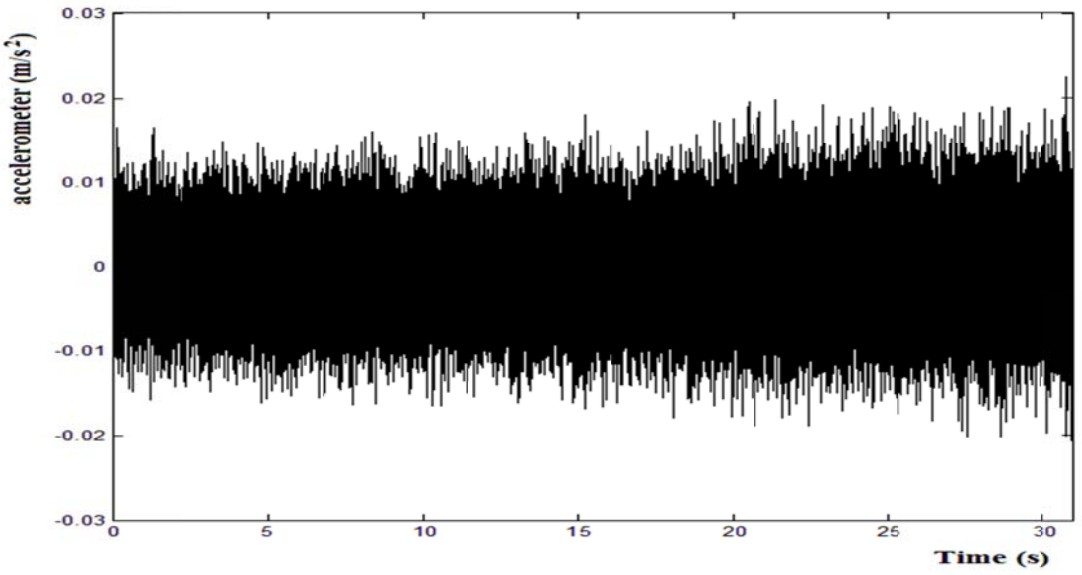

Figure 5.6: Acceleration acquired during cutting of titanium. Spindle speed: *3500 rpm*, Cutting Speed: *280 mm/min*, a_p: *0-2 mm*, a_e: *3 mm* (Trial No.5).

From the milling duration, the optimum length of time segments is determined and for the study test runs it is chosen to use *10 s* time segments (9 segments in total) with *7 s* overlap. The time series is reconstructed in the form of a state vector and the corresponding cross sections of the phase space attractor at $j=1$ is plotted for every time segment. For this study, the time delay is computed by calculating the first zero cross value of autocorrelation of the $x_{(t)}$. The value of time delay is then equal to 16, and the corresponding cross section of the reconstructed phase space attractor related to $x_{(t-16)}$ versus $x_{(t)}$ can be now plotted (Figure 5.7).

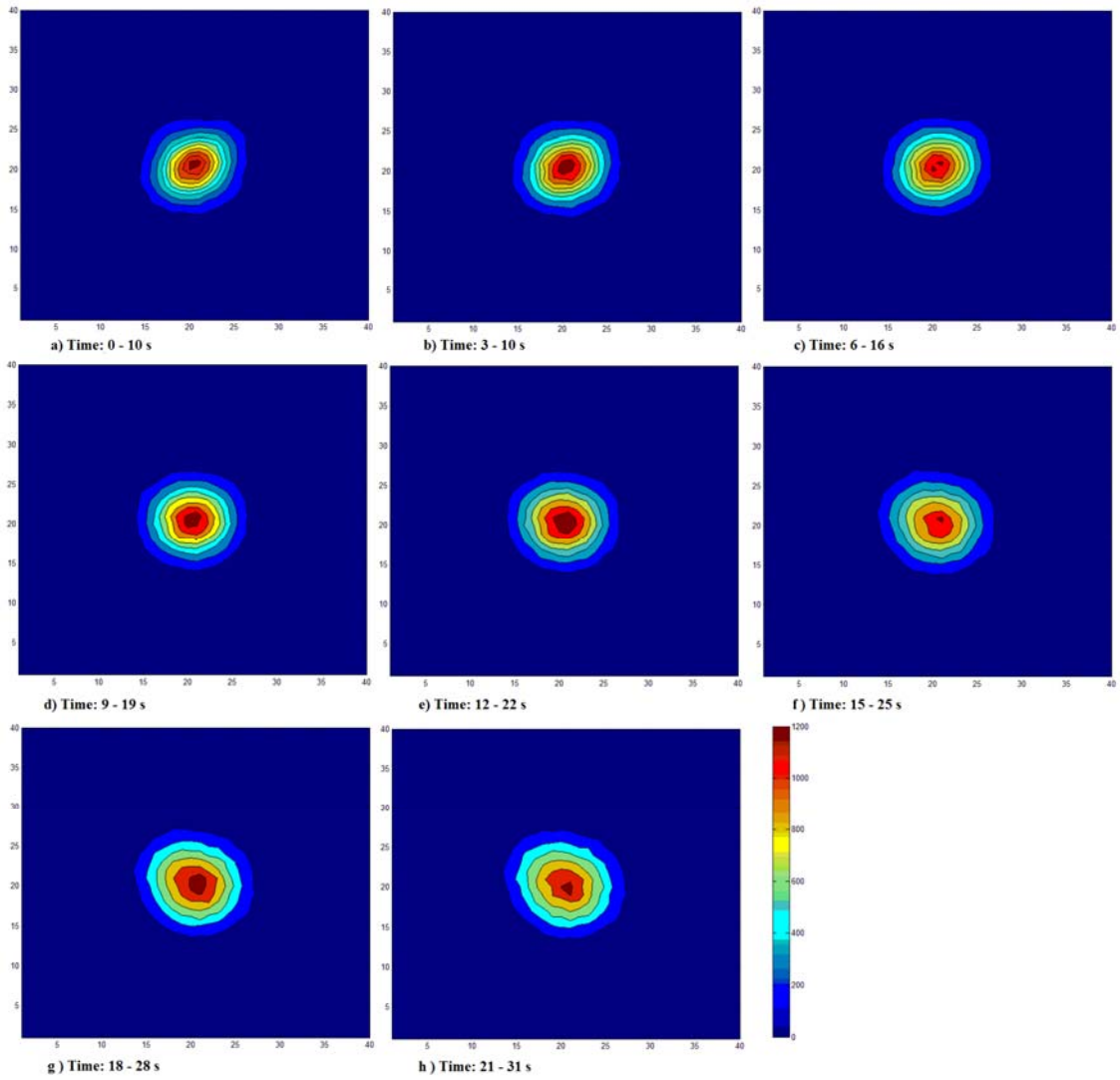

Figure 5.7: Poincaré sections along milling process. Spindle speed: *3500 rpm*, Cutting Speed: *280 mm/min*, a_p: *0-2 mm*, a_e: *3 mm*.

The Pearson's coefficient is computed between corresponding Poincaré sections representing each time segment and the reference Poincaré section (Time = *0 – 10* seconds). The Pearson's coefficient value between phase space attractor at time segment 2 and the reference pattern is *0.999* (*99%*). The coefficient only changes slightly over the test run, with the final value being *0.956* (*95.6%*) for the last Poincaré section. The results are plotted in Figure 5.8. The evaluation of the minimal change in Pearson's coefficient demonstrates that the milling run is stable.

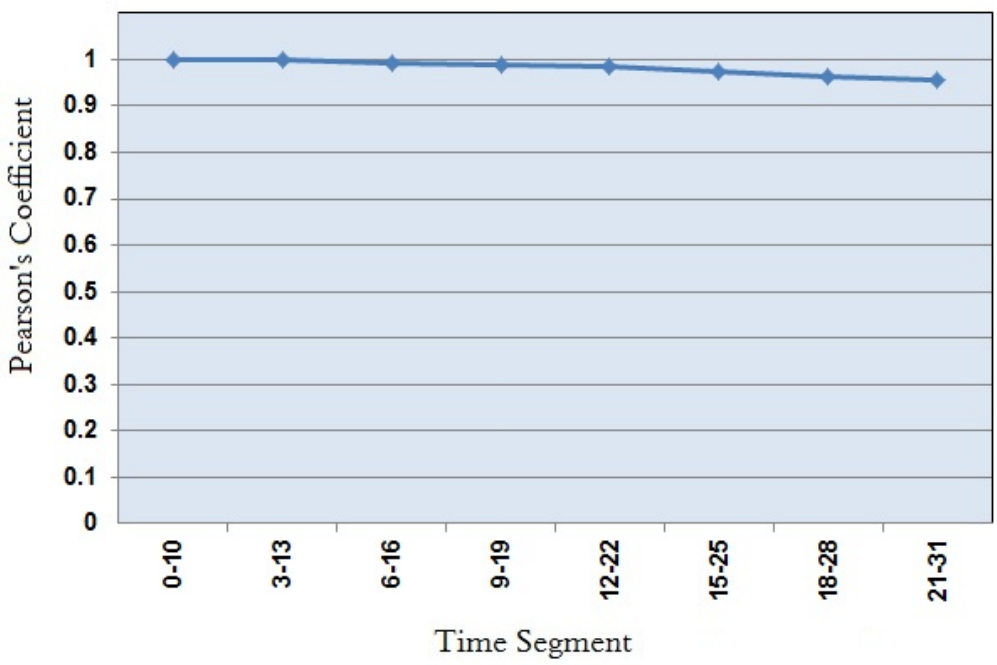

Figure 5.8: Pearson's coefficient deviation along trial no. 5. No sudden changes can be seen in the coefficient deviation. The trial has run stable.

5.5 Phase Space Attractor Evaluation in other Embedding Dimensions

In the last section, it was shown how the phase space attractor varies in its Poincaré section corresponding to $j=1$. However, it is required to determine whether the phase space attractor has similar variation in other cross sections during milling, specifically when the process moves to an unstable state. In other words, the dependency of the Pearson's coefficient to the space dimension (j) must be investigated. For this purpose, Poincaré sections of the phase space attractor is plotted at each time segment for $j= 2$ and 3.

To verify the effect of embedding dimensions, the signal from Test no. 7 (cutting parameters are demonstrated in Table 5.1) is used. For $j=2$, the phase space attractor Poincaré sections are plotted by $x_{(t-2\tau)}$ against $x_{(t)}$, while they are plotted by $x_{(t-3\tau)}$ against $x_{(t)}$ for the value of $j=3$.

The Pearson's coefficient of each Poincaré section is computed against the reference section. The values are tabulated in Table 5.2 and plotted in Figure 5.9.

Table 5.2: Pearson's coefficient for different space dimension values.

Time Segment (s)	Pearson's Coefficient in different space dimension		
	j = 1	*j = 2*	*j = 3*
0 - 6	1	1	1
1.5 - 7.5	0.9998	0.9996	0.9996
3 - 9	0.995	0.996	0.995
(4.5 - 10.5)[3]	0.9	0.91	0.91
6 - 12	0.81	0.82	0.81
7.5 - 13.5	0.64	0.64	0.63
9 - 15	0.57	0.58	0.57
10.5 - 16.5	0.56	0.58	0.57
12 - 18	0.54	0.55	0.53
13.5 - 19.5	0.53	0.53	0.52
15 - 21	0.52	0.52	0.51

The onset of chatter has been identified as occurring at the 4^{th} time segment (*4.5 – 10.5s*). The correlation between the phase space attractor cross section at this time segment and reference pattern is high-lighted in the Table 5.2. As shown, the tolerance of Pearson's coefficient for space dimensions *1*, *2*, and *3* is only *±0.01*, or *±%1*, which is very small and well within experimental error and can be ignored. Therefore, it is concluded that the proposed chatter threshold indicator is insensitive to the space dimension value.

[3] Time interval that chatter begins.

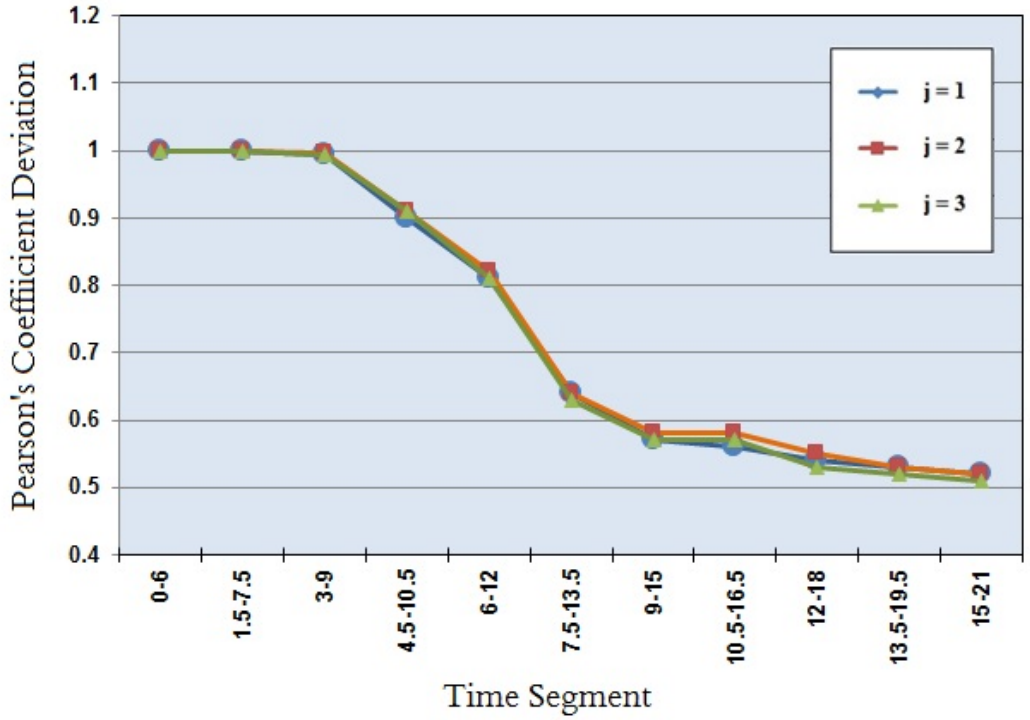

Figure 5.9: Corresponding variation of Pearson's coefficient to different space dimensions along trial no. 7.

5.6 The Evaluation of Chatter Occurrence

To evaluate whether the combination of phase space attractor Poincaré sections and image correlation could successfully detect the onset of chatter, it is required to validate the proposed method with another accepted method. For this purpose, two methods, visual inspection and Fast Fourier Transform (FFT), are used to detect the occurrence of chatter and the time of onset.

5.6.1 Visual Inspection

The simplest method for detection of chatter is inspection of the milled surface. In the laboratory environment, the surface can be inspected with digital microscopes. The method is not a prediction technique but only provides confirmation that chatter has occurred after finishing milling.

Previously, this was used to determine the occurrence of chatter. The surface is inspected by imaging different parts of the milled path. Chatter marks and their location on the surface indicate whether chatter occurred during the process and the position of chatter onset.

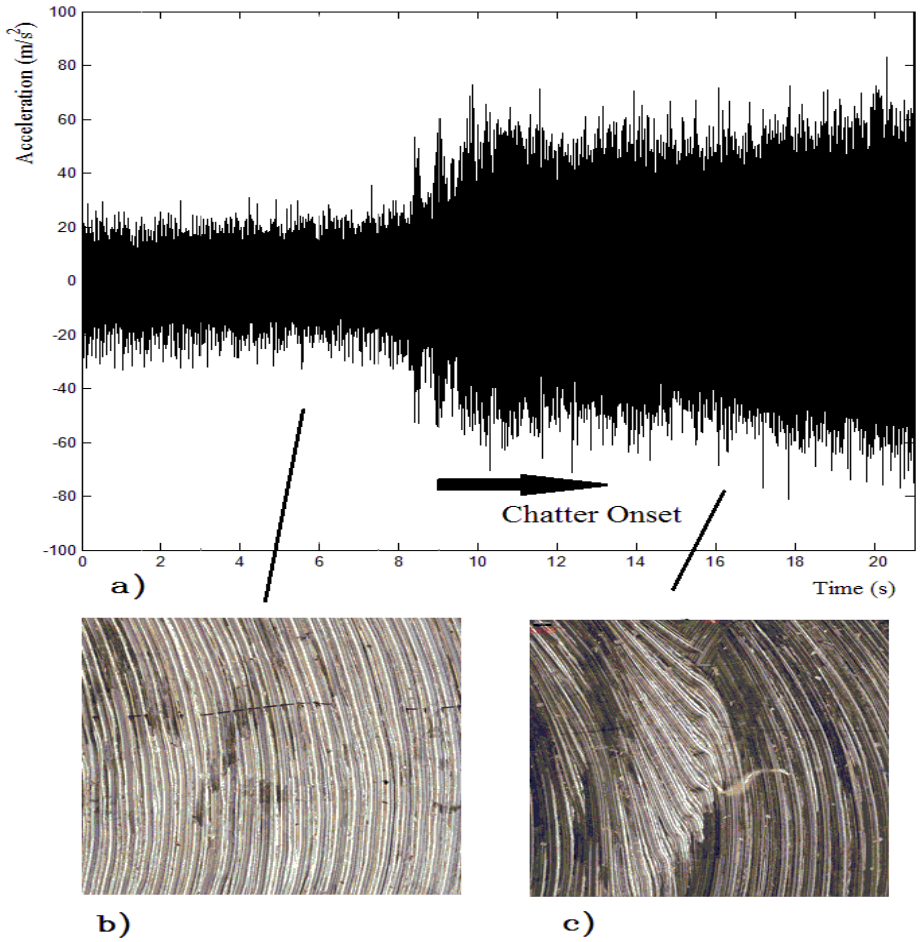

Figure 5.10: a). Acquired acceleration signal along milling trial no. 7. b) Cutting surface at stable condition. c). Chatter marks on the cutting surface.

Figure 5.10 shows the acceleration signal during milling trial no. 7 (Table 5.1) and the captured image of the surface at the stable and chatter conditions. This method cannot be considered a consistent technique, thus the Fast Fourier Transform method is used to determine the onset or boundary of chatter.

5.6.2 Fast Fourier Transform (FFT) Method

To determine the occurrence of chatter by FFT method, the acquired cutting force signal during the test run is transformed into the power spectrum by Fast Fourier Transform (FFT). The chatter energy is reflected in the FFT power spectrum diagram. Harmonic frequencies are identified as multiples of the tooth passing frequency. When chatter occurs, a frequency which is a harmonic of the tooth passing frequency but with significantly higher power can be identified as being chatter frequency [207].

Milling trial no. 7 was evaluated to determine the outline chatter threshold from the regression analysis with FFT method. The power spectrum diagram is illustrated for the acquired signal, as shown in Figure 5.11. The FFT Power spectrum diagram indicates the chatter frequency after the third harmonic frequency of tooth passing frequency.

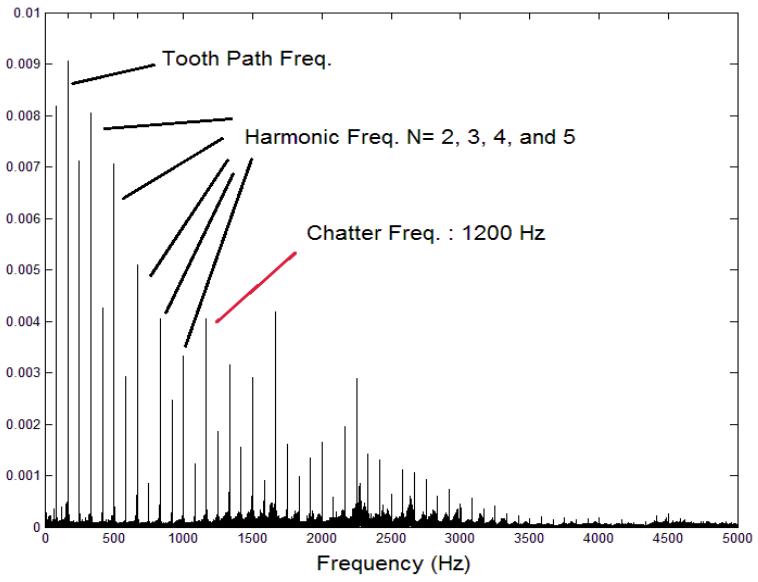

Figure 5.11 FFT power spectrum of cutting force acquired during milling trial no.7: Spindle speed 4000 rpm, a_p: 0-2 mm and a_e: 1.5 mm (0.25D).

To determine the moment of chatter onset, the cutting force signal is divided into the time intervals similar to what was done for evaluation of the phase space attractor Poincaré sections. The FFT power spectrum is then plotted for each time interval.

As shown in Figure 5.12, the range of harmonic frequencies is generated with some regularity in time segments (*0-6 s*), (*1.5-7.5 s*), and (3-9 s). Then an irregular jump in power levels occurred in the harmonic frequencies at time segment (*4.5-10.5 s*). Accordingly, the onset of chatter occurred in time interval (*4.5-10.5 s*). This is the same time segment where the value of the Pearson's coefficient was considered for the chatter threshold boundary. Similarly, the procedure is repeated for other experiments. The outcome of the experiments represents that the value of the regression coefficient can be considered as the boundary for onset of chatter.

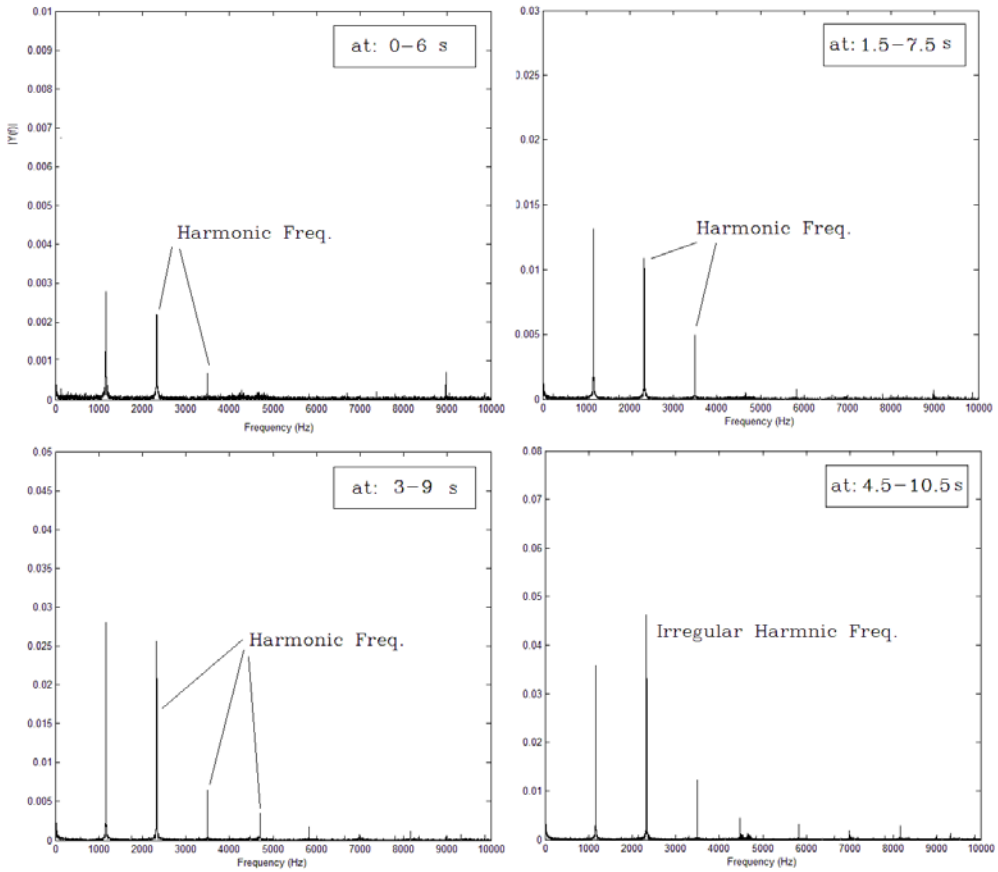

Figure 5.12 FFT power spectrums for each time interval during milling trial no. 7.

5.7 Evaluation of the Image Correlation for Other Trials

Related time series for the trials no. 1, 2, 4, and 8 are reconstructed in the form of state vectors. As per trial no. 7, every time series is divided into time segments with overlap. Hence, the corresponding cross section of phase space attractor to each time segment is plotted by considering an embedding dimension equal to *2* (or *j=1*). The deviation of the phase space attractor during each trial is indicated by computing Pearson's coefficient between the attractors at the time segments and the relevant reference pattern. The result is demonstrated in Figure 5.13 (a) to (d).

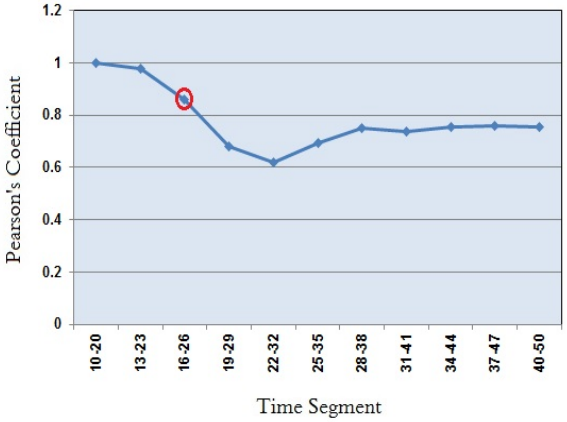

a). Trial no. 1, Onset of chatter at *r=0.86*

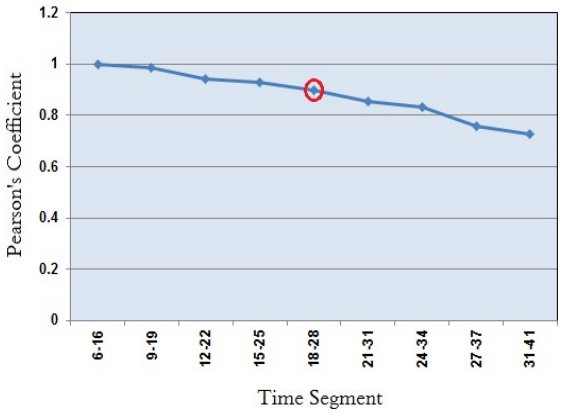

b). Trial no. 2, Onset of chatter at *r*= 0.88

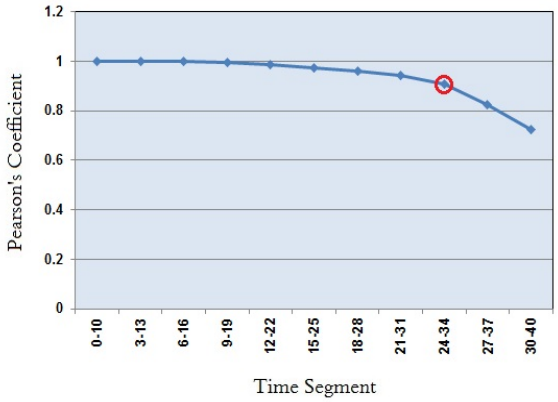

c). Trial no. 4, Onset of chatter at *r=0.91*

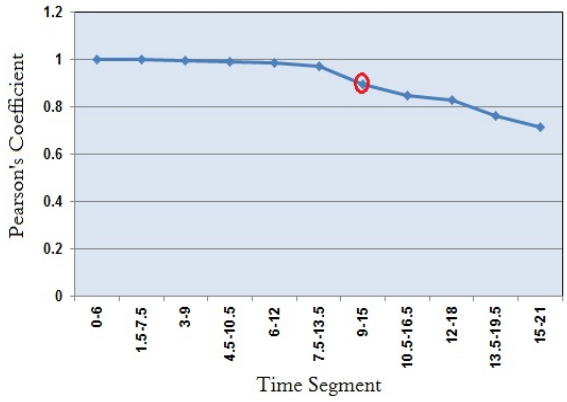

d). Trial no. 8, Onset of chatter at *r=0.89*

Figure 5.13: Corresponding Pearson's coefficient to phase space attractor Poincaré sections along 4 milling operations.

The Poincaré sections patterns obtained during the trials are similar to the patterns attained from experimental trial no. 7. When milling moves from a stable condition to chatter, the patterns from main experiments present a similar variation to the primary experiment. During the stable phase of milling, the attractor is dense and circular while it expands during state transformation to chatter.

5.8 DISCUSSION

A trend analysis algorithm has been developed to indicate when to stop milling before it enters the chatter state. It is expected that the method works well in modelling and prediction. It should use data while the cutting process is occurring to predict new values for an outcome given measured values for an explanatory variable. The prediction must be consistent. Furthermore, it is required to test a hypothesized mechanistic model of a system against data, or we wish to use a mechanistic model we believe in to predict new data.

This chapter describes the analysis algorithm based on image correlation principle. Starting with a reasonable stable cut, the analysis algorithm, if it is implemented in a computer, can continue its operation to analyse the cutting process while cutting continues. The algorithm will distinguish the transition of process from stable to unstable. In this algorithm, the milling processes are divided into equal time segments with an overlap. Phase space attractor is then demonstrated along milling trials by plotting the cross section of attractor at each time segment. The outcome shows that shape and size of the attractor is continuously changed during the milling operation. The attractor has significant variation by transferring to the unstable condition or chatter.

By transforming the phase space attractor into two dimensional Poincaré sections, the reference section is identified. Pearson's coefficient is then computed according to the reference section. As milling continues, the Pearson's coefficient will decrease and will reach a threshold value indicating chatter, at which the point milling should stop damaging to the workpiece.

Besides the technical advantages of using the correlation coefficient application in definition of chatter threshold, it further provides a simple method with minimal or acceptable processing time. The correlation coefficient is invariant to linear transformation of two variables [203]. It is also unit-less, which allows calculating the correlation coefficient on different data sets with different units. Furthermore, the coefficient condenses the comparison of two images down to a single scalar value, r.

The image correlation method has some limitations in detecting the chatter, which can effect on the resulted chatter onset boundary. Firstly it cannot measure correlation accuracy where there is a poor signal-to-noise ratio and negative spikes. Hence, it only measures the observed correlation without been able to consider any confounding or spurious effects. Secondly, the biggest disadvantage of it as an indicator for the onset of chatter is the coefficient only demonstrates the existing relationship between two Poincaré sections that have already been observed. It cannot provide any prediction or extra information about the second Poincaré section or dependent variable.

To overcome these key disadvantages of the Pearson's coefficient, linear regression is proposed in the following chapter 6. Similarly to image correlation, linear regression will be applied to the reconstructed phase space attractor to indicate the variation of the attractor when milling moves to the unstable state or chatter.

Chapter 6

Modeling of the Phase Space Attractor Deviation by Linear Regression

6.1 Introduction

Pearson's correlation coefficient has some mathematical limitations determining the precise relationship between different Poincaré sections during milling. These limitations have been discussed in the last chapter. It is necessary to search for another mathematical tool that can cover these limitations. A literature review shows that linear regression can be used to approach the same problem [208]. Therefore, both linear regression and image correlation can be used to measure or determine the relationship between two or more variables.

In this chapter, a model is developed based on the linear regression technique to parameterize the deviation of Poincaré sections. It is developed to give a consistent numerical indicator for the variation between Poincaré sections of phase space attractor in the same way as image correlation can be done. Linear regression, multiple regression and simple regression, are investigated to see if they can parameterize the variation of the Poincaré sections such that regression coefficients are considered as the numerical indicator to represent the boundary between a stable state and chatter. The Poincaré sections are interpreted in the form of a matrix and are regressed with the reference Poincaré section.

In this chapter, we investigate whether the method can resolve the disadvantages over image correlation. Hence, the method has to be able to provide a timely forecast of chatter occurrence, as well as being insensitive to the dynamics of milling and cutting parameters.

6.2 Linear Regression

Several mathematical techniques are used to present the relationships between sets of variables. The most common techniques are; Moving Average (MA), Exponential Smoothing, Auto Regressive Integrated Moving Average (ARIMA), and Linear Regression. Linear regression is a powerful technique that explores the linearity between two or more variables. By this method, mean of variable U is

defined as a straight line function of V plus an error term or residual. Usually the undetermined variable, which is also known as dependent or criterion variable, is regressed with one or more independent (predictor) variables [209].

Linear regression is predominantly used for the purpose of indicating phase space attractor deviation, in the same way as image correlation. MA is a statistical tool to analyse time series by creating a series of averages of different subsets of the full data set [210]. MA plots an interval of the averages but it does not produce a specific number as is required for determining the chatter onset boundary. In MA, equal weight must be given to every time period that makes the forecasts lag behind the underlying trend, or the actual data values have to be multiplied by some weightings, which makes calculation difficult. Therefore the inherent nature of MA, means the outcomes always lag behind and making it insensitive for prediction purposes.

ARIMA is used to fit data to a time series. The choice of the model structure demands great experience from the developer. The complexity increases the computation time, which is not desirable with on-line chatter detection methods [211]. The ARIMA method firmly models the variable with information about the past values of the same variable, and has difficulty handling multiple variables. Hence, the model is complicated to use and is not flexible as the parameters are fixed over time [212].

The exponential smoothing method produces smoothed data as the recent observations are given relatively more weight in forecasting than the older observations. Compared with MA, exponential smoothing is faster, more accurate, and has less complexity. However, it cannot provide a model and interval for prediction [213].

6.2.1 Linear Regression Application on Modelling Dynamic Systems

Linear regression has been used to analyse trends in wide range of dynamic systems. It characterizes the relationship between independent variables and

dependent variables, which is useful for forecasting the future values of the dependent variable [214].

The linear regression method has been applied to many engineering processes. Bukkapatnam *et al.* [215] used linear regression to characterize the material removal rate in the chemical-mechanical planarization of SiO2 film. To improve the predictability (more than 40%), they applied statistical features along with the process parameters and polishing time. Ic [216] advanced TOPSIS to define critical selection attributes and their interactions by fitting a polynomial to the experimental data in a multiple linear regression analysis. On the subject of TOPSIS, the regression model reduced the process cost, time and the computing complexity. Xue *et al.* [217] modelled the robotic arc-welding process by using fuzzy linear regression to promote the automated welding system. Su and Dingwell [218] employed linear regression to demonstrate scaling coefficient effects on stability of walking model on an irregular surface. Kaunda [219] combined linear regression with numerical integration to analyse deep-seated landslides, at slow to extremely slow episodic displacement rates. The technique predicted volumetric rates of mass flow in a specific direction, based on measured surface velocities. Foucart [220] evaluated the inverse of a correlation matrix stability by looking at the squared length of the regression vector's derivatives.

Linear regression is used in models that are linearly dependent on their independent parameters. It has also been applied to machining processes for various purposes. Huang *et al.* [221] tried to provide a multiple linear regression model to detect the tool breakage on-line during machining. Chen *et al.* [222] provided a model with multiple regression to monitor the wearing of cutting tools during milling. Korkut *et al.* [223] compared the regression and artificial neural network (ANN) in order to predict tool‑chip interface temperatures during machining, which is dependent on cutting parameters. The result demonstrates that in comparing with ANN model, regression provides stronger predicted values in performance. Regression analysis is used even to estimate the cost of machining processes [224].

The summary of literature search above indicates that linear regression analysis is well fitted to appoint independent variables to changing dependent variables. Therefore, linear regression was chosen and applied on reconstructed phase space attractor Poincaré sections in this study to predict the state of milling processes.

The literature review demonstrates that linear regression is consistent and precise, such that the slope (trend) is able to provide useful and accurate information [214]. This aspect makes the linear regression method most suitable and reliable on forecasting data in regards to chatter.

6.3 The Mathematical Format of Poincaré Section

A Poincaré section based on section 4.5, is considered at this point to design a certain mathematical format. The mathematical design must be applicable for linear regression modelling. It can then be applied for all phase space attractor Poincaré sections. The Poincaré sections of relevance are those resulting from analysing acceleration signals acquired during the milling trials.

To interpret a Poincaré section, it is divided into k equal segments in each direction of X and Y, as shown in Figure 6.1. A number of ordered pairs $(x_l, x_{l-\tau})$ are perched inside of each pixel. k is the optimum value that is determined by minimum and maximum values of ordered pairs $(x_l, x_{l-\tau})$, as well as the total number of ordered pairs in the Poincaré section. Therefore, the Poincaré section at time interval i is divided into the number of $k \times k$ pixels, each pixel including a number of ordered pairs. Accordingly, the Poincaré section is shown in the form of a $k \times k$ matrix, named $\mathbf{S_i}$. In matrix $\mathbf{S_i}$ that is sown by Equation (6.1), the total quantity of the ordered pairs in each pixel can be the value of the array corresponding to the pixel.

$$\boldsymbol{S_i} = \begin{bmatrix} S_{11} & \cdots & S_{1k} \\ \vdots & \ddots & \vdots \\ S_{k1} & \cdots & S_{kk} \end{bmatrix} \tag{6.1}$$

By accomplishing the above procedure for each Poincaré section at each time segment, a set of matrices are resulted. The matrices are the desired mathematical format of the phase space attractor Poincaré section, as two or more matrices can be easily subjected to linear regression.

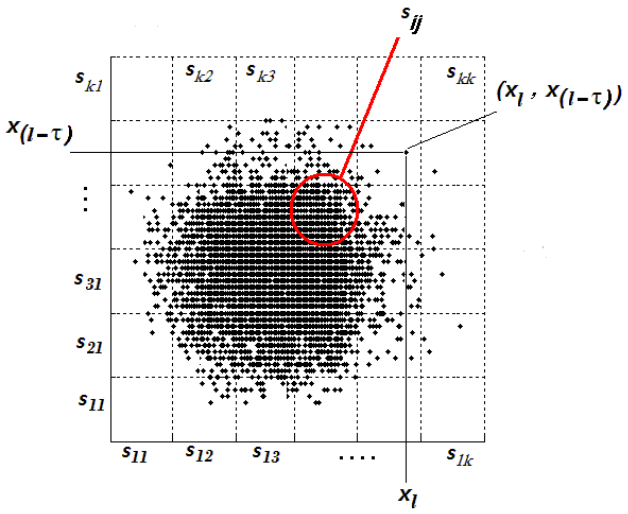

Figure 6.1: phase space attractor cross section divided into $k \times k$ pixels.

6.4 Poincaré Section Deviation Modelling

Having reviewed the linear regression method, this section describes how it can be used to analyse the Poincaré sections generated from phase space attractor during milling, as explained in chapter 4.

In modelling with linear regression a minimum of two variables are required, one independent variable and one dependent. The independent variable is the reference variable which has been controlled in the milling process.

Linear regression models the relationship for two variables with a line equation as shown in Equation (6.2).

$$U = \beta + \alpha . V \tag{6.2}$$

Where:

U is dependent and V independent variable. Hence, α is the regression coefficient that represents the variation of dependent variable when the independent variable varies by one unit. Consequently, β is the intercept.

Similarly, multiple variable linear regression models can be formatted. Equation (6.2) is expanded to a new form of the Equation (6.3), which incorporates multiple variables. Using this model, a dependent variable can be modelled by considering all distinguishable independent variables.

$$U = \beta + \alpha_1 V_1 + \alpha_2 V_2 + \cdots + \alpha_n V_n \tag{6.3}$$

where:

V_1 to V_n are independent variables that dependent variable U is modelled based on its relationship with them. Hence, α_1 to α_n are regression coefficients.

In the regression model, the regression coefficient is the slope of the line that explains the linear association between U and V_i. In the other word, it represents the rate of change of one variable (U) as a function of changes in the other variables V_i. Accordingly in order to indicate whether the milling process is going to chatter, the regression coefficient is the consistent indicator that reflects the variations between Poincaré sections.

6.4.1 Multiple Variables Linear Regression Model

Linear regression modelling of the Poincaré sections deviation requires an initial state reference. A milling process starts at a stable condition, then according to the dynamics self-excited vibration occurs. So in the linear regression model, the corresponding matrix of the Poincaré section at the first time interval (beginning of the process) is considered as the reference variable. The relationship between the corresponding matrix of Poincaré section at the second time interval and

reference Poincaré section is evaluated by Equation (6.4), where $\mathbf{S_1}$ and $\mathbf{S_2}$ are the corresponding matrices to the Poincaré sections at time segment one and two.

$$\boldsymbol{S_2} = \beta + \alpha_1 . \boldsymbol{S_1} \tag{6.4}$$

Similarly, the multiple variables regression model of third time segment can be calculated by using Poincaré sections prior to the time segment 3, as shown in Equation (6.5).

$$\boldsymbol{S_3} = \beta + \alpha_{1(3)} . \boldsymbol{S_1} + \alpha_2 . \boldsymbol{S_2} \tag{6.5}$$

The regression coefficients α_2 represents the rate of change of the Poincaré sections with respect to the closest section $\mathbf{S_2}$. It is noted that the regression coefficient α_1 for $\mathbf{S_1}$ is different and is labelled as $\alpha_{1(3)}$.

Correspondingly, Equation (6.6) is the expanded form of Equation (6.5), where the dependent variable $\boldsymbol{S_i}$ is modelled by using distinguishable variables $\mathbf{S_1}$ to $\mathbf{S_{i-1}}$. In this model, all matrices prior to the $\mathbf{S_i}$ have been considered as independent variables. $\mathbf{S_i}$ is the corresponding matrix of Poincaré section at time segment *i*, while $\mathbf{S_1}$ to $\mathbf{S_{i-1}}$ are corresponding matrices of Poincaré sections at time segments *1* to *i-1*.The association of each Poincaré section with prior Poincaré sections is then expanded in the Equation (6.6).

$$\boldsymbol{S_i} = \beta + \alpha_{1(i)} . \boldsymbol{S_1} + \alpha_{2(i)} . \boldsymbol{S_2} + \cdots + \alpha_{i-1(i)} . \boldsymbol{S_{i-1}} \tag{6.6}$$

The regression coefficients $\alpha_{(i)}$ are the potential indicators that define the boundary between the stable and unstable states of milling. However, the question is:

What is the value of the regression coefficient that indicates the boundary of chatter onset?

To answer this question, a set of real data that is acquired during milling should be used, and the proposed multiple variables regression model has to be applied

to it. For this purpose, the same set of acquired data that was previously used in section 5.4, chapter 5 is analysed (Milling trial no. 7, Table 5.1).

Milling trial no. 7 is divided into the 10 time intervals. Poincaré sections of related phase space attractor to the milling process are illustrated by plotting $x_{(t-10)}$ versus $x_{(t)}$. To apply linear regression, every Poincaré section is considered dependent to the prior Poincaré sections. Consequently by considering a Poincaré section at time segment i as the dependent variable, prior Poincaré sections are considered independent variables. Accordingly, the outlined matrix corresponding to each Poincaré section is placed in the Equation (6.6). Regression Coefficients α_1 to α_{10} are then calculated and tabulated in Table 6.1.

To answer the above question, the variation of regression coefficient must be investigated during the milling trial. Based on the tabulated information in Table 6.1, the investigation can be done in two ways:

- Deviation of each coefficient (α_1 to α_{10}) during different time intervals, or
- Deviation of all regression coefficients at each time segment.

Considering the value of α_1 during milling, there does not appear to be a consistent and predictable trend for its variation as shown in Figure 6.2, especially when the milling trial enters into the chatter at time interval (*4.5 – 10.5 s*). Similarly, the investigation of other regression coefficients provides a similar result. For better visualization of the regression coefficient deviation during milling, the deviation of every regression coefficient along milling process is plotted in Figure 6.3.

Table 6.1: The regression coefficient deviation for each time interval based on the multiple linear regression by using acquired data during milling trial no. 7.

Regression coefficient	α_1	α_2	α_3	α_4	α_5	α_6	α_7	α_8	α_9	α_{10}
Time Interval *(s)*										
1.5-7.5	0.99									
3-9	-1.21	2.13								
4.5-10.5[4]	0.19	-1.20	1.92							
6-12	0.37	-0.33	-1.02	1.91						
7.5-13.5	0.51	-0.49	-0.40	-0.21	1.58					
9-15	-0.41	1.06	-0.76	-0.29	0.01	1.37				
10.5-16.5	-0.15	0.08	0.43	-0.50	-0.02	-0.09	1.23			
12-18	0.00	-0.05	-0.06	0.48	-0.54	0.12	-0.17	1.22		
13.5-19.5	0.31	-0.32	-0.25	-0.05	1.03	-0.99	-0.07	-0.04	1.34	
15-21	-0.27	0.53	-0.19	-0.18	-0.25	0.82	-0.62	0.05	-0.51	1.56

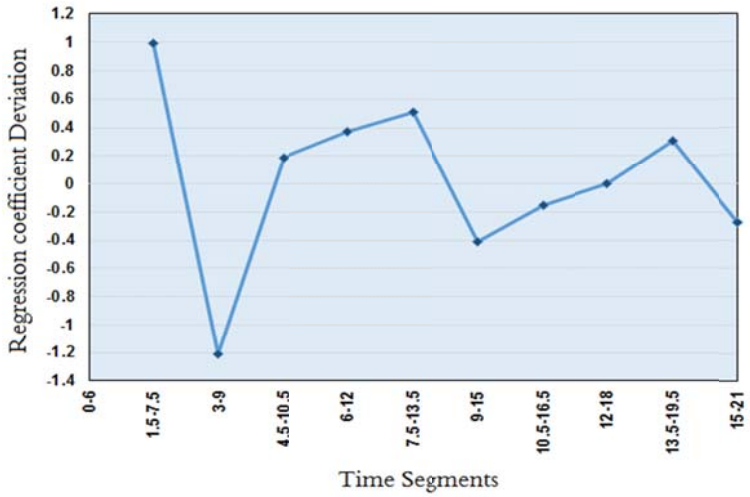

Figure 6.2: Deviation of regression coefficient (α_1) in multiple variable regression modelling and during milling trial no. 7.

[4] Time interval that chatter begins.

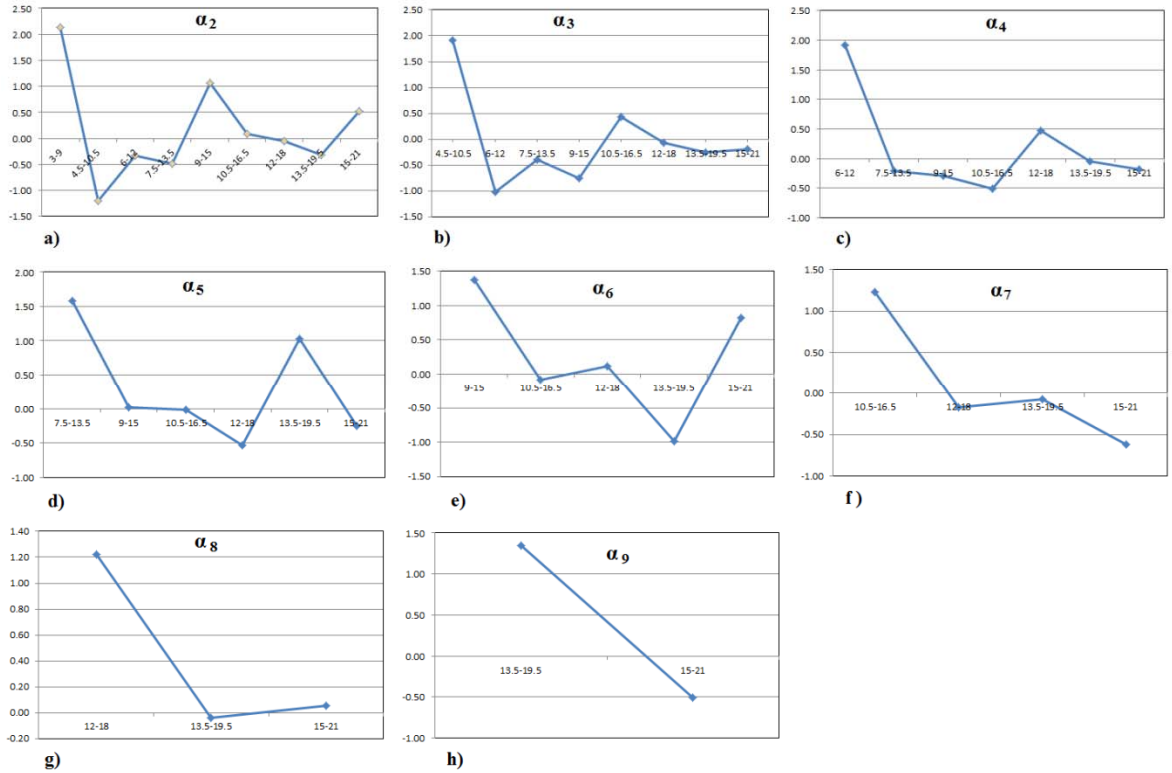

Figure 6.3 (a) – (h): deviation of α_2 to α_9 during milling trial.

The variation of regression coefficients (α_1 to α_{10}) is also investigated at each time segment. The variation of resulted regression coefficients from modelling of corresponding Poincaré section to time interval (*15-21 s*) are shown in Figure 6.4. The observation from the figure shows that the variation of regression coefficients belonging to each time interval (*15-21 s*) does not show any consistency or rule. Similarly, the variation of α_1 to α_{10} during other time intervals is not consistent and predictable, as shown in Figure 6.5 (a) to (h).

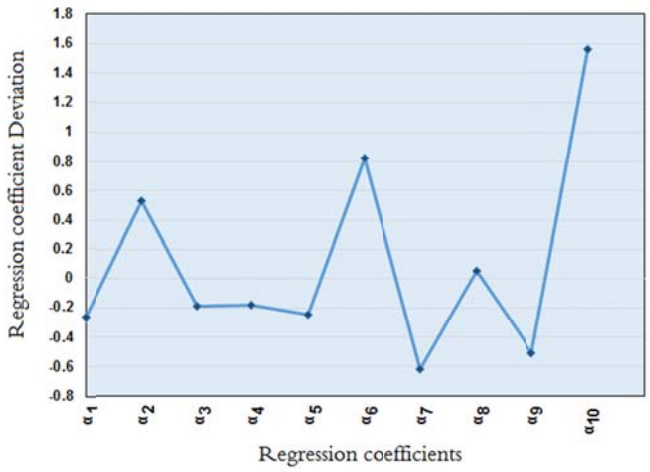

Figure 6.4: Deviation of regression coefficients (α_1 to α_{10}) for during the modelling of corresponding Poincaré section to time interval (*15 – 21s*).

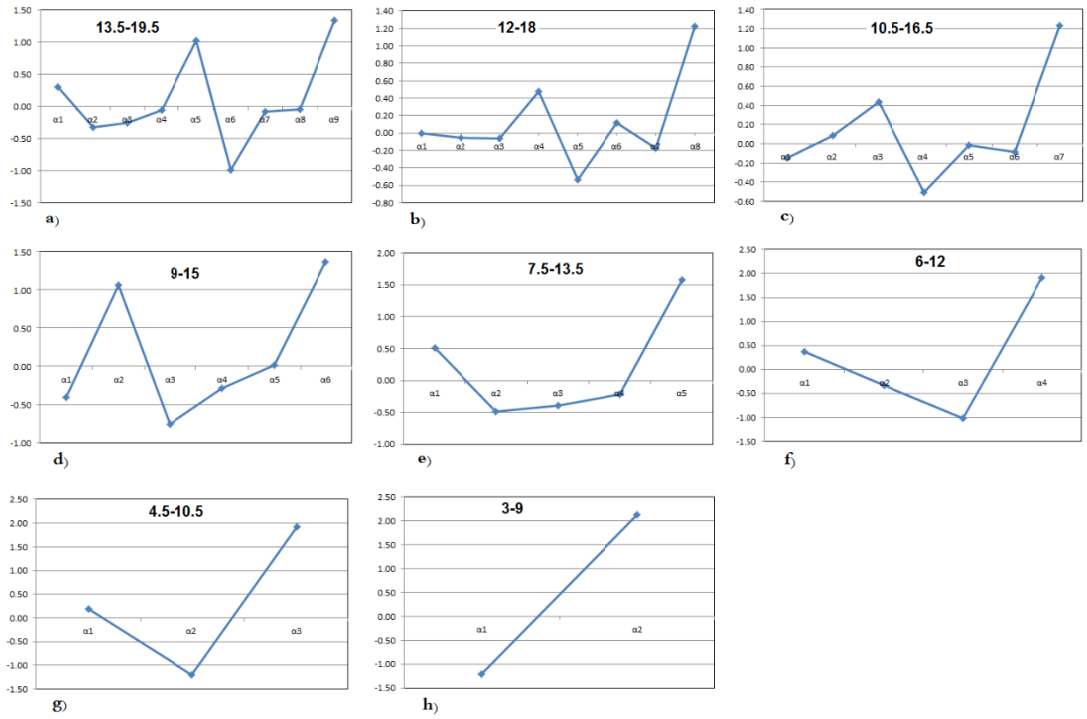

Figure 6.5 (a) - (h): Deviation of regression coefficients for each time interval.

By investigation of the regression coefficient deviation in the proposed multiple variable regression model, it is impossible to find a consistent relationship between regression coefficient deviation and Poincaré sections deviation. Therefore, the multiple linear regression model cannot provide the desired indicator for detection of chatter threshold. Therefore, it is necessary to investigate further and choose another linear regression modelling technique.

6.4.2 Fixed Reference Linear Regression Model

The investigation of using the multiple variable regression model shows that it is not successful in determining the chatter onset boundary. An alternative regression model is proposed in this section based on the simple linear regression model. In this model, every Poincaré section of reconstructed phase space attractor is compared with one fixed reference variable.

Normally, milling starts within a stable state. Gradually due to incomplete process parameters and interaction between cutting tool and workpiece, the milling process degenerates into chatter. Consequently to measure the deviation of Poincaré sections, the most suitable reference variable could be a corresponding matrix of a Poincaré section at the beginning of the cutting process, or in the first time segment. Accordingly, this matrix is considered as an independent variable and all other matrices are regressed with regard to that. Due to using a constant reference, the proposed model is titled, fixed reference linear regression. The model is represented by the simple linear regression Equation (6.9), and correlates each Poincaré section with the initial Poincaré section.

$$\boldsymbol{S_i} = \beta_i + \alpha_i . \boldsymbol{S_1} \qquad i = 2, 3, \ldots, n \qquad (6.9)$$

Having values of matrix $\mathbf{S_1}$ to $\mathbf{S_i}$, regression coefficient (α_i) is then calculated. The variation of phase space attractor along the milling process can now be measured by a regression coefficient (α_i) and the state of milling would be appointed during the milling time.

The fixed reference model is applied again on data acquired during trial no. 7 (Table 5.1) in order to determine whether the proposed model can indicate the onset of chatter. Corresponding matrix of Poincaré section at time segment (*0 - 6 s*) is considered as the fixed reference variable. The other ten corresponding matrices of phase space attractor Poincaré sections are correlated with the reference one. The regression coefficient must demonstrate the relationship between each Poincaré section and the initial Poincaré section. The variation of the regression coefficient can then be used to evaluate the deviation of Poincaré sections. For this purpose, the regression coefficient variation is demonstrated in Table 6.2, as well as Figure 6.6.

Table 6.2: Regression coefficient deviation during milling trial no. 7 analysed based on fixed reference regression model.

Time Intervals (s)	Regression Coefficient (α1)
0-6	Reference
1.5-7.5	0.987
3-9	0.891
(4.5-10.5)[5]	0.718
6-12	0.514
7.5-13.5	0.332
9-15	0.210
10.5-16.5	0.177
12-18	0.178
13.5-19.5	0.160
15-21	0.143

[5] Time interval that chatter begins.

The regression coefficient starts with the value of *0.987* for regression between Poincaré section at time interval (*1.5-7.5 s*) and reference one. The value of the coefficient continuously drops until it reaches a final value of *0.143* for regression between the last Poincaré section of time interval (*15-21 s*) and the reference. As shown in Figure 6.6, the variation of regression coefficient shows a consistent trend over the period of the experiment. It reduces consistently during the process. The value of regression coefficient is *0.718* at corresponding time interval (*4.5 – 10.5 s*), is the time interval representing the onset of chatter.

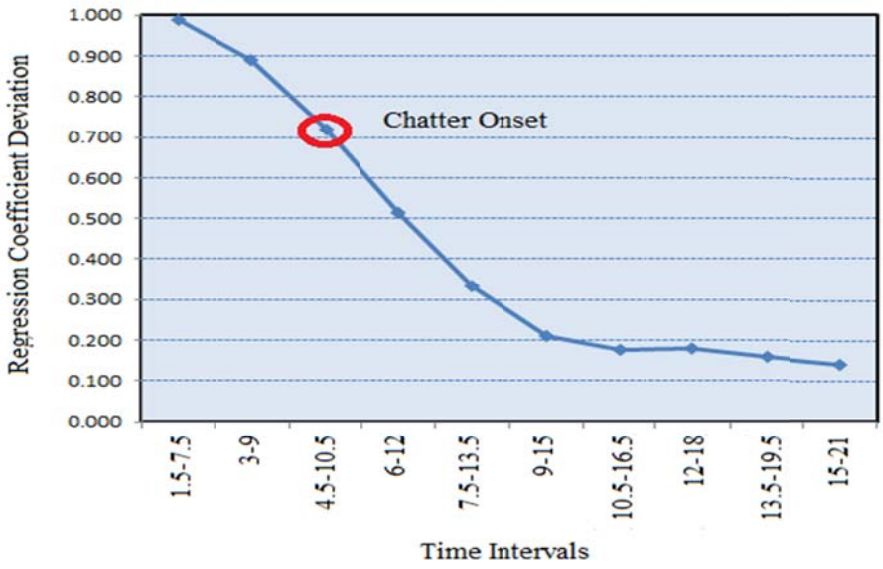

Figure 6.6: Regression coefficient deviation during unstable milling process (trial no. 7), based on the fixed reference linear regression model.

6.4.2.1 Fixed Linear Regression for Stable Milling Process

The deviation of Poincaré sections during unstable milling was successfully modelled by the fixed reference linear regression model. Next, the implication to stable state is examined. If the variation of regression coefficient is similar to the unstable milling state, then the model is not applicable. For this purpose, milling trial no. 5 is considered (Table 5.1), where the milling is stable during the entire trial.

Similar to experiment no. 7, the acquired time series was reconstructed and Poincaré sections were plotted for each time segment. The fixed reference linear regression was applied to measure the attractor variation during milling, and hence the regression coefficients were computed. The variation of regression coefficient is demonstrated in Table 6.3, as well as Figure 6.7.

The regression coefficient starts with the value of *0.997* for regression between Poincaré section at time interval (*3-13 s*) and the reference. The value of coefficient drops until the final value of *0.912* for regression between Poincaré section of time interval (*21-31 s*) and the reference. As shown in Figure 6.7, the regression coefficient does not have excessive variation during the stable milling operation and its value varies descending and smoothly from *1* to *0.9*.

Table 6.3: Regression coefficient deviation during milling trial no. 5 analysed based on fixed reference regression model.

Time Intervals (s)	Regression Coefficient (α_1)
0-10	Reference
3-13	0.997
6-16	0.982
9-19	0.975
12-22	0.945
15-25	0.931
18-28	0.905
21-31	0.912

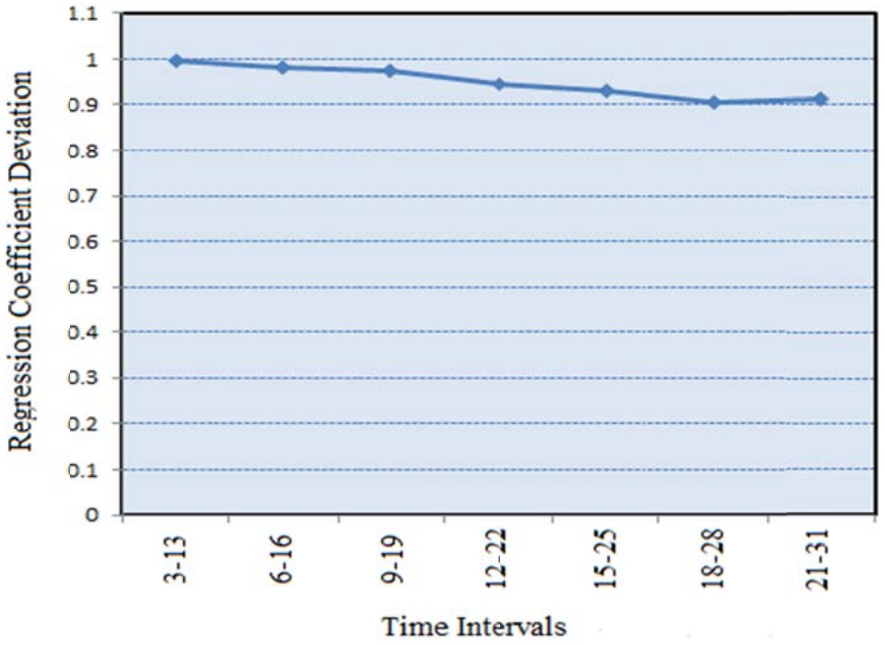

Figure 6.7: Regression coefficient deviation during stable milling process (trial no. 5), based on the fixed reference linear regression model.

6.5 Evaluation of the Fixed Reference Linear Regression Model for Other Trials

Similar to trial no. 7, the Poincaré sections related to the trials no. 1, 2, 4, and 8 (Table 5.1) are interpreted in the form of a matrix. Other milling trials ran stable. The deviation of the phase space attractor during each trial is indicated by computing the regression coefficient between Poincaré sections at time segments and the reference Poincaré section. The result is demonstrated in Figure 6.8 (a) to (d).

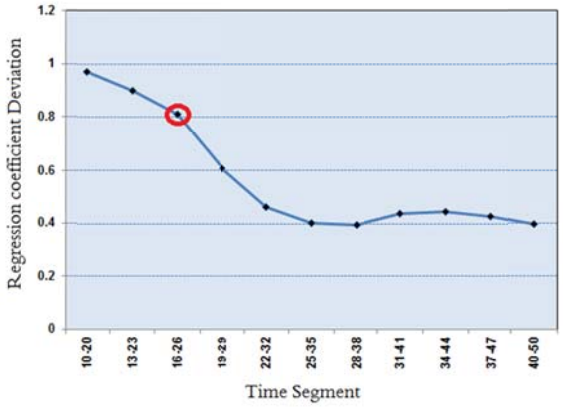

a). Trial no. 1: Onset of chatter at α_1=*0.81*

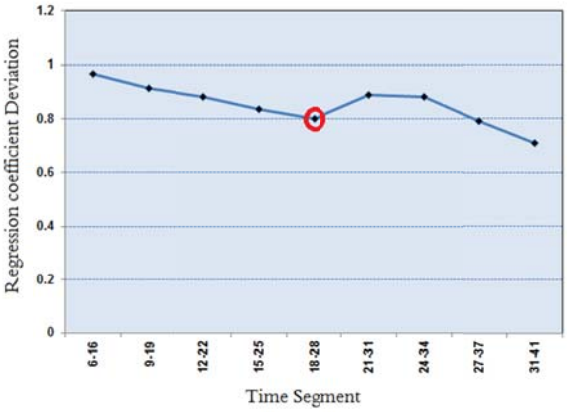

b). Trial no. 2, Onset of chatter at α_1= 0.8

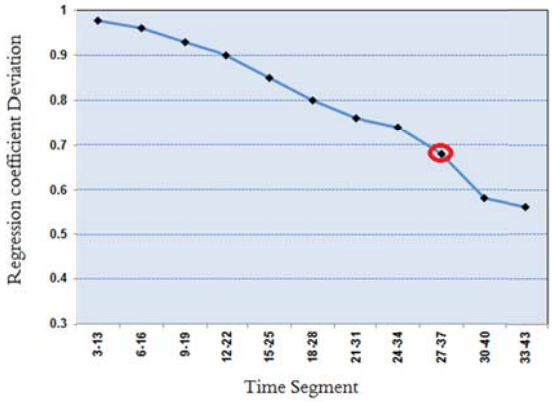

c). Trial no. 4, Onset of chatter at α_1=*0.67*

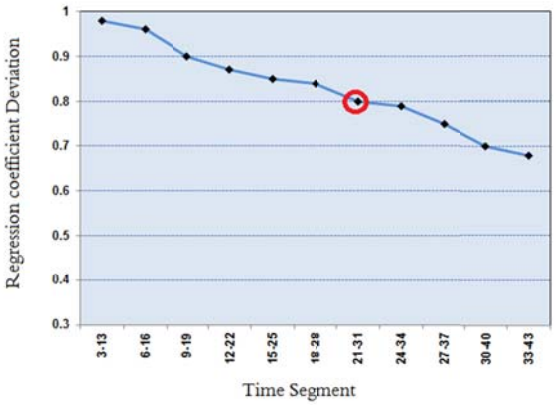

d). Trial no. 8, Onset of chatter at α_1=*0.78*

Figure 6.8: Corresponding regression coefficient to phase space attractor Poincaré sections along 4 milling operations.

The resulting regression coefficient deviations related to the four trials are similar to the patterns in experimental trial no. 7. When milling moves from a stable condition to chatter, the regression coefficients derived from the fixed reference linear regression model show similar variations to the primary experiment, where the value of the coefficient reduces smoothly during milling.

6.6 Discussion

In chapter 5, the correlation coefficient was applied to determine the relationship between Poincaré sections. The chatter onset boundary was determined by using the correlation coefficient variation during milling, even though; the method is not consistent and has some limitations. In the other hand and from this study, linear regression overcomes those limitations and could successfully provide a consistent indicator for chatter onset.

The use of the correlation coefficient is fast, easy, and straightforward, although it measures the closeness of the relationship between two or more variables without any information about their functional relationships. Hence, a high value of the correlation coefficient (more than 0.8) explains about *50%* of the variability. Image correlation can establish the relationship between only two variables, and obviously only makes sense if both variables are observed.

Unlike image correlation, linear regression, which is also known as a statistical technique, demonstrates the form of the relationship between independent and dependent variables. The basic linear relationship forms such as polynomial, exponential and logarithmic regression have low correlation coefficients but are high on the regression function. Regression analysis can also explain one variable with more than one independent variable simultaneously.

As mentioned in chapter 5, image correlation cannot prove dependency between two variables. It only gives an estimation of the degree of the relationship between two variables. On the other hand, the regression analysis is used if a fixed, or dependent variable is available, and if the aim is to use the measurement of the relationship to predict values of the random variable based on values of the fixed variable. Regression analysis attempts to describe the dependence of a variable on one (or more) explanatory variables; it implicitly assumes that there is a one-way causal effect from the explanatory variable(s) to the response variable, regardless of whether the path of effect is direct or indirect. There are advanced regression methods that allow a non-dependence based relationship to be described.

6.7 Conclusion

In this chapter, a new model based on the principle of linear regression is proposed to determine the deviation of phase space attractor towards chattering state during milling. As opposed to traditional use of linear regression analysis with multiple variables, the innovation in this new model is to use fixed reference linear regression that provides a consistent trend indicator. Furthermore, the indicator has been proved to be a reliable indicator for chatter threshold, based on predicting the relationship between Poincaré sections during milling. The fixed reference linear regression method overcomes the limitations of the image correlation.

Based on the results from linear regression modelling for sets of data acquired during trial 7 for milling titanium, the fixed reference model could successfully provide a trend to demonstrate the variation of the phase space attractor Poincaré sections during milling. The regression coefficient is the indicator that measures the variation of Poincaré section.

The method described must be further validated by more titanium milling experiments. The outlined threshold regression coefficients are therefore applicable to for machining activities. For validation purposes more milling trials including other materials, cutting tools, and cutting parameters have been run. The proposed linear regression method has been applied on the acquired data in order to further validate the proposed model. The results are discussed in the next chapter.

Chapter 7

Evaluation of Fixed Reference Regression Model

7.1 Introduction

The variation of phase space attractor Poincaré sections was demonstrated as a tool to visualize the state of milling process in time. The variation was successfully parameterized by the fixed reference linear regression model. This model supplied a regression coefficient as a numeric indicator, which can be used in the online monitoring process to predict chatter onset. The method described has been validated by a series of experiments milling titanium.

To further validate the proposed regression model, it is applied to numerous milling processes based on workpiece material and cutting tool size. The milling trials are also run with different cutting parameters. The study objective is to determine whether the variation regression coefficient is similar for different milling processes. The aim is also to determine whether the proposed chatter threshold boundary in the initial study results is applicable for new cutting runs, or it is required to determine specific boundaries based on each new milling condition.

In this chapter, the milling operations are classified based on the workpiece material and the cutting tool size. In the first studies the regression model is applied to trials cutting titanium, stainless steel, and aluminium with a 6-mm cutter. These engineering materials are the most common materials used for milled products. The studies carried out in this section use the same materials but with a 4 mm cutting tool. The results are a database of regression coefficient values based on the cutting conditions. This database can then be used in industry and in the format of software that the operator can use to determine whether the milling process is going to enter into chatter, thereby the prevention of this will be beneficial.

7.2 Analysing Milling Trials Cut with a 6-mm Cutter

A set of milling cuts is done with a 6-mm long cutter. The cutter is made of tungsten carbide material which is suitable to cut titanium and stainless steel.

Moreover, the cutting tool varies in the number of flutes. Workpieces are cut by cutters with two different numbers of flutes, two and four.

7.2.1 Titanium

The advantages of titanium are given in chapter 1. Comparing with other engineering materials such as steel, aluminium and composites, titanium is more susceptible to chatter. Consequently, it is classified as a hard-to-cut material. Consequently the, detection of chatter during milling of titanium is the main objective of this study.

One set of experiments including nine titanium milling trials was completed by using a ball-nose cutter, and the proposed methods of chatter detection, image correlation and regression model, were applied to determine the chatter threshold boundary. However, more investigation is required to verify the application of chatter detection methods for different milling conditions. This was done with different cutting tools and cutting parameters.

For titanium, chatter occurrence is more likely when the cutting parameters are in the range is shown in Table 7.1. Accordingly, the trials had cutting parameters within the ranges shown in the table and also with the condition that milling begins with a stable state and continuously moves to an unstable condition or chatter.

Table 7.1 The range of cutting parameters for occurrence of chatter.

Cutting Parameters	Range
Spindle speed (V_s)	4500-5000 (rpm)
Cutting Speed (V_c)	225-250 (mm/min)
Axial Depth of Cut (a_p)	1-2 (mm)
Radial Depth of Cut (a_e)	0.25 D - 0.75 D (mm)

Stability lobes diagrams are usually plotted by Axial Depth of Cut (a_p) versus spindle speed. Accordingly to have stable condition at the start of milling process and continuously move to chatter, the trial can be designed in a way that axial depth of cut or cutting speed changes continuously during milling. To continuously increase axial depth of cut during a trial means a ball-nose cutting tool is required, but for end-milling this cannot be done so axial depth of cut in this case is invariable. Therefore, two distinctly different forms of milling; ball-nose and end mill are investigated.

7.2.1.1 Ball-Nose Milling

To increase D_A continuously during the milling trial, the cutting path must be considered as a form of inclined slot. Two kinds of a 6-mm ball-nose cutting tool with 2 and 4 flutes are used to cut titanium.

Considering the numbers of flutes, two sets of milling process are performed with each set including nine milling trials. The cutting process starts with zero axial depth of cut, and then it is continuously increased to the final value of 2 mm. The immersion rate varies between *25%* and *75%* during the trials. The cutting parameters are shown in Tables 5.1 for a 4-flute cutter, and in Table 7.2 for a 2-flute cutter.

Table 7.2 Cutting parameters for a ball-nose, 2 flutes, and 6 mm cutting tool.

Test No.	V_s *(rpm)*	V_c *(mm/min)*	a_p *(mm)*	a_e *(mm)*
1	4500	225	0-2	0.25D
2	4500	225	0-2	0.50D
3	4500	225	0-2	0.75D
4	5000	250	0-2	0.25D
5	5000	250	0-2	0.50D
6	5000	250	0-2	0.75D
7	5500	275	0-2	0.25D
8	5500	275	0-2	0.50D

9	5500	275	0-2	0.75D

The observations from the experiments shows that milling trials no. 2, 5, and 6 ran in a stable condition. The acceleration signal is recorded in the form of a time series. The corresponding time series is shown for each trial in Figure 7.2. The time series is reconstructed to state vectors and phase space attractor Poincaré sections related to each milling trial and are plotted (the procedure has been explained particularly in chapter 4). Thereafter the fixed reference linear regression method models the variation of Poincaré sections along each of the milling trials, as discussed previously.

Earlier in chapter 6, the chatter threshold boundary was established for the set of milling trials that cut the titanium workpiece with a *6 mm* ball-nose cutter with 4 flutes. In this case the same process is done for another set of milling trials that cut titanium workpieces with a *6 mm* ball-nose cutter but with only two flutes. The regression coefficient is calculated and its variation is established for each milling trial, as shown in Figure 7.1.

Determining the Poincaré section variation between time intervals that chatter onsets and the reference one by using the fixed reference linear regression method, the regression coefficient values have been established at the chatter threshold. The value of regression coefficient at the onset of chatter varies between *0.69* and *0.83*.

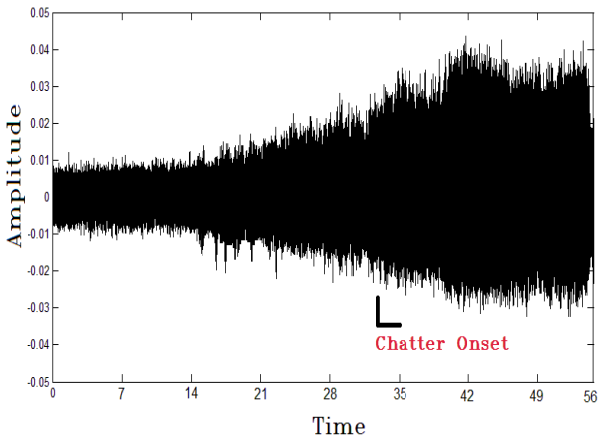

Acquired Signal during trial no. 1.

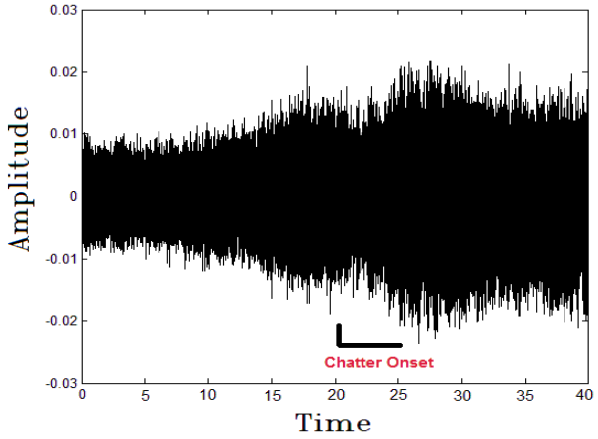

Acquired Signal during trial no. 3.

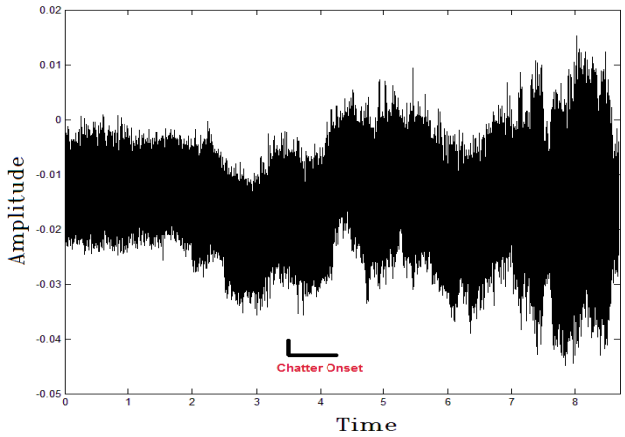

Acquired Signal during trial no. 4.

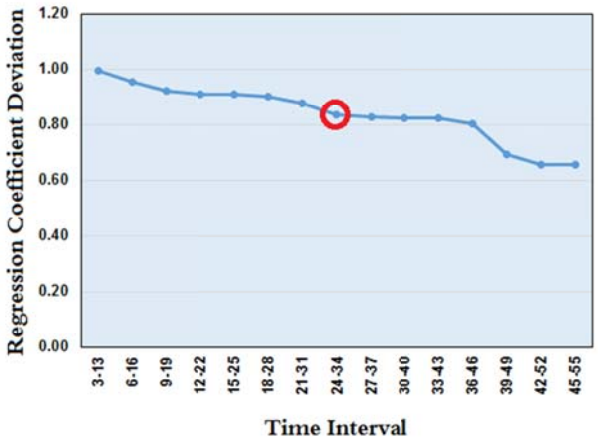

a). Trial no. 1, Onset of chatter at r=0.83

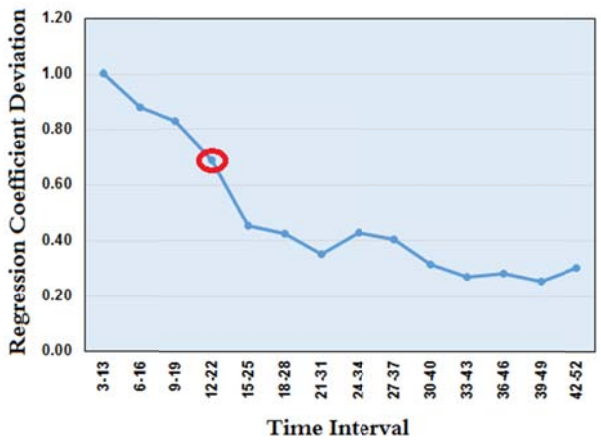

b). Trial no. 3, Onset of chatter at r= 0.69

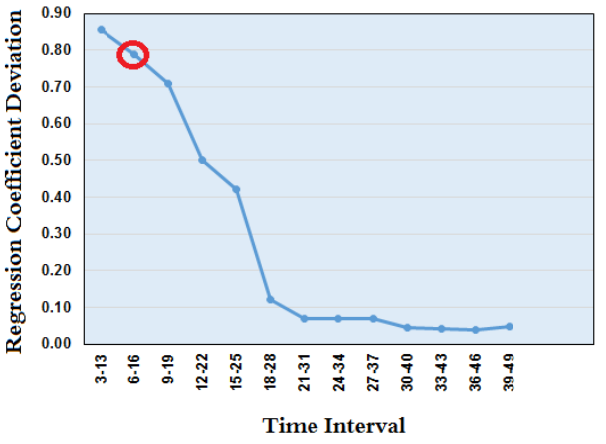

c). Trial no. 4, Onset of chatter at r=0.79

Figure 7.1(a) to (c): Regression coefficient variation during titanium cutting trials by a 6-mm with two flutes ball-nose cutter.

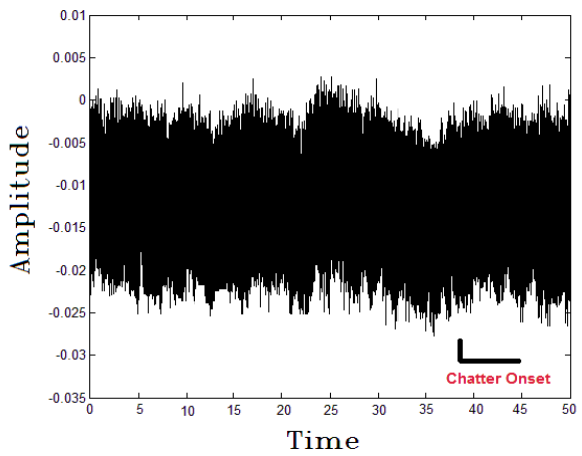

Acquired Signal during trial no. 7.

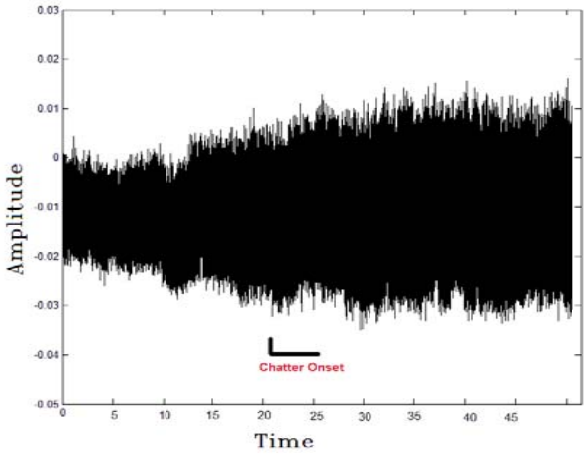

Acquired Signal during trial no. 8.

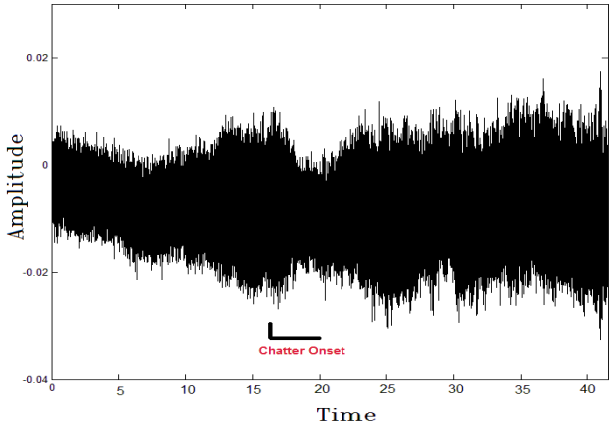

Acquired Signal during trial no. 9.

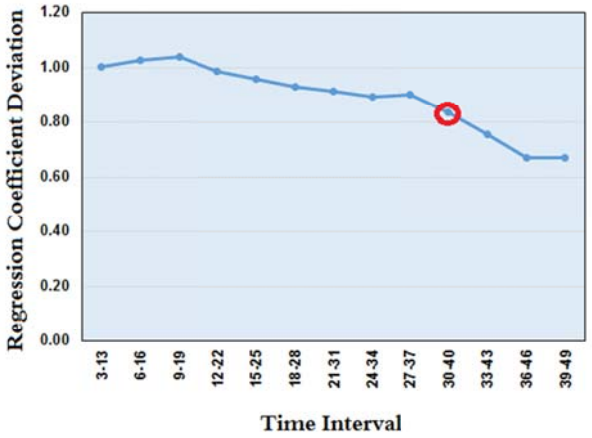

d). Trial no. 7 Onset of chatter at r=0.83

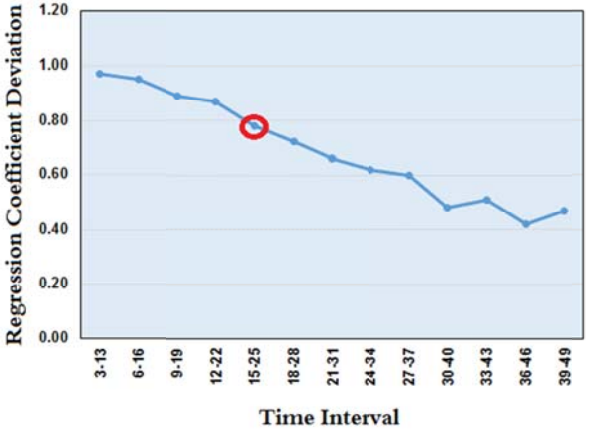

e). Trial no. 8, Onset of chatter at r=0.78

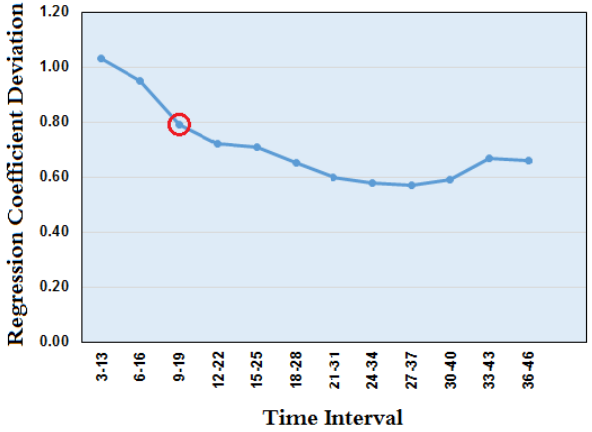

f). Trial no. 9 Onset of chatter at r=0.79

Figure 7.1 (d) to (f): Regression coefficient variation during titanium cutting trials by a 6-mm with two flutes ball-nose cutter.

7.2.1.2 End Milling

Changing the spindle speed can also affect the state of milling and change it from stable to chatter condition. An end mill must run at a constant axial depth of cut therefore, for the trials the cutting speed was varied by increasing it during the run. The cutting path is a straight slot, which is cut by different cutters with 2 and 4 flutes.

For each milling trial, the CNC code is written in a way that cutting speed continuously increases in three steps. Axial depth of cut is constant during the milling trials; and the immersion rate varies between *25%* and *75%* during the trials. The cutting parameters are shown in Tables 7.3 for a 4-flute cutter and in Table 7.4 for a 2-flute cutter.

Table 7.3: Cutting parameters for end-mill, 4 flutes, and *6 mm* cutting tool.

Test No.	V_s *(rpm)*	V_c *(mm/min)*	a_p *(mm)*	a_e *(mm)*
1	3500-4500	240-360	1.0	0.25 D
2	3500-4500	240-360	1.0	0.5 D
3	3500-4500	240-360	1.0	0.75 D

Table 7.4: Cutting parameters for end-mill, 2 flutes, and *6 mm* cutting tool.

Test No.	V_s *(rpm)*	V_c *(mm/min)*	a_p *(mm)*	a_e *(mm)*
1	3500-4500	140-180	1	0.25D
2	3500-4500	140-180	1	0.5D
3	3500-4500	140-180	1	0.75D

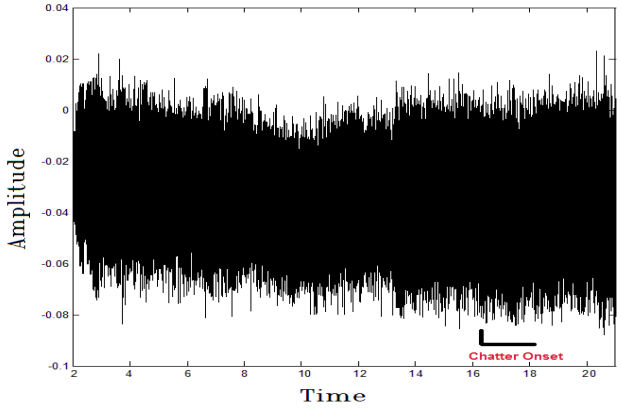

Acquired Signal during trial no. 1.

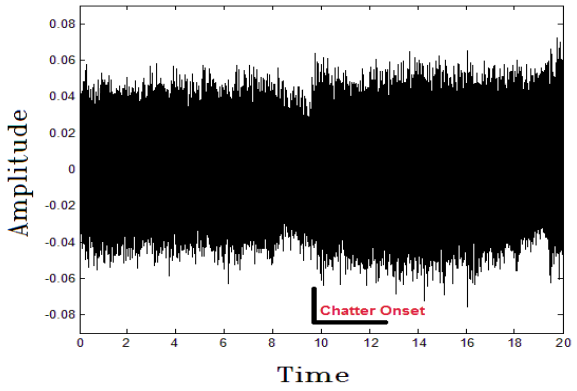

Acquired Signal during trial no. 2.

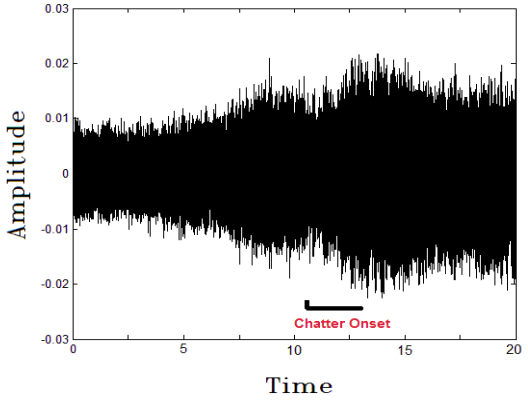

Acquired Signal during trial no. 3.

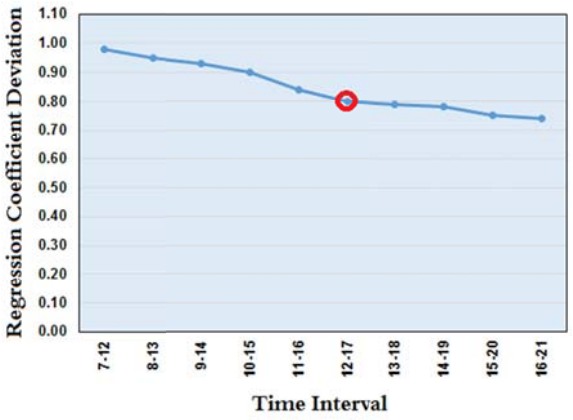

a). Trial no. 1, Onset of chatter at r=0.8

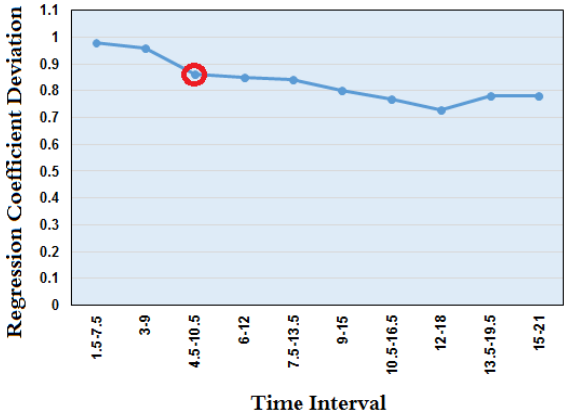

b). Trial no. 2, Onset of chatter at r= 0.86

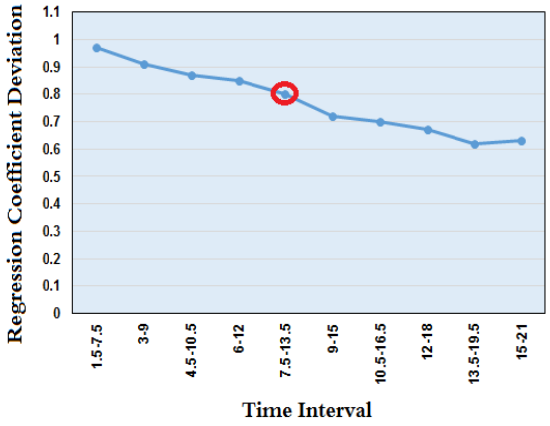

c). Trial no. 3, Onset of chatter at r=0.89

Figure 7.2: Regression coefficient variation of titanium cut using a 6-mm end-mill cutter with four flutes.

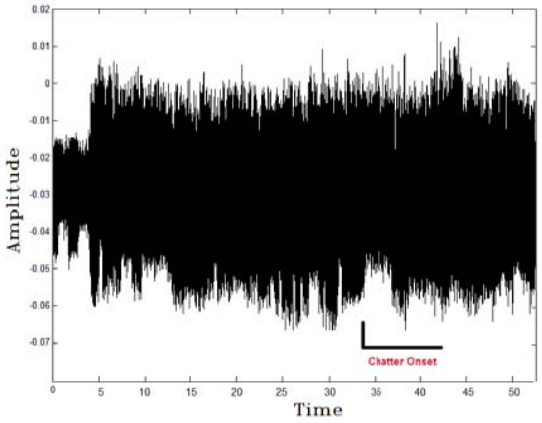

Acquired Signal during trial no. 1.

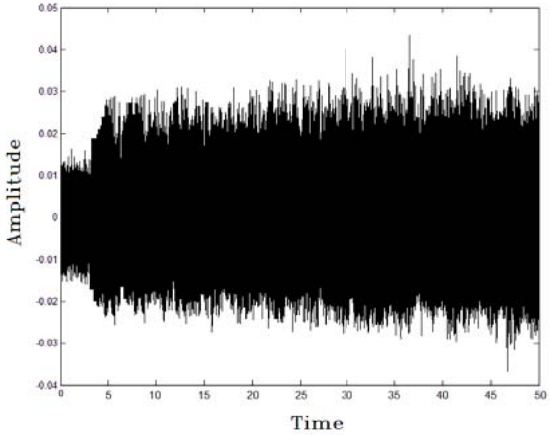

Acquired Signal during trial no. 2.

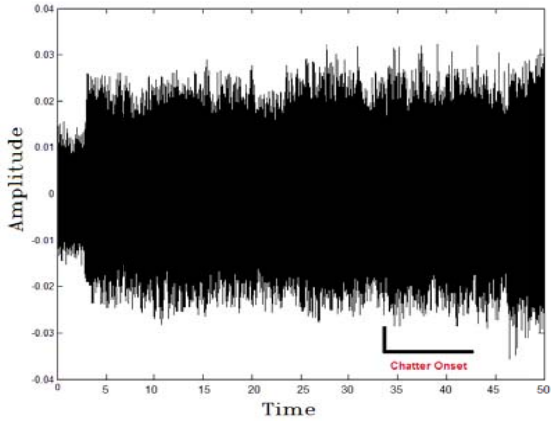

Acquired Signal during trial no. 3.

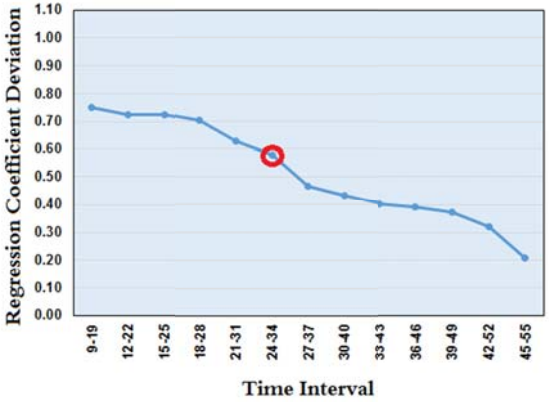

a). Trial no. 1 Onset of chatter at r=0.58

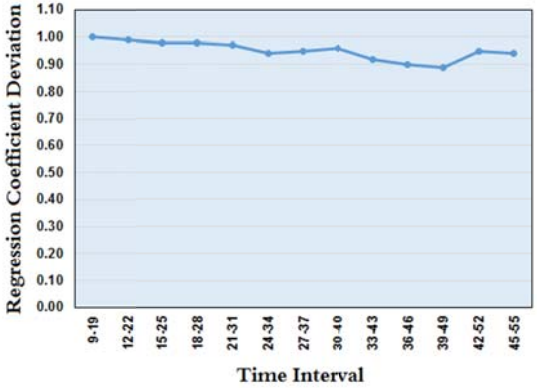

b). Trial no. 2, Stable cutting process.

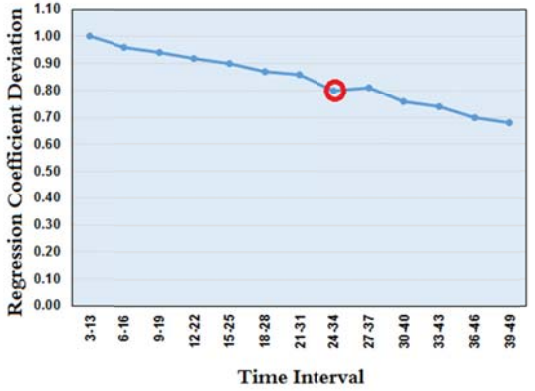

c). Trial no. 3 Onset of chatter at r=0.8

Figure 7.3: Regression coefficient variation of titanium cut using a 6-mm end-mill cutter with two flutes.

The observations from the experiments show that milling trials no. 1 ran in a stable condition. Time series are reconstructed in the form of a state vector and phase space attractor Poincaré sections related to each milling trial are plotted. Consequently, the regression coefficient is calculated and its variation is demonstrated during each milling trial, as shown in Figure 7.2. The value of the regression coefficient at the onset of chatter varies between *0.89* and *0.8*. The acquired signals during the trials are displayed in figure 7.2.

Similarly, three end-milling trials were implemented by using a 6 mm end mill cutter with 2 flutes. The acquired accelerations during the cutting trials were reconstructed and the variations of Poincaré sections are modelled by regression coefficient, which is shown in Figure 7.3. The value of regression coefficient at the onset of chatter varies between *0.58* and *0.8*. The acquired signals during trials are displayed in figure 7.3.

7.2.2 Stainless Steel

The grade of stainless steel chosen for this milling trials was Grade 316, a common and widely used grade in industry. The broad number of preliminary cutting trials determines that the occurrence of chatter during milling of stainless steel is most likely when the cutting parameters are in the range shown in Table 7.5. Similar to titanium, the milling trials are designed to have a stable process at the beginning and then move into chatter. Two milling processes were used, which were exactly the same as for titanium.

Table 7.5 Cutting parameters for chatter occurrence during milling stainless steel.

Cutting Parameters	Range
Spindle speed (V_s)	5000 rpm
Cutting Speed (V_c)	500 mm/min
Axial Depth of Cut (a_p)	0 – 2 mm
Radial Depth of Cut (a_e)	0.25 D - 0.75 D mm

7.2.2.1 Ball-Nose Milling

Two ball-nose cutting tools are used to mill stainless steel. Two sets of milling process, each set including nine milling trials, are performed to cut a stainless steel block in the form of steep slots. The cutting process starts with zero axial depth of cut, and then it is continuously increased to the final value. The immersion rate varies between *25%* and *75%* during the trials. The cutting parameters are shown in Tables 7.6 for a 4-flute cutter, and in Table 7.7 for a 2-flute cutter.

Table 7.6 Cutting parameters for a ball-nose, 4 flutes, and 6 mm cutting tool.

Test No.	V_s *(rpm)*	V_c *(mm/min)*	a_p *(mm)*	a_e *(mm)*
1	4500	450	0-2	0.25D
2	4500	450	0-2	0.50D
3	4500	450	0-2	0.75D
4	5000	500	0-2	0.25D
5	5000	500	0-2	0.50D
6	5000	500	0-2	0.75D
7	5500	550	0-2	0.25D
8	5500	550	0-2	0.50D
9	5500	550	0-2	0.75D

The acceleration signal in the form of time series is reconstructed to a state vector and the related phase space attractor Poincaré sections are plotted for each trial. Fixed reference linear regression models the variation of Poincaré sections during each milling trial, as discussed previously.

Table 7.7 Cutting parameters for a ball-nose, 2 flutes, and 6 mm cutting tool.

Test No.	V_s *(rpm)*	V_c *(mm/min)*	a_p *(mm)*	a_e *(mm)*
1	4500	400	0-1.5	0.25D
2	4500	400	0-1.5	0.5D
3	4500	400	0-1.5	0.75D
4	5000	450	0-1.5	0.25D
5	5000	450	0-1.5	0.5D
6	5000	450	0-1.5	0.75D
7	5500	495	0-1.5	0.25D
8	5500	495	0-1.5	0.5D
9	5500	495	0-1.5	0.75D

Considering milling trials with 6mm ball-nose cutter with 4 flutes, milling trials no. 3, 5, also 6 and 9 ran stable. While for trials 1, 2, 4, 7, and 8 chatter did occur and for these trials, the value of the regression coefficient at the onset of chatter varies between *0.64* and *0.8*, while its variation is demonstrated for different cutting trials in Figure 7.4. Consequently, the variation of regression coefficient is demonstrated in Figure 7.5 for cutting of stainless steel with 2 flutes cutter shows chatter did occur for trials 1, 3, 6, 7, and 9 and its variation is between *0.6* and *0.82*; hence milling trials no. 2, 4, 5, and 8 are stable.

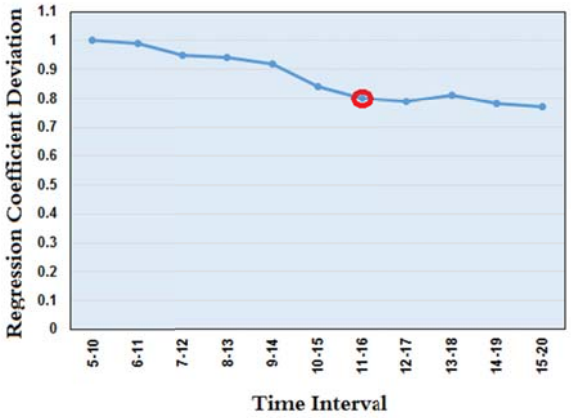

a). Trial no. 1, Onset of chatter at *r=0.8*

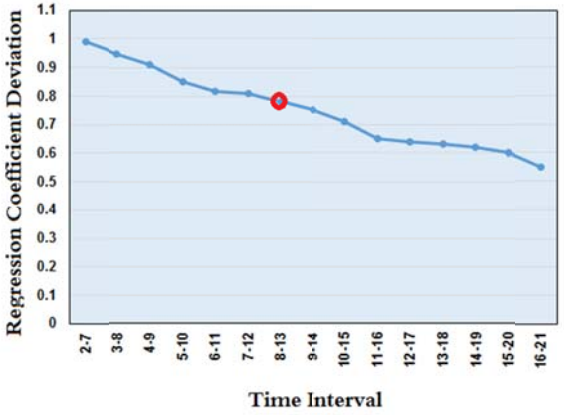

b). Trial no. 2, Onset of chatter at *r*= 0.78

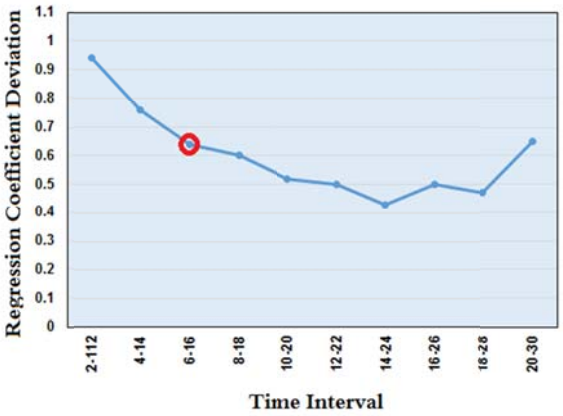

c). Trial no. 4, Onset of chatter at *r=0.64*

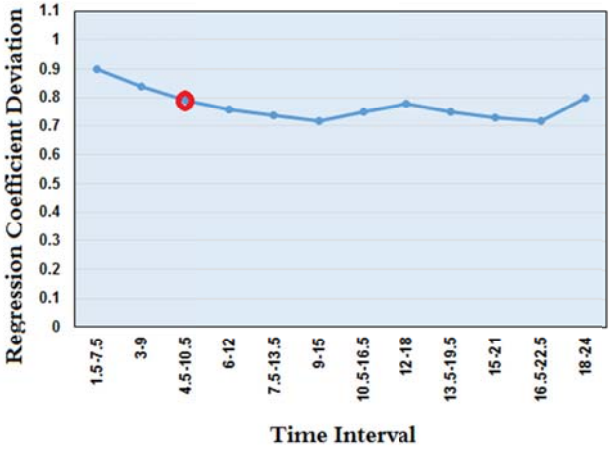

d). Trial no. 7 Onset of chatter at r=0.79

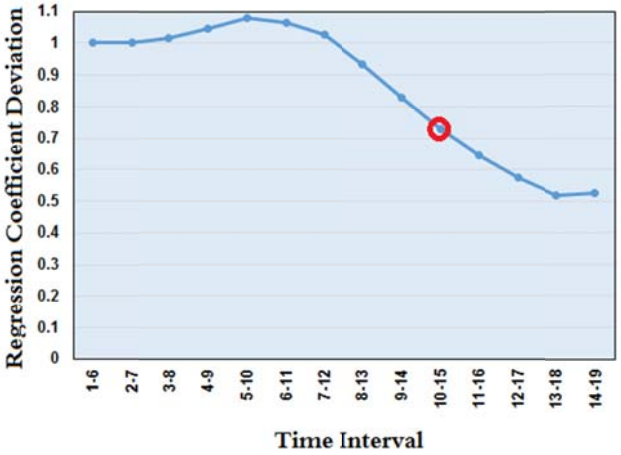

e). Trial no. 8, Onset of chatter at r=0.73

Figure 7.4: Regression coefficient variation along stainless steel milling trials by a 6-mm and four flutes ball-nose cutter.

a). Trial no. 1, Onset of chatter at *r=0.82*

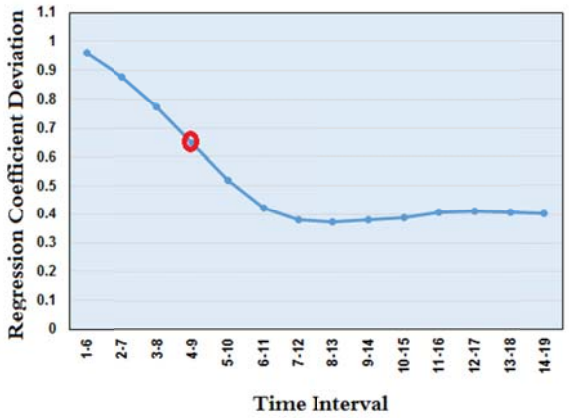

b). Trial no. 3, Onset of chatter at *r*= 0.64

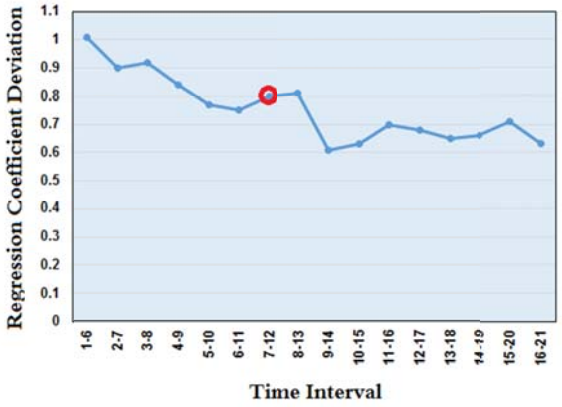

c). Trial no. 6, Onset of chatter at *r=0.8*

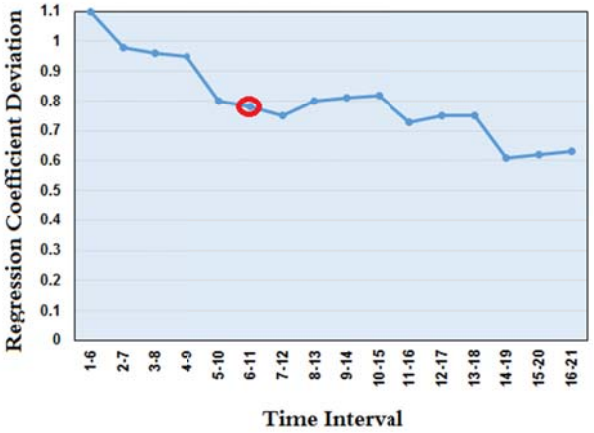

d). Trial no. 7 Onset of chatter at r=0.78

e). Trial no. 9, Onset of chatter at r=0.6

Figure 7.5: Regression coefficient variation along stainless steel milling trials by a 6-mm and two flutes ball-nose cutter.

7.2.2.2 End-Milling

Changing the spindle speed can also affect the state of milling and change it from stable to chatter condition. An end mill must run at a constant depth therefore, for the trials the cutting speed was varied by increasing it during the run. The cutting path is a straight slot, which is cut by different cutters with two and four flutes.

For each milling trial, the CNC code is written in a way that cutting speed continuously increases in 3 steps. Axial depth of cut is constant during the milling trials; and the immersion rate varies between *25%* and *75%* during the trials. The cutting parameters are similar for both two and four flutes cutters. So, one Table 7.8 demonstrates the cutting parameters for both sets of milling trials.

Table 7.8: Cutting parameters for 6 mm cutting tool.

Test No.	V_s *(rpm)*	V_c *(mm/min)*	a_p *(mm)*	a_e *(mm)*
1	5000-6000	500-600	1.5	0.25D
2	5000-6000	500-600	1.5	0.5D
3	5000-6000	500-600	1.5	0.75D

Similarly, the regression coefficient is calculated and its variation is determined during each milling trial, as shown in Figure 7.6 (a) to (c). The value of regression coefficient at the onset of chatter varies between *0.89* and *0.86*. A 6-mm end-mill cutter with two flutes is also used. The variation of regression coefficient is shown in Figure 7.6 (d) to (f), which varies between *0.85* and *0.82*.

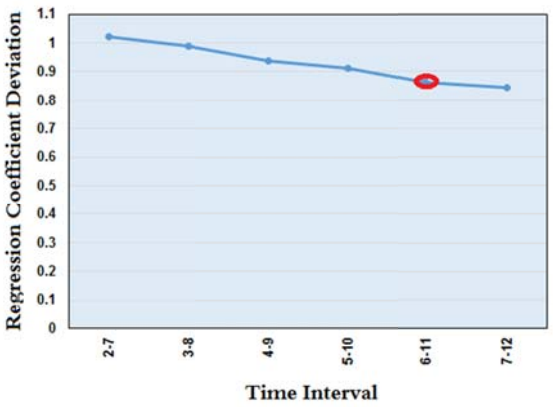

a). Trial no. 1, Onset of chatter at *r=0.86*

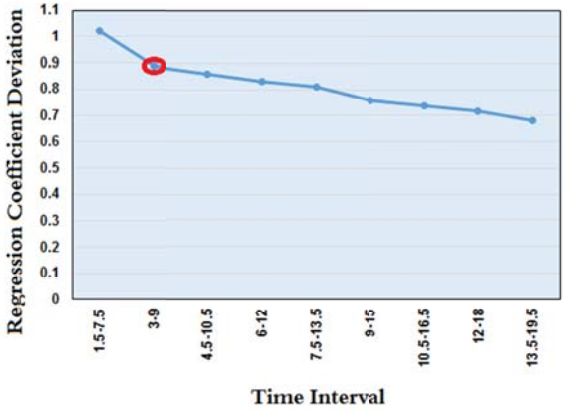

b). Trial no. 2, Onset of chatter at *r*= 0.89

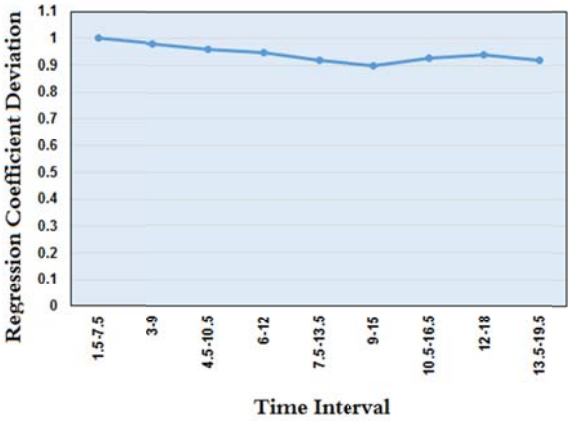

c). Trial no. 3, Stable Process.

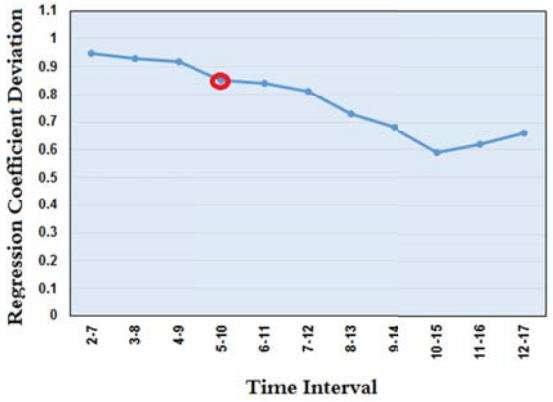

d). Trial no. 1 Onset of chatter at r=0.84

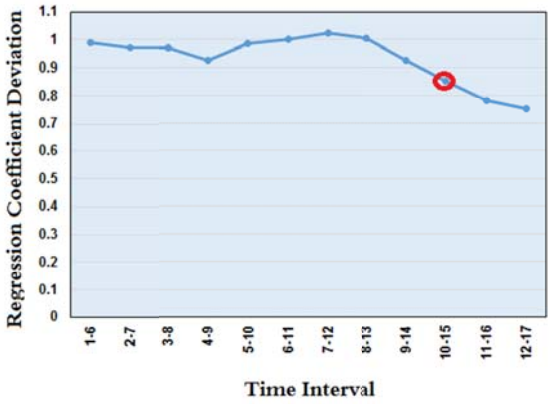

e). Trial no. 2, Onset of chatter at r=0.85

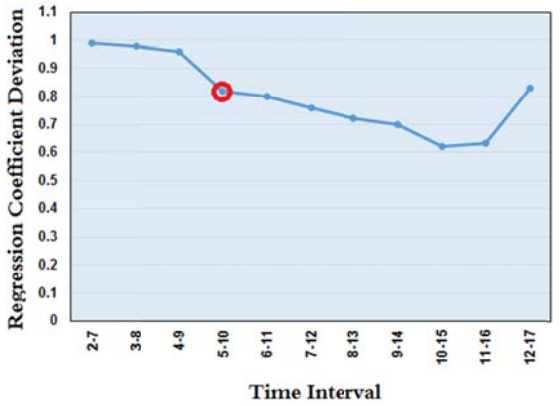

f). Trial no. 3 Onset of chatter at r=0.82

Figure 7.6 Regression coefficient variation for: a) to c). A 6-mm end-mill cutter with 4 flutes. d) to f): with 2 flutes.

7.2.3 Aluminium

The preliminary milling trials of aluminium material determined that the occurrence of chatter is most likely when the milling parameters are in the range shown in Table 7.9.

Table 7.9 the milling parameters for chatter occurrence during milling aluminium.

Cutting Parameters	Range
Spindle speed (V_s)	8500 rpm
Cutting Speed (V_c)	150 mm/min
Axial Depth of Cut (a_p)	0 – 2 mm
Radial Depth of Cut (a_e)	0.25 D - 0.75 D mm

Similar to experiment design developed for other two materials, two milling processes are also designed to cut the aluminium. Axial depth of cut varies during the ball-nose process, and cutting speed changes during end-mill process. Furthermore, cutting tools with *4 mm* and *6 mm* diameter are used for each milling process. They have a different numbers of flutes, two and four flutes.

7.2.3.1 Ball-Nose Milling Process

To cut an inclined slot, two ball-nose cutting tools are used to cut aluminium. The cutters are both *6 mm* in diameter and with two and four flutes.

Two sets of milling process, each set including nine milling trials, are performed. The immersion rate varies between *25%* and *75%* during the trials. The cutting parameters are shown in Tables 7.10 for a 4-flute cutter, also in Table 7.11 for a 2-flute cutter. Furthermore, the value of regression

coefficient at the onset of chatter is displayed in the tables for each milling process.

Table 7.10: Cutting parameters for a ball-nose, 4 flutes, and 6 mm cutting tool.

Test No.	V_s *(rpm)*	V_c *(mm/min)*	a_p *(mm)*	a_e *(mm)*	α
1	8000	1000	0-3	0.25D	0.81
2	8000	1000	0-3	0.5D	0.78
3	8000	1000	0-3	0.75D	Stable
4	9000	1125	0-3	0.25D	0.63
5	9000	1125	0-3	0.5D	0.57
6	9000	1125	0-3	0.75D	0.79
7	9800	1225	0-3	0.25D	0.77
8	9800	1225	0-3	0.5D	0.76
9	9800	1225	0-3	0.75D	0.79

Considering the regression model between time intervals that chatter onsets and the reference one, the value of regression coefficient indicates chatter threshold. The value of regression coefficient at the onset of chatter varies between *0.57* and *0.81* when aluminium cuts with four flutes cutter; and it is between *0.54* and *0.77* for a 2-flute cutter.

Table 7.11: Cutting parameters for a ball-nose, 2 flutes, and 6 mm cutting tool.

Test No.	V_s *(rpm)*	V_c *(mm/min)*	a_p *(mm)*	a_e *(mm)*	α
1	8000	1000	0-3	0.25D	Stable
2	8000	1000	0-3	0.5D	"
3	8000	1000	0-3	0.75D	"
4	9000	1125	0-3	0.25D	0.54
5	9000	1125	0-3	0.5D	0.68
6	9000	1125	0-3	0.75D	0.75
7	9500	1187	0-3	0.25D	0.77
8	9500	1187	0-3	0.5D	0.63
9	9500	1187	0-3	0.75D	0.72

7.2.3.2 End-Millings

Similar to other two materials, an end-mill milling process was designed to cut aluminium. In the milling trials, axial depth of cut is constant and cutting speed varies along the cutting trial. The cutting path is a straight slot, which is cut with two different cutting tools, with two and four flutes.

Two sets of milling process, each set including three milling trials, were performed to cut slots in aluminium blocks. Axial depth of cut is constant during the milling trials; hence the immersion rate varies between *25%* and *75%* during the trials. The milling parameters are shown in Tables 7.12 for a 4-flute cutter, and in Table 7.13 for a 2-flute cutter. Furthermore, the value of regression coefficient at the onset of chatter is displayed in the tables for each milling process.

Table 7.12: Cutting parameters for end-mill, 4 flutes, and 4 mm cutting tool.

Test No.	V_s *(rpm)*	V_c *(mm/min)*	a_p *(mm)*	a_e *(mm)*	α
1	8000-9800	800-980	3 mm	0.25D	0.89
2	8000-9800	800-980	3 mm	0.5D	0.59
3	8000-9800	800-980	3 mm	0.75D	0.84

Table 7.13: Cutting parameters for end-mill, 2 flutes, and 6 mm cutting tool.

Test No.	V_s *(rpm)*	V_c *(mm/min)*	a_p *(mm)*	a_e *(mm)*	α
1	8000-9500	800	2	0.25D	0.52
2	"	"	"	0.5D	0.84
3	"	"	"	0.75D	0.86

The regression coefficient variation is demonstrated during each milling trial, as shown in Figure 7.18 (a) to (c). The value of the regression coefficient at the onset of chatter varies between *0.59* and *0.89*. Similarly, three end-milling trials were completed using a 6-mm end mill cutter with two flutes. The value of regression coefficient at the onset of chatter varied between *0.52* and *0.86*.

7.3 Analysing milling trials cut with a 4-mm cutter

At this stage, all procedures were repeated for the three materials with a 4-mm cutting tool. The aim was to determine the effect of milling tool diameter on the chatter threshold boundary. Additionally two and four flutes cutting tools were used.

7.3.1 Titanium

7.3.1.1 Ball-nose Milling Process

Similar to the previous section, two sets of milling processes each set including nine milling trials were performed. A cutting tool with *4 mm* diameter is used to cut steep slots in the block of titanium. The axial depth of cut varied between *0* and *1 mm*; hence the immersion rate varies between *25%* and *75%* during the trials. The milling parameters are shown in Tables 7.14 for a 4-flute cutter and in Table 7.15 for a 2-flute cutter.

Table 7.14: Cutting parameters for a ball-nose, 4 flutes, and 4 mm cutting tool.

Test No.	V_s *(rpm)*	V_c *(mm/min)*	a_p *(mm)*	a_e *(mm)*
1	3500	175	0-1	0.25D
2	3500	175	0-1	0.5D
3	3500	175	0-1	0.75D
4	4000	200	0-1	0.25D
5	4000	200	0-1	0.5D
6	4000	200	0-1	0.75D
7	4500	225	0-1	0.25D
8	4500	225	0-1	0.5D
9	4500	225	0-1	0.75D

a). Trial no. 3, Onset of chatter at *r=0.86*

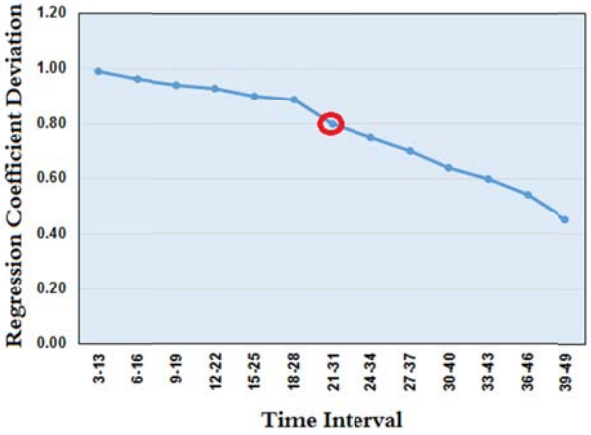

b). Trial no. 4, Onset of chatter at *r*= 0.80

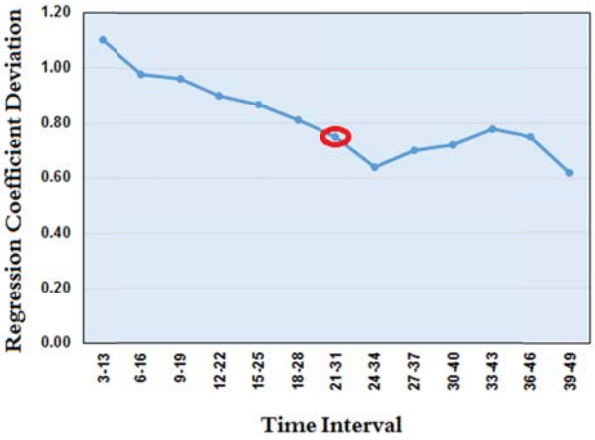

c). Trial no. 6, Onset of chatter at *r=0.75*

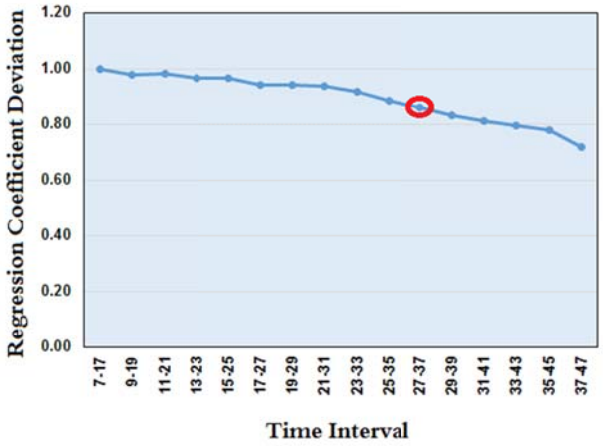

d). Trial no. 8 Onset of chatter at *r=0.85*

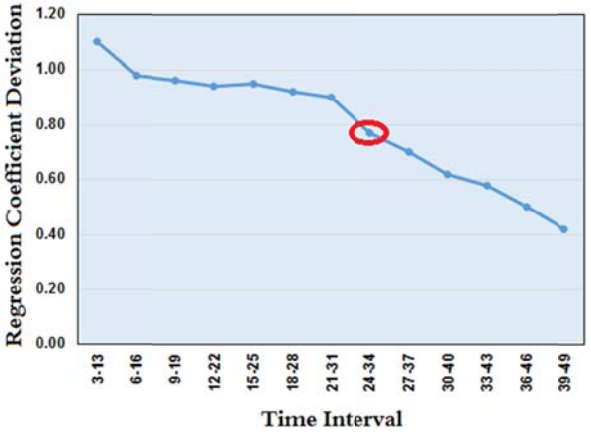

e). Trial no. 9, Onset of chatter at *r=0.77*

Figure 7.7: Regression coefficient variation along titanium milling trials by a 4-mm and four flutes ball-nose cutter.

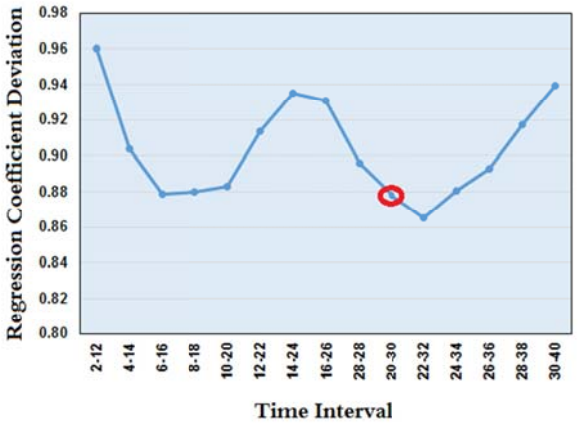

a). Trial no. 1, Onset of chatter at *r=0.88*

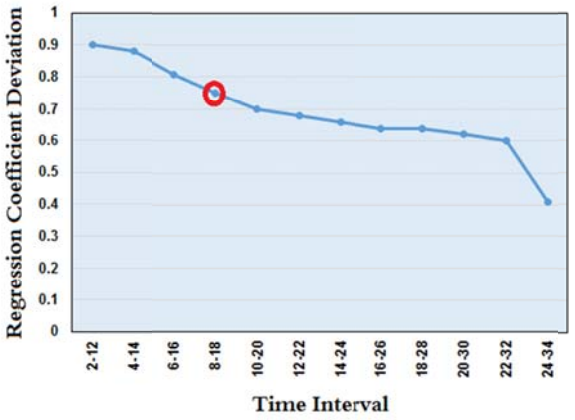

b). Trial no. 4, Onset of chatter at *r*= 0.75

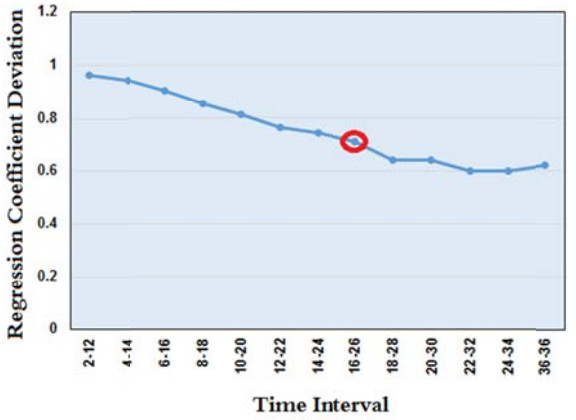

c). Trial no. 5, Onset of chatter at *r=0.71*

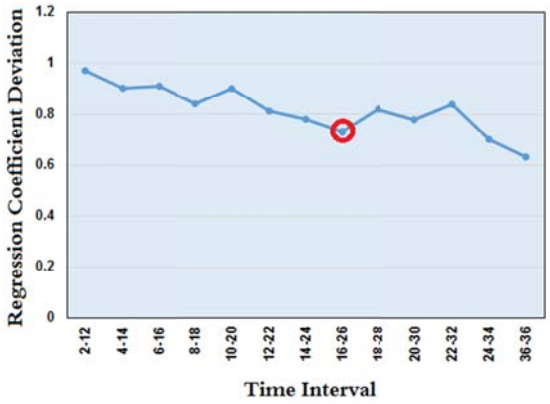

d). Trial no. 6 Onset of chatter at *r=0.73*

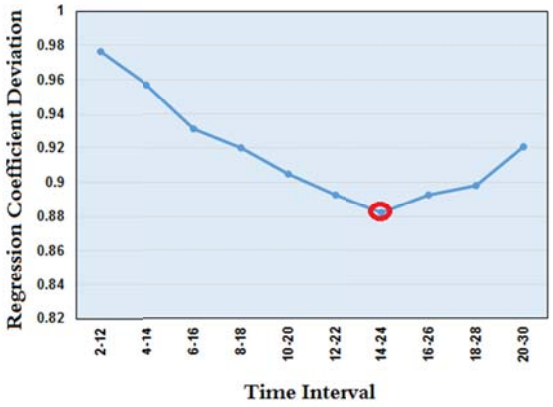

e). Trial no. 7, Onset of chatter at *r=0.87*

Figure 7.8: Regression coefficient variation along titanium milling trials by a 4-mm and two flutes ball-nose cutter.

Table 7.15: Cutting parameters for a ball-nose, 2 flutes, and 4 mm cutting tool.

Test No.	V_s *(rpm)*	V_c *(mm/min)*	a_p *(mm)*	a_e *(mm)*
1	3000	180	0-1	0.25D
2	3000	180	0-1	0.5D
3	3000	180	0-1	0.75D
4	4000	240	0-1	0.25D
5	4000	240	0-1	0.5D
6	4000	240	0-1	0.75D
7	4500	315	0-1.5	0.25D
8	4500	315	0-1.5	0.5D
9	4500	315	0-1.5	0.75D

Similarly, the acquired time series are reconstructed and the related phase space attractor Poincaré sections are plotted. Consequently, the fixed reference linear regression models the variation of Poincaré sections during each milling trial. The milling trials with a 4-flute cutter, trials no. 1, 2, 5, and 7 ran in stable condition. The regression coefficient is calculated and its variation is demonstrated during each milling trial, as shown in Figure 7.7 for cuts are implemented by four flutes cutting tool. The value of the regression coefficient at the onset of chatter varies between *0.75* and *0.87* for milling trials carried out by a 4-flute cutting tool.

Figure 7.8 demonstrates the variation of regression coefficients for cutting trials with a 2-flute cutter. The regression coefficient for chatter onset varied between *0.71* and *0.87*. While, milling trials no. 2, 3, 8 and 9 ran in stable state.

7.3.1.2 End Milling

Two sets of milling processes, each set including three milling trials, were performed on a titanium block with a 4-mm cutting tool. Similar to the *6 mm* end-mill cutter, axial depth of cut is constant during the milling trials. The cutting parameters are shown in Tables 7.16 for a 4-flute cutter, also in Table 7.17 for a 2-flute cutter.

Table 7.16: Cutting parameters for end-mill, 4 flutes, and 4 mm milling tool.

Test No.	V_s *(rpm)*	V_c *(mm/min)*	a_p *(mm)*	a_e *(mm)*
1	3500-4500	175	0-1	0.25D
2	3500-4500	175	0-1	0.5D
3	3500-4500	175	0-1	0.75D

Table 7.17: Cutting parameters for end-mill, 2 flutes, and 4 mm cutting tool.

Test No.	V_s *(rpm)*	V_c *(mm/min)*	a_p *(mm)*	a_e *(mm)*
1	4000-4800	160	1	0.25
2	4000-4800	160	1	0.5D
3	4000-4800	160	1	0.75D

For each milling trial, the CNC code is written in a way that milling speed continuously increases in 3 steps. Time series are reconstructed in the form of a state vector and phase space attractor Poincaré sections related to each cutting process being plotted. Consequently, the regression coefficient is calculated and its variation is demonstrated during each milling trial, as shown in Figure 7.9 (a) to (c). The value of regression coefficient at the onset of chatter varies between *0.63* and *0.83*.

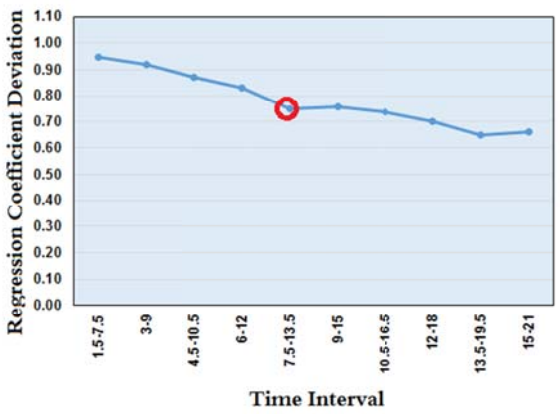

a). Trial no. 1, Onset of chatter at *r=0.75*

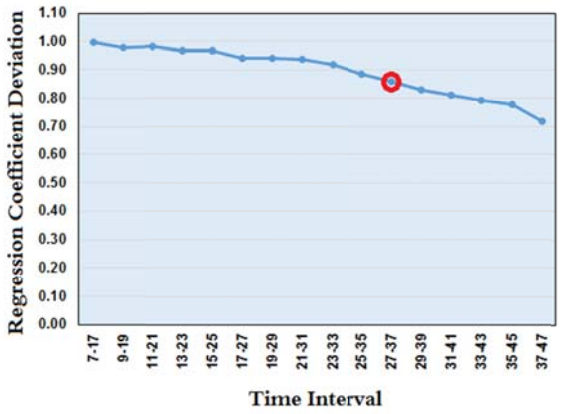

b). Trial no. 2, Onset of chatter at *r*= 0.84

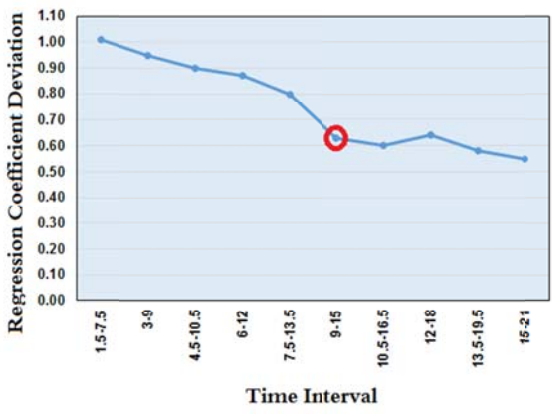

c). Trial no. 3, Onset of chatter at *r=0.63*

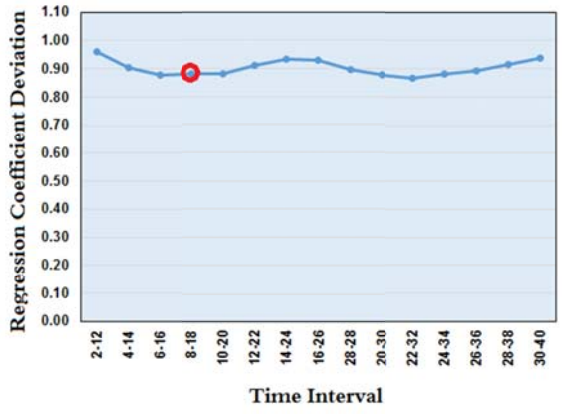

d). Trial no. 1 Onset of chatter at *r=0.89*

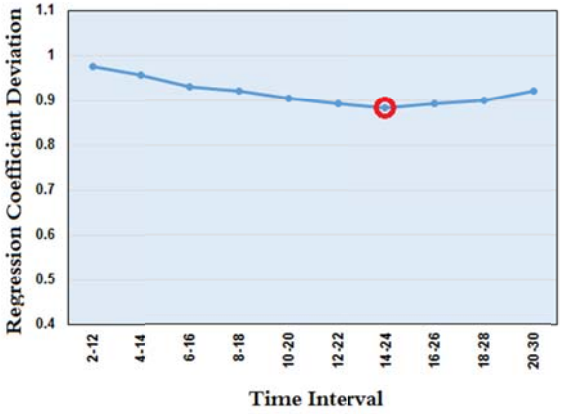

e). Trial no. 2, Onset of chatter at *r=0.88*

f). Trial no. 3 Onset of chatter at *r=0.74*

Figure 7.9 Regression coefficient variation for: a) to c). A 4-mm end-mill cutter with 4 flutes. d) to f): with 2 flutes.

Similarly, three end-milling trials were carried out by using a 4 mm end mill cutter with 2 flutes. The acquired accelerations during the cutting trials were reconstructed and the variations of Poincaré sections are modelled by regression coefficient, which are shown in Figure 7.9 (d) to (f).The value of regression coefficient at the onset of chatter varies between *0.74* and *0.89*.

7.3.2 Stainless Steel

7.3.2.1 Ball-nose Milling

A cutting tool with 4mm diameter is used to cut inclined slots in the block of stainless steel. The axial depth of cut varies between *0* and *1.5 mm*; hence the immersion rate varies between *25%* and *75%* during the trials. The cutting parameters are shown in Tables 7.18 for a 4-flute cutter, also in Table 7.19 for a 2-flute cutter.

Table 7.18 Cutting parameters for a ball-nose, 4 flutes, and 4 mm cutting tool.

Test No.	V_s *(rpm)*	V_c *(mm/min)*	a_p *(mm)*	a_e *(mm)*
1	4500	450	0-1.5	0.25D
2	4500	450	0-1.5	0.5D
3	4500	450	0-1.5	0.75D
4	5000	500	0-1.5	0.25D
5	5000	500	0-1.5	0.5D
6	5000	500	0-1.5	0.75D
7	5500	550	0-1.5	0.25D
8	5500	550	0-1.5	0.5D
9	5500	550	0-1.5	0.75D

Table 7.19 Cutting parameters for a ball-nose, 2 flutes, and 4 mm cutting tool.

Test No.	V_s *(rpm)*	V_c *(mm/min)*	a_p *(mm)*	a_e *(mm)*
1	3000	180	0-1	0.25D
2	3000	180	0-1	0.5D
3	3000	180	0-1	0.75D
4	4000	240	0-1	0.25D
5	4000	240	0-1	0.5D
6	4000	240	0-1	0.75D
7	4500	315	0-1.5	0.25D
8	4500	315	0-1.5	0.5D
9	4500	315	0-1.5	0.75D

Similarly, the acquired time series are reconstructed and the phase space attractor Poincaré sections related to each milling process are plotted. Consequently, the fixed reference linear regression models the variation of Poincaré sections during each milling trial. The regression coefficient is calculated and its variation is demonstrated during each milling trial, as shown in Figure 7.10 for cuts carried out by a 4-flute cutting tool, and Figure 7.11 for a 2-flute cutter. The value of regression coefficient at the onset of chatter varies between *0.57* and *0.79* for cutting trials implemented by a 4-flute cutting tool; and it varies between *0.75* and *0.82* for cutting trials implemented by a 2-flute cutting tool.

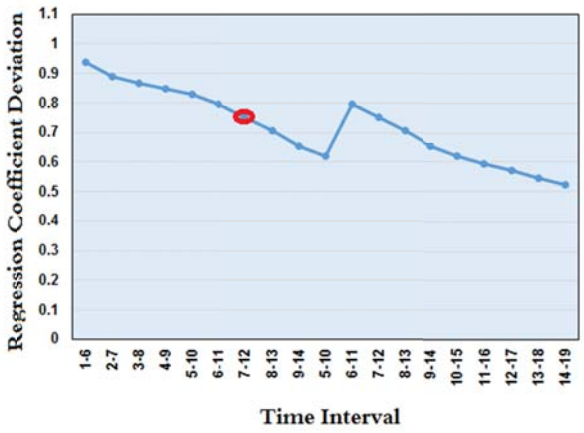

a). Trial no. 1, Onset of chatter at $r=0.75$

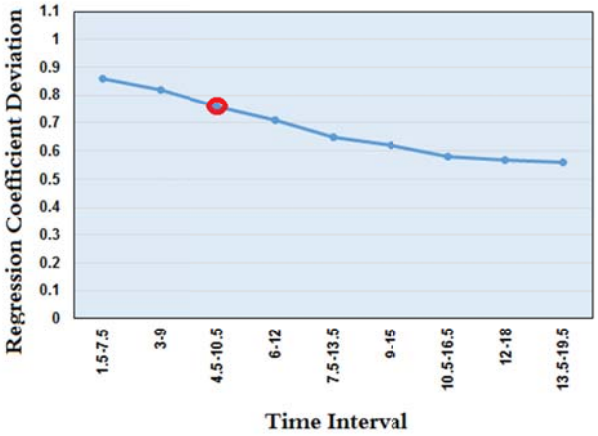

b). Trial no. 2, Onset of chatter at $r= 0.76$

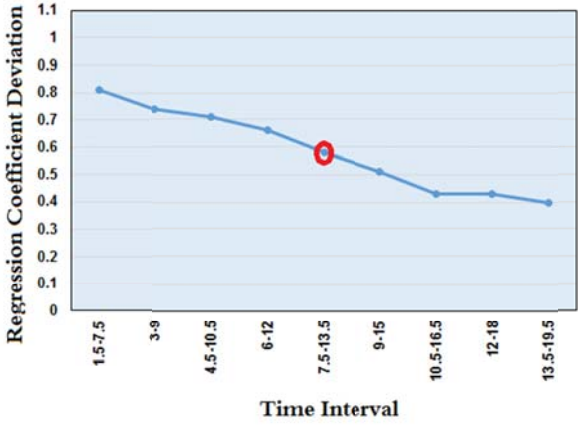

c). Trial no. 3, Onset of chatter at $r=0.57$

d). Trial no. 4 Onset of chatter at $r=0.74$

e). Trial no. 9, Onset of chatter at $r=0.79$

Figure 7.10: Regression coefficient variation along milling trials of stainless steel with a ball-nose, *4 mm* with four flutes cutter.

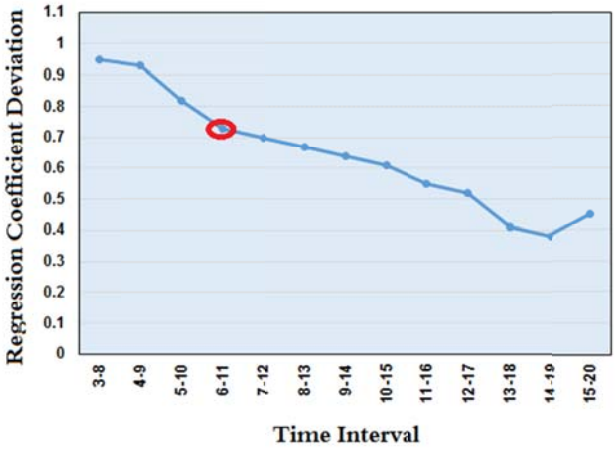

a). Trial no. 2, Onset of chatter at *r=0.75*

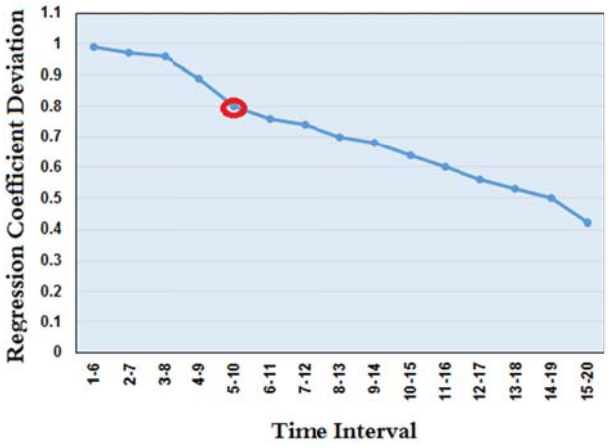

b). Trial no. 6, Onset of chatter at *r=0.8*

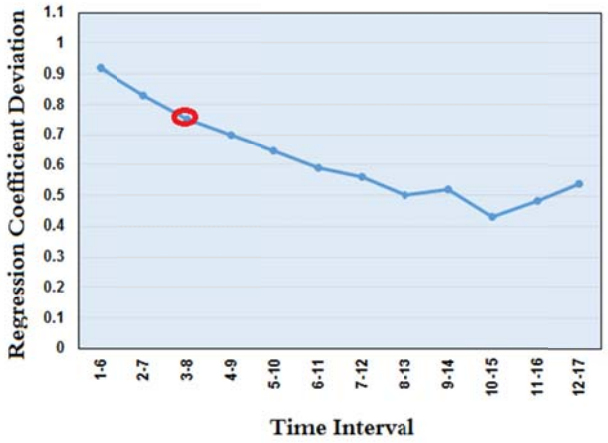

c). Trial no. 8 Onset of chatter at *r=0.76*

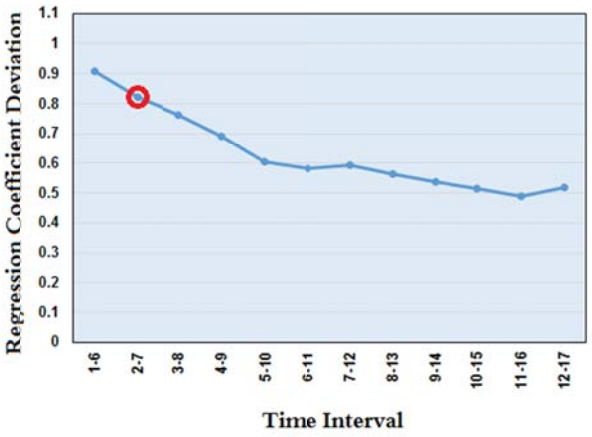

d). Trial no. 9, Onset of chatter at *r=0.82*

Figure 7.11: Regression coefficient variation along milling trials of stainless steel with a ball-nose, *4 mm* with two flutes cutter.

7.3.2.2 End-Milling

Two sets of milling process, each set including three milling trials, were carried out on stainless steel with a 4-mm cutting tool. Similar to *6 mm* end-mill cutter, axial depth of cut is constant during the milling trials. The cutting parameters are shown in Tables 7.20 for a 4-flute cutter, also in Table 7.21 for a 2-flute cutter.

Table 7.20: Cutting parameters for end-mill, 4 flutes, and 4 mm cutting tool.

Test No.	V_s *(rpm)*	V_c *(mm/min)*	a_p *(mm)*	a_e *(mm)*
1	4500-5500	360-435	1	0.25D
2	4500-5500	360-435	1	0.5D
3	4500-5500	360-435	1	0.75D

Table 7.21: Cutting parameters for end-mill, 2 flutes, and 4 mm cutting tool.

Test No.	V_s *(rpm)*	V_c *(mm/min)*	a_p *(mm)*	a_e *(mm)*
1	4500-5400	315-380	0.7	0.25D
2	4500-5400	315-380	0.7	0.5D
3	4500-5400	315-380	0.7	0.75D

The regression coefficient is calculated and its variation is determined during each milling trial, as shown in Figure 7.12 (a) to (c). The value of regression coefficient at the onset of chatter varies between *0.64* and *0.81*.

Similarly, three end-milling trials were carried out by using a 4 mm end mill cutter with two flutes. The variations of Poincaré sections are modelled by regression coefficient, which is shown in Figure 7.12 (d) to (f).The value of the regression coefficient at the onset of chatter varies between *0.56* and *0.84*.

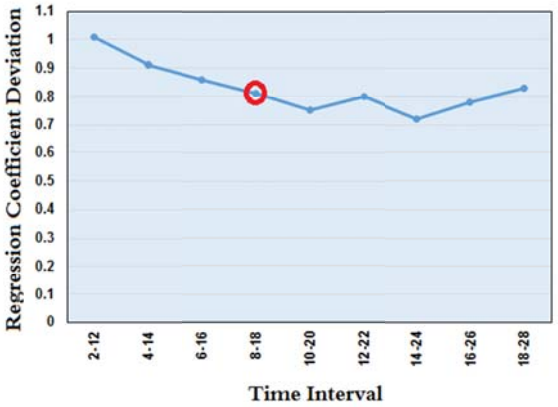

a). Trial no. 1, Onset of chatter at *r=0.81*

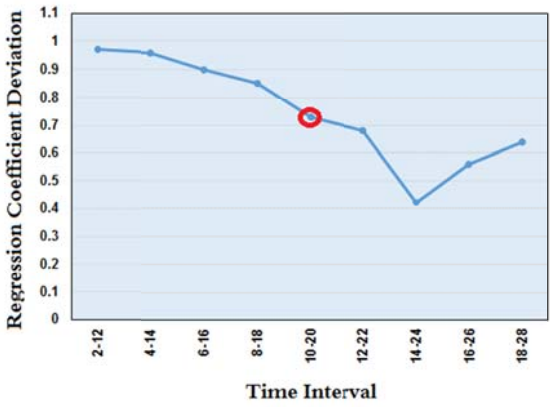

b). Trial no. 2, Onset of chatter at *r*= 0.73

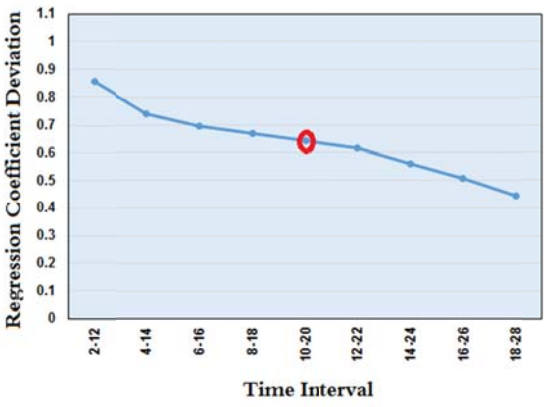

c). Trial no. 3, Onset of chatter at *r=0.64*

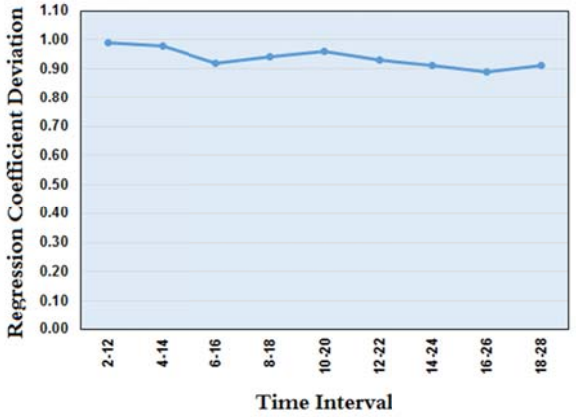

d). Trial no. 1 Stable milling process.

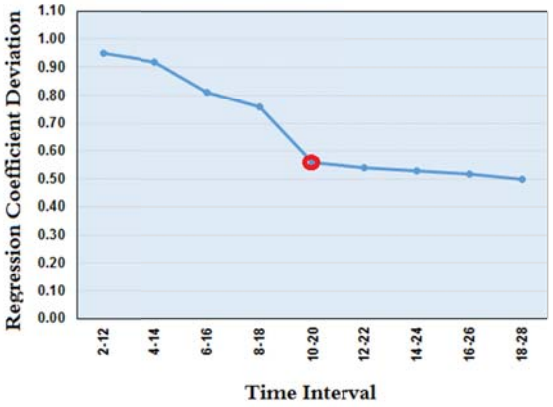

e). Trial no. 2, Onset of chatter at *r=0.56*

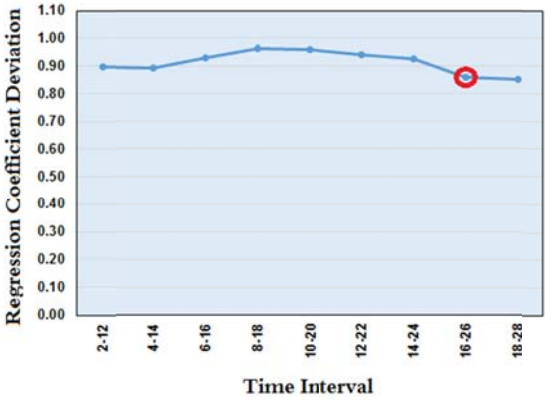

f). Trial no. 3 Onset of chatter at *r=0.84*

Figure 7.12 Regression coefficient variation for: a) to c). *4 mm* end-mill cutter with 4 flutes. d) to f): with 2 flutes.

7.3.3 Aluminium

7.3.3.1 Ball-nose Milling

Two sets of milling process were also performed with a 4-mm cutter. The immersion rate also varies between *25%* and *75%* during the trials. The cutting parameters are shown in Tables 7.22 for a 4-flute cutter, also in Table 7.23 for a 2-flute cutter. Furthermore, the value of regression coefficient at the onset of chatter is displayed in the tables for each milling process.

Table 7.22: Cutting parameters for a ball-nose, 4 flutes, and 4 mm cutting tool.

Test No.	V_s *(rpm)*	V_c *(mm/min)*	a_p *(mm)*	a_e *(mm)*	α
1	7500	750	0-2	0.25D	Stable
2	"	"	"	0.5D	"
3	"	"	"	0.75D	"
4	8500	1275	0-2	0.25D	0.84
5	"	"	"	0.5D	0.8
6	"	"	"	0.75D	0.82
7	9000	1350	0-2	0.25D	0.86
8	"	"	"	0.5D	Stable
9	"	"	"	0.75D	0.63

The value of the regression coefficient at the onset of chatter varies between *0.63* and *0.86* when aluminium cuts with four flutes cutter; and it is between *0.61* and *0.8* for a 2-flute cutter.

Table 7.23: Cutting parameters for a ball-nose, 2 flutes, and 4 mm cutting tool.

Test No.	V_s *(rpm)*	V_c *(mm/min)*	a_p *(mm)*	a_e *(mm)*	α
1	8000	1200	0-2	0.25D	Stable
2	"	"	"	0.5D	0.61
3	"	"	"	0.75D	Stable
4	8500	1275	0-2	0.25D	0.8
5	"	"	"	0.5D	Stable
6	"	"	"	0.75D	Stable
7	9000	1350	0-2	0.25D	0.72
8	"	"	"	0.5D	0.79
9	"	"	"	0.75D	0.64

7.3.3.2 End-Milling

Two sets of milling process, each set including three milling trials, are carried out in aluminium blocks. Similar cutting parameters are used during cutting aluminium with cutters with different flutes, which is shown in Tables 7.24 and 7.25. Furthermore, the value of regression coefficient at the onset of chatter is displayed in the tables for each milling process.

Table 7.24: Cutting parameters for 4 mm end-mill cutters with 4 flutes.

Test No.	V_s *(rpm)*	V_c *(mm/min)*	a_p *(mm)*	a_e *(mm)*	α
1	7000-8500	700-850	0-1	0.25D	0.83
2	"	"	"	0.5D	0.89
3	"	"	"	0.75D	0.52

Table 7.25: Cutting parameters for 4 mm end-mill cutters with 2 flutes.

Test No.	V_s *(rpm)*	V_c *(mm/min)*	a_p *(mm)*	a_e *(mm)*	α
1	7000-8500	700-850	0-1	0.25D	0.85
2	"	"	"	0.5D	0.66
3	"	"	"	0.75D	0.86

The value of regression coefficient at the onset of chatter varies between *0.52* and *0.89*. Similarly, three end-milling trials were implemented by using a 6-mm end mill cutter with two flutes. The value of regression coefficient at the onset of chatter varies between *0.66* and *0.86*.

7.4 Conclusion

In this chapter, a broad range of different milling trials were run with different cutting tools, workpiece materials, and cutting parameters. The value of the regression coefficient between the Poincaré section at the onset of chatter and reference Poincaré sections was calculated. The outline variation of the regression coefficient during milling operations verifies that the fixed reference linear regression method can model the transition of milling processes from a stable condition to the chatter condition. Based on the computed value for each set of experiments, an onset chatter boundary is proposed.

Chapter 8

Conclusion & Future Work

8.1 Research Contribution

In chapter 2, the state of the art indicated that recent chatter detection methods consider dynamics of cutting process as well as cutting parameters in order to determine the occurrence of chatter. Experimentally or analytically, they determine a boundary for choosing cutting parameters in a way that a milling process runs in a stable condition. However as milling is a nonlinear dynamic system, the methods cannot precisely detect chatter in a timely manner due to incomplete process parameters and any sudden changes in the dynamics of milling.

This thesis focuses on the prediction of chatter during milling while being insensitive to the cutting parameters and cutting dynamics. A set of five goals were previously determined in chapter 1. By completion of the research, the following conclusions are drawn from the results obtained and the analysis performed afterwards. They can correctly address the designed goals in section 1.3.

8.1.1 A novel method which is able to detect chatter on-line, and is applicable in industry

A new novel experimental method for the prediction of chatter during milling process of metals has been developed. The new method is based on the chaos theory and in particular, the transformation of time domain signals during cutting to Poincare sections from which a new process analysis algorithm has been developed. The new method is independent of the cutting parameters and dynamics of the milling process, and can be integrated in the cutting machines to detect chatter on-line during the cutting process, as aimed in section 1.3, number one.

8.1.2 A novel method that is not time consuming

The new method is simple in transformation from time domain signals to Poincare section format. Phase space attractor Poincaré sections have been

plotted for each time interval. The variation in outlined Poincaré sections has been indicated by image correlation. The variation has been demonstrated by Pearson coefficient. The coefficient shows transition of milling process from stable condition into the chatter; hence it determines the onset of chatter during cutting of titanium.

Recognition of the onset of chatter can be done either by simple image correlation computation or by linear regression coefficient analysis. The computational time on the experimental computers are in fractions of a second, as aimed in section 1.3, number two.

8.1.3 A clear set of criteria for demarcation of stable and unstable conditions is developed

A complete experimental setup has been designed for material removal, chatter creation, acquiring vibration between cutting tool and workpiece, and recording the cutting force during milling. Two kinds of milling paths have been designed based on the end-mill and ball nose cutting tools. Accessible and reasonably priced equipment that can be used easily by industries and in the workshop are used during the trials.

The acceleration signal has been analysed. A mathematical model based on the chaos theory and by reconstruction of phase space attractor has been developed to determine the state of milling continuously during the milling process. For this purpose, the milling process is divided into time intervals with overlap. Time delay is calculated based on the first cross zero value of autocorrelation factor of the recorded acceleration signal. The existence of noise can be ignored or easily removed in this model. The FFT power spectrum diagram verified detection of chatter has been developed by the proposed method.

The variation of the phase space attractor is evaluated for embedding dimensions equal to 1, 2, and 3. The designed boundary for the onset of chatter is applicable for different embedding dimensions.

A fixed reference regression method has also been modelled to measure the variation of the Poincaré sections. The regression coefficient was calculated between every Poincaré section and the reference Poincaré section. The obtained regression coefficient is a numerical indicator that is able to determine the boundary of chatter onset during milling of titanium, as aimed in section 1.3, number 3.

8.1.4 The new chatter prediction method can be used for monitoring cutting process of all metallic materials

Chatter threshold has been successfully derived for three engineering materials; titanium, aluminium, and stainless steel. The result demonstrates that the method can be applied to any material to determine the chatter threshold, as aimed in section 1.3, number four. It is also verified that the result can be applicable for different cutting tool and cutting path.

The outlined chatter threshold is applicable for milling processes with various immersion rates, as well as various cutting parameters. Accordingly, the designed method can be considered insensitive to the cutting parameters and dynamics of cutting process. Detection of chatter can be easily predicted in less than a minute.

8.1.5 The new method does not require expensive signal analysis equipment

Development of a chatter detection method insensitive to the cutting parameter and dynamics of milling process in a reasonable time provides ability to detect chatter on-line. The mathematical model allows the detection of chatter for a wide class of problems from the use of a very simple equation. The method can be used in the workshop environment with a set of low cost accelerometer and force sensors mounting on an adaptor on the spindle, as aimed in section 1.3, number five.

8.2 Recommendations for Future Work

The variation of phase space attractor Poincaré sections is measured directly for the first time to determine the chatter threshold boundary. It is a starting point for detection of chatter while taking into account the continuous change in the state of milling processes. The following topics could be pursued for future research work:

- Develop expert software that can automatically detect the occurrence of chatter by using the proposed numeric indicators.
- Running more machining trials with different cutting tools, cutting parameters, and workpiece materials in order to acquire large enough data for establishing a database. It is required to extend the method to deal with more complex and arbitrary component shapes of cutting paths.
- Using the fixed reference regression method, a database of chatter threshold for various cutting trials can be generated.
- Extending the chatter threshold boundary to deal with other materials and cutting parameters.
- Extending the chatter threshold boundary to deal with other machining processes such as turning, grinding, drilling, etc.
-

Publication

The work presented in this thesis has been published, or is under review in the following:

1. Koohestani A, Mo J, and Yang S. Stability prediction of titanium milling with data driven reconstruction of phase-space. *International Journal of Machining Science and Technology*. 2014; **18**(1).

2. Koohestani A, Mo J, Yang S, Application of linear regression model on chatter threshold delineation, *Proc IMechE Part B: Journal of Engineering Manufacture.* 2014; 1-11.

3. Koohestani A, Mo J, Yang S, The development of chatter threshold boundary during milling process of metals using regression coefficient, International Journal of Machine Tools & Manufacture, *Under Review*.

4. Koohestani A, Mo J, The application of image correlation in order to define chatter during milling of titanium. In: *ASME 2012 International Mechanical Engineering Congress and Exposition: Design, Materials and Manufacturing, Parts A, B, and C*; November 9–15, 2012; Houston, USA. ASME; 2012.

5. Koohestani A and Mo J. Detection of Chatter during High Speed Milling Using Chaos Theory. In: *Mechanical, Industrial, and Manufacturing Engineering. Proceedings of International Conference on Mechanical, Industrial, and Manufacturing Engineering*; January 15-16 2011; Melbourne, Australia. MIME; 2011.

References

1. Ali, S.M., N.R. Dhar, and S.K. Dey, *Effect of minimum quantity lubrication (MQL) on cutting performance in turning medium carbon steel by uncoated carbide insert at different speed-feed combinations.* Advances in production engineering and management, 2011. **6**(3): p. 185-196.
2. Trent, E.M. and P.K. Wright, *Metal Cutting*. 2000: Butterworth-Heinemann.
3. Ezugwu, E.O., W.F. Sales, and J. Landre, Jr., *Machining Dynamics in Turning Processes*, in *Machining Dynamics*, K. Cheng, Editor. 2009, Springer London. p. 151-166.
4. Gajate, A., et al., *Tool wear monitoring using neuro-fuzzy techniques: a comparative study in a turning process.* Journal of Intelligent Manufacturing, 2012. **23**(3): p. 869-882.
5. Tlusty, J., *Analysis of the state of research in cutting dynamics.* Annals of the CIRP, 1978. **27**: p. 583-589.
6. Chen, S.-G., A. Ulsoy, and Y. Koren, *Computational stability analysis of chatter in turning.* Journal of manufacturing science and engineering, 1997. **119**(4A): p. 457-460.
7. Schmitz, T. and K. Smith, *Milling Dynamics*, in *Machining Dynamics*. 2009, Springer US. p. 99-171.
8. Coelho, R.T., et al., *Experimental evaluation of cutting force parameters applying mechanistic model in orthogonal milling.* Journal of the Brazilian Society of Mechanical Sciences and Engineering, 2003. **25**: p. 247-253.
9. Cheng, K., *Machining Dynamics: Fundamentals, Applications and Practices*. 2008: Springer.
10. Merdol, S.D. and Y. Altintas, *Multi Frequency Solution of Chatter Stability for Low Immersion Milling.* Journal of Manufacturing Science and Engineering, 2004. **126**(3): p. 459-466.
11. Faassen, R.P.H., et al., *Prediction of regenerative chatter by modelling and analysis of high-speed milling.* International Journal of Machine Tools and Manufacture, 2003. **43**(14): p. 1437-1446.
12. Salomon, C., *Critical Machining Velocities*. 1931: German Patent No. 523594. .
13. Darcy, P., et al., *Process and methodology for selecting cutting parameters for titanium*. 2004, Google Patents.
14. Yao, C.-f., et al., *Influence of high-speed milling parameter on 3D surface topography and fatigue behavior of TB6 titanium alloy.* Transactions of Nonferrous Metals Society of China, 2013. **23**(3): p. 650-660.

15. Hamdan, A., A.D. Sarhan, and M. Hamdi, *An optimization method of the machining parameters in high-speed machining of stainless steel using coated carbide tool for best surface finish.* The International Journal of Advanced Manufacturing Technology, 2012. **58**(1-4): p. 81-91.

16. Wang, T., et al., *Surface Integrity of High Speed Milling of Al/SiC/65p Aluminum Matrix Composites.* Procedia CIRP, 2013. **8**(0): p. 475-480.

17. Schmitz, Y., et al., *The application of high-speed CNC machining to prototype production.* International journal of machine tools & manufacture, 2001. **41**(8): p. 1209-1228.

18. Stephenson, D.A. and J.S. Agapiou, *Metal Cutting Theory and Practice*. 2005: Taylor & Francis.

19. Ehrich, F.F., *Chapter 5: Self-Excited Vibration*, in *Harris' shock and vibration handbook*, C.M. Harris and A.G. Piersol, Editors. 2002, McGraw-Hill New York.

20. Totis, G., *RCPM—A new method for robust chatter prediction in milling.* International Journal of Machine Tools and Manufacture, 2009. **49**(3–4): p. 273-284.

21. Kayhan, M. and E. Budak, *An experimental investigation of chatter effects on tool life.* Proceedings of the Institution of Mechanical Engineers, Part B: Journal of Engineering Manufacture, 2009. **223**(11): p. 1455-1463.

22. Budak, E. and L. Kops, *Improving Productivity and Part Quality in Milling of Titanium Based Impellers by Chatter Suppression and Force Control.* CIRP Annals - Manufacturing Technology, 2000. **49**(1): p. 31-36.

23. Yusoff, A.R. and N.D. Sims, *Optimisation of variable helix end millings tools by minimising self excited vibration.* Journal of Physics: Conference Series 2009. **181**(1): p. 1-8.

24. Chae, J., *Development and Analysis of the Precision Micro Milling System*. 2006: University of Calgary (Canada).

25. Araujo, A.C., P. Pacheco, and M.A. Savi. *Dynamical analysis of an end milling process*. in *International Congress of Mechanical Engineering-COBEM*. 2009. Gramado, RS, Brazil.

26. Quintana, G. and J. Ciurana, *Chatter in machining processes: A review.* International Journal of Machine Tools and Manufacture, 2011. **51**(5): p. 363-376.

27. Wiercigroch, M. and E. Budak, *Sources of nonlinearities, chatter generation and suppression in metal cutting.* Philosophical Transactions of the Royal Society of London. Series A: Mathematical, Physical and Engineering Sciences, 2001. **359**(1781): p. 663-693.

28. Davies, M.A. and B. Balachandran, *Impact Dynamics in Milling of Thin-Walled Structures.* Nonlinear Dynamics, 2000. **22**(4): p. 375-392.

29. Van de Wouw, N., et al., *Modeling of High-Speed Milling for Prediction of Regenerative Chatter*, in *Nonlinear Dynamics of Production Systems*. 2005, Wiley-VCH Verlag GmbH & Co. KGaA. p. 169-186.

30. Guo, Q., et al., *Prediction of stability limit for multi-regenerative chatter in high performance milling.* International Journal of Dynamics and Control, 2014: p. 1-11.

31. Dandekar, C.R., Y.C. Shin, and J. Barnes, *Machinability improvement of titanium alloy (Ti–6Al–4V) via LAM and hybrid machining.* International Journal of Machine Tools and Manufacture, 2010. **50**(2): p. 174-182.

32. Mhamdi, M.B., et al., *Surface Integrity of Titanium Alloy Ti-6Al-4 V in Ball end Milling.* Physics Procedia, 2012. **25**(0): p. 355-362.

33. Abele, E. and B. Fröhlich, *High speed milling of titanium alloys.* Advances in production engineering and management, 2008. **3**(3): p. 131-140.

34. Boyer, R.R., *Attributes, characteristics, and applications of titanium and its alloys.* JOM, 2010. **62**(5): p. 21-24.

35. Froes, F.H., et al., *Titanium in the family automobile: The cost challenge.* JOM, 2004. **56**(2): p. 40-44.

36. Ítalo Sette Antonialli, A., A. Eduardo Diniz, and R. Pederiva, *Vibration analysis of cutting force in titanium alloy milling.* International Journal of Machine Tools and Manufacture, 2010. **50**(1): p. 65-74.

37. Huang, P., et al., *Milling force vibration analysis in high-speed-milling titanium alloy using variable pitch angle mill.* The International Journal of Advanced Manufacturing Technology, 2012. **58**(1-4): p. 153-160.

38. Afazov, S.M., et al., *Chatter modelling in micro-milling by considering process nonlinearities.* International Journal of Machine Tools and Manufacture, 2012. **56**(0): p. 28-38.

39. Leckie, H.P. and H.H Uhlig, *Environmental Factors Affecting the Critical Potential for Pitting in 18–8 Stainless Steel.* Journal of Electrochemical Society, 1966. **113**(12): p. 1262-1267.

40. Nikulin, I., R. Kaibyshev, and V. Skorobogatykh, *High temperature properties of an austenitic stainless steel.* Journal of Physics: Conference Series; 15th International Conference on the Strength of Materials (ICSMA-15) 2010. **240**(012071): p. 1-4.

41. Gardner, L., *The use of stainless steel in structures.* Progress in Structural Engineering and Materials, 2005. **7**(2): p. 45-55.

42. Makkus, R.C., et al., *Use of stainless steel for cost competitive bipolar plates in the SPFC.* Journal of Power Sources, 2000. **86**(1–2): p. 274-282.

43. Shao, H., L. Liu, and H.L. Qu, *Machinability study on 3%Co–12%Cr stainless steel in milling.* Wear, 2007. **263**(1–6): p. 736-744.

44. Paro, J., H. Hänninen, and V. Kauppinen, *Tool wear and machinability of HIPed P/M and conventional cast duplex stainless steels.* Wear, 2001. **249**(3–4): p. 279-284.

45. Vargel, C., *Corrosion of Aluminium*. 2004: Elsevier.

46. Gale, W.F. and T.C. Totemeier, *Smithells Metals Reference Book*. 2003: Elsevier Science.

47. Ismail, F. and R. Ziaei, *Chatter suppression in five-axis machining of flexible parts.* International Journal of Machine Tools and Manufacture, 2002. **42**(1): p. 115-122.

48. Taylor, F.W., *On the Art of Cutting Metals*. 1907: American society of mechanical engineers.

49. Arnold, R.N., *The mechanism of tool vibration in the cutting of steel.* Proc. Inst. Mech. Engrs (Lond.), 1946. **154**: p. 261-284.

50. Tobias, S. and W. Fishwick, *Theory of regenerative machine tool chatter.* The Engineer-London 1958.

51. Tlusty, J. and M. Polacek, *The stability of machine tools against self-excited vibrations in machining.* International Research in Production Engineering, 1963: p. 465-474.

52. Olgac, N. and M. Hosek, *A new perspective and analysis for regenerative machine tool chatter.* International Journal of Machine Tools and Manufacture, 1998. **38**(7): p. 783-798.

53. Ozoegwu, C.G. and S.N. Omenyi, *Time domain chatter stability comparison of turning and milling processes.* International Journal of Multidisciplinary science and engineering, 2012. **3**(11): p. 25-30.

54. Insperger, T. and G. Stépán, *Updated semi-discretization method for periodic delay-differential equations with discrete delay.* International Journal for Numerical Methods in Engineering, 2004. **61**(1): p. 117-141.

55. Koenigsberger, F. and J. Tlustý, *Machine tool structures—Vol. 1: stability against chatter*. 1967, Oxford, UK: Pergamon Press.

56. Tobias, S.A., *Machine-tool vibration*. 1965: J. Wiley.

57. Sridhar, R., R.E. Hohn, and G.W. Long, *A Stability Algorithm for the General Milling Process: Contribution to Machine Tool Chatter Research—7.* Journal of Engineering for Industry, 1968. **90**(2): p. 330-334.

58. Ozlu, E. and E. Budak, *Analytical Modeling of Chatter Stability in Turning and Boring Operations—Part I: Model Development.* Journal of Manufacturing Science and Engineering, 2007. **129**(4): p. 726-732.

59. Fu, Q., A. Rashid, and C.M. Nicolescu, *Improving machining performance against regenerative tool chatter*

through adaptive normal pressure at the tool clamping interface. Journal of Machine Engineering, 2013. **13**(1): p. 93-105.

60. Sims, N.D., *Dynamics Diagnostics: Methods, Equipment and Analysis Tools*, in *Machining Dynamics*, K. Cheng, Editor. 2009, Springer London. p. 85-115.

61. Nair, U., et al., *Permutation entropy based real-time chatter detection using audio signal in turning process.* The International Journal of Advanced Manufacturing Technology, 2010. **46**(1-4): p. 61-68.

62. Schmitz, T.L., *Chatter recognition by a statistical evaluation of the synchronously sampled audio signal.* Journal of Sound and Vibration, 2003. **262**(3): p. 721-730.

63. Bayly, P.V., et al., *Effects of radial immersion and cutting direction on chatter stability in end milling.* ASME International Congress and Exposition, 2002. **13**: p. 351-363.

64. Godwin, O.C., et al., *Comparing chatter stability of end-milling processes of different number of teeth.* Industrial Engineering Letters, 2012. **2**(9): p. 11-22.

65. Zhongqun, L. and L. Qiang, *Solution and Analysis of Chatter Stability for End Milling in the Time-domain.* Chinese Journal of Aeronautics, 2008. **21**(2): p. 169-178.

66. Wan, M. and W.H. Zhang, *Calculations of chip thickness and cutting forces in flexible end milling.* The International Journal of Advanced Manufacturing Technology, 2006. **29**(7-8): p. 637-647.

67. Smith, S. and J. Tlusty, *Update on high-speed milling dynamics.* Journal of Engineering for Industry 1990. **112**: p. 142-149.

68. Smith, S. and J. Tlusty, *Current Trends in High-Speed Machining.* Journal of Manufacturing Science and Engineering, 1997. **119**(4B): p. 664-666.

69. Sims, N.D., *The Self-Excitation Damping Ratio: A Chatter Criterion for Time-Domain Milling Simulations.* Journal of Manufacturing Science and Engineering, 2004. **127**(3): p. 433-445.

70. Saleh, K. and N.D. Sims, *The self-excitation damping ratio in variable speed milling.* Proceedings of the World Congress on Engineering 2012, 2012. **3**.

71. Eppel, A., et al., *Feasibility Study of Optical Detection of Chatter Vibration During Milling.* International Journal of Optomechatronics, 2010. **4**(2): p. 195-214.

72. Ganguli, A., A. Deraemaeker, and A. Preumont, *Regenerative chatter reduction by active damping control.* Journal of Sound and Vibration, 2007. **300**(3–5): p. 847-862.

73. Ganguli, A., *Chatter reduction through active vibration damping.* PhD Thesis: Universite Libre de Bruxelles, 2005: p. 120 pages.

74. Surmann, T. and D. Enk, *Simulation of milling tool vibration trajectories along changing engagement conditions.* International Journal of Machine Tools and Manufacture, 2007. **47**(9): p. 1442-1448.

75. Broughton, S.A. and K.M. Bryan, *Discrete Fourier analysis and wavelets applications to signal and image processing* John Wiley and Sons, Hoboken, N.J, 2009: p. 360 Pages.

76. Altintaş, Y. and E. Budak, *Analytical Prediction of Stability Lobes in Milling.* CIRP Annals - Manufacturing Technology, 1995. **44**(1): p. 357-362.

77. Patwari, M.A.U., A.K.M.N. Amin, and W.F. Faris, *Influence of Chip Serration Frequency on Chatter Formation During End Milling of Ti6Al4V.* Journal of Manufacturing Science and Engineering, 2011. **133**(1): p. 1-12.

78. Toh, C.K., *Vibration analysis in high speed rough and finish milling hardened steel.* Journal of Sound and Vibration, 2004. **278**(1–2): p. 101-115.

79. Ding, S., et al., *Chatter detection in high speed machining of Titanium alloys.* Key Engineering Materials, 2011. **458**: p. 289-294.

80. Schmitz, T.L., K. Medicus, and B. Dutterer, *Exploring once-per-revolution audio signal variance as a chatter indicator.* Machining Science and Technology, 2002. **6**(2): p. 215-233.

81. Dong, W., Y.H. Joe Au, and A. Mardapittas, *Machine tool chatter monitoring by coherence analysis.* International Journal of Production Research, 1992. **30**(8): p. 1901.

82. Li, X.Q., Y.S. Wong, and A.Y.C. Nee, *Tool wear and chatter detection using the coherence function of two crossed accelerations.* International Journal of Machine Tools and Manufacture, 1997. **37**(4): p. 425-435.

83. Zaghbani, I., et al., *High speed machining of aluminum alloys with the robots.* Journal of advanced materials research, 2011. **188**: p. 584-588.

84. Gradišek, J., E. Govekar, and I. Grabec, *Using coarse-grained entropy rate to detect chatter in cutting.* Journal of Sound and Vibration, 1998. **214**(5): p. 941-952.

85. Pérez-Canales, D., et al., *Analysis of the entropy randomness index for machining chatter detection.* International Journal of Machine Tools and Manufacture, 2012. **62**(0): p. 39-45.

86. Gradišek, J., et al., *Automatic chatter detection in grinding.* International Journal of Machine Tools and Manufacture, 2003. **43**(14): p. 1397-1403.

87. Thaler, T., et al., *Chatter detection in band sawing based on discriminant analysis of sound features.* Applied Acoustics, 2014. **77**: p. 114-121.

88. Messaoud, A., C. Weihs, and F. Hering, *Detection of chatter vibration in a drilling process using multivariate control charts.* Computational Statistics & Data Analysis, 2008. **52**(6): p. 3208-3219.

89. Tangjitsitcharoen, S., *Analysis of Chatter in Ball End Milling by Wavelet Transform.* World Academy of Science, Engineering & Technology, 2012. **71**: p. 1048-1054.

90. Ma, L., *PVDF sensor based wireless monitoring of milling process.* Georgia Institute of Technology, 2013.

91. Tangjitsitcharoen, S., T. Saksri, and S. Ratanakuakangwan, *Advance in chatter detection in ball end milling process by utilizing wavelet transform.* Journal of Intelligent Manufacturing, 2013: p. 1-15.

92. Mallat, S.G., *A theory for multiresolution signal decomposition: the wavelet representation.* Pattern Analysis and Machine Intelligence, IEEE Transactions on, 1989. **11**(7): p. 674-693.

93. Addison, P.S., *The Illustrated Wavelet Transform Handbook: Introductory Theory and Applications in Science, Engineering, Medicine and Finance*. 2002: Taylor & Francis.

94. Graps, A., *An introduction to wavelets.* Computational Science & Engineering, IEEE, 1995. **2**(2): p. 50-61.

95. Bijaoui, A. and G. Jammal, *On the distribution of the wavelet coefficient for a Poisson noise.* Signal Processing, 2001. **81**(9): p. 1789-1800.

96. Hsin, H.-C. and C.-C. Li, *The adaptive modulated wavelet transform image representation.* Pattern Recognition Letters, 2002. **23**(14): p. 1817-1823.

97. Seleghim, P. and F.E. Milioli, *Improving the determination of bubble size histograms by wavelet de-noising techniques.* Powder Technology, 2001. **115**(2): p. 114-123.

98. Kuljanic, E., G. Totis, and M. Sortino, *Development of an intelligent multisensor chatter detection system in milling.* Mechanical Systems and Signal Processing, 2009. **23**(5): p. 1704-1718.

99. Yongtao, J. and Z. Chunliang, *Hybrid HMM/SVM method for predicting of cutting chatter.* Proc. of 3rd International Symposium on Precision Mechanical Measurements, Urumqi, China, 2006: p. 404-411.

100. Khraisheh, M.K., C. Pezeshki, and A.E. Bayoumi, *Time series based analysis for primary chatter in metal cutting.* Journal of Sound and Vibration, 1995. **180**(1): p. 67-87.

101. Bickraj, K., et al., *Inspection of Chatter Damage in End Milling Operations by Using Wavelet Transformations.* 5th International Latin American and Caribbean Conference for Engineering and Technology. Tempaco, Mexico, 2007.

102. Lange, J.H. and N.H. Abu-Zahra, *Tool Chatter Monitoring in Turning Operations Using Wavelet Analysis of Ultrasound Waves.* The International Journal of Advanced Manufacturing Technology, 2002. **20**(4): p. 248-254.

103. Wang, L. and M. Liang, *Chatter detection based on probability distribution of wavelet modulus maxima.* Robotics and Computer-Integrated Manufacturing, 2009. **25**(6): p. 989-998.

104. Huang, P., et al., *Vibration analysis in milling titanium alloy based on signal processing of cutting force.* The International Journal of Advanced Manufacturing Technology, 2013. **64**(5-8): p. 613-621.

105. Ji, Y., et al., *Feature extraction with discrete wavelet transform for drill wear monitoring.* Journal of Vibration and Control, 2005. **11**: p. 1375+.

106. Fang, N., P.S. Pai, and N. Edwards, *A comparative study of high-speed machining of Ti-6Al-4V and Inconel 718—part II: Effect of dynamic tool*

edge wear on cutting vibrations. The International Journal of Advanced Manufacturing Technology, 2013. **68**(5-8): p. 1417-1428.

107. Ninness, B., *Analysis of Wavelet Based Maximum Likelihood Estimation of= f Noise.*

108. Choi, T. and Y.C. Shin, *On-Line Chatter Detection Using Wavelet-Based Parameter Estimation.* Journal of Manufacturing Science and Engineering, 2003. **125**(1): p. 21-28.

109. Mallat, S., *A Wavelet Tour of Signal Processing*. 1999: Elsevier Science.

110. Berger, B.S., et al., *Wavelet based cutting state identification.* Journal of Sound and Vibration, 1998. **213**(5): p. 813-827.

111. Cao, H., et al., *End milling tool breakage detection using lifting scheme and Mahalanobis distance.* International Journal of Machine Tools and Manufacture, 2008. **48**(2): p. 141-151.

112. NARAHARISETTI, V.G.P., *An Image Fusion Technique For Colour Images Using Dual-Tree Complex Wavelet Transform.* International Journal of Engineering, 2012. **1**(8).

113. Palpandian, P., R.V. Prabhu, and B.S. Satish, *Stability Lobe Diagram for High Speed Machining Processes:Comparison of Experimental and Analytical Methods – A Review.* International Journal of Innovative Research in Science, Engineering and Technology, 2013. **2**(3): p. 747-752.

114. Tobias, S.A., *Vibraciones en Máquinas-Herramientas.* URMO, Spain, 1961.

115. Smith, S. and J. Tlusty, *Update on High-Speed Milling Dynamics.* Journal of Engineering for Industry, 1990. **112**(2): p. 142-149.

116. Stepan, G., Z. Dombovari, and J. Muñoa, *Identification of cutting force characteristics based on chatter experiments.* CIRP Annals - Manufacturing Technology, 2011. **60**(1): p. 113-116.

117. Pal Pandian, P., V. Prabhu Raja, and K. Sakthimurugan, *Identification of stability lobes in high-speed machining of thin ribs.* International Journal of Engineering and Science, 2012. **1**(8): p. 1-6.

118. Thevenot, V., et al., *Integration of dynamic behaviour variations in the stability lobes method: 3D lobes construction and application to thin-walled structure milling.* The International Journal of Advanced Manufacturing Technology, 2006. **27**(7-8): p. 638-644.

119. Kareem, A. and M.F. Azeem, *A novel soft computing based algorithm for the control of dynamic uncertain systems – An application to DC-DC converters.* International Journal of Artificial Intelligence & Applications, 2011. **2**(2): p. 21-30.

120. Zadeh, L.A., *What is soft computing?* Soft computing, 1997. **1**(1).

121. Pal, S.K., A. Ghosh, and M.K. Kundu, *Soft Computing for Image Processing*. 2010: Physica-Verlag HD.

122. Faris, H., A. Sheta, and E. Öznergiz, *Modelling hot rolling manufacturing process using soft computing techniques.* International Journal of Computer Integrated Manufacturing, 2013. **26**(8): p. 762-771.

123. Patnaik, S. and Y.-M. Yang, *Soft Computing Techniques in Vision Science*. 2012: Springer Publishing Company, Incorporated. 230.

124. Oosterom, M., R. Babuska, and H.B. Verbruggen, *Soft computing applications in aircraft sensor management and flight control law reconfiguration.* Systems, Man, and Cybernetics, Part C: Applications and Reviews, IEEE Transactions on, 2002. **32**(2): p. 125-139.

125. Lee, K.H., *First Course on Fuzzy Theory and Applications*. 2004: Springer.

126. Xu, D., *A fuzzy logic approach for chatter detection and suppression in end milling*. 2003: University of Ottawa.

127. Sims, N.D., G. Manson, and B. Mann, *Fuzzy stability analysis of regenerative chatter in milling.* Journal of Sound and Vibration, 2010. **329**(8): p. 1025-1041.

128. Kim, D. and D. Jeon, *Fuzzy-logic control of cutting forces in CNC milling processes using motor currents as indirect force sensors.* Precision Engineering, 2011. **35**(1): p. 143-152.

129. Haykin, S.S., *Neural networks: a comprehensive foundation*. 1994: Macmillan.

130. Tansel, I.N., A. Wagiman, and A. Tziranis, *Recognition of chatter with neural networks.* International Journal of Machine Tools and Manufacture, 1991. **31**(4): p. 539-552.

131. Lamraoui, M., et al., *Chatter detection in milling machines by neural networks classification and feature selection.* Journal of Vibration and Control, 2013: p. 1-16.

132. Pontes, F.J., et al., *Optimization of Radial Basis Function neural network employed for prediction of surface roughness in hard turning process using Taguchi's orthogonal arrays.* Expert Systems with Applications, 2012. **39**(9): p. 7776-7787.

133. Ayala-Ramirez, V., et al., *Scene Reconstruction, Pose Estimation and Tracking. Chapter 5: Soft Computing Applications in Robotic Vision Systems.* edited by: Rustam Stolkin, 2007: p. 530 pages.

134. Wilamowski, B.M. *Advantages and problems of soft computing*. in *Industrial Informatics (INDIN), 9th IEEE International Conference on*. 2011. Caparica, Lisbon, Potugal.

135. Dote, Y. and S.J. Ovaska, *Industrial applications of soft computing: a review.* Proceedings of the IEEE, 2001. **89**(9): p. 1243-1265.

136. Werbos, P.J., *Neurocontrol and elastic fuzzy logic: capabilities, concepts, and applications.* Industrial Electronics, IEEE Transactions on, 1993. **40**(2): p. 170-180.

137. Zuperl, U., F. Cus, and M. Reibenschuh, *Modeling and adaptive force control of milling by using artificial techniques.* Journal of Intelligent Manufacturing, 2012. **23**(5): p. 1805-1815.

138. Quintana, G., M.L. Garcia-Romeu, and J. Ciurana, *Surface roughness monitoring application based on artificial neural networks for ball-end milling operations.* Journal of Intelligent Manufacturing, 2011. **22**(4): p. 607-617.

139. Seguy, S., et al., *Supression of period doubling chatter in high-speed milling by spindle speed variation.* Machining Science and Technology, 2011. **15**(2): p. 153-171.

140. Nurul Amin, A.K.M., et al., *Surface Roughness Optimization in End Milling of Stainless Steel AISI 304 with Uncoated WC-Co Insert Under Magnetic Field.* Advanced Materials Research, 2012. **576**: p. 119-122.

141. Kuttolamadom, M.A., S. Hamzehlouia, and L. Mears, *Effect Of machining feed on surface roughness in cutting 6061 aluminum.* 2010.

142. Outeiro, J.C., J.P. Costes, and J.R. Kornmeier, *Cyclic Variation of Residual Stress Induced by Tool Vibration in Machining Operations.* Procedia CIRP, 2013. **8**: p. 493-497.

143. Nayfeh, A.H. and B. Balachandran, *Applied nonlinear dynamics*. 2008: Wiley. com.

144. Rusinek, R.I., A. Weremczuk, and J. Warmi nski, *Regenerative Model of Cutting Process with Nonlinear Duffing Oscillator.* Mechanics and Mechanical Engineering, 2011. **15**(4): p. 131-145.

145. Wiercigroch, M. and A.M. Krivtsov, *Frictional chatter in orthogonal metal cutting.* Philosophical Transactions of the Royal Society of London. Series A: Mathematical, Physical and Engineering Sciences, 2001. **359**(1781): p. 713-738.

146. Davies, M.A., et al., *On the Dynamics of High-Speed Milling with Long, Slender Endmills.* CIRP Annals - Manufacturing Technology, 1998. **47**(1): p. 55-60.

147. Zhao, M.X. and B. Balachandran, *Dynamics and stability of milling process.* International Journal of Solids and Structures, 2001. **38**(10–13): p. 2233-2248.

148. Liu, M.-K., E.B. Halfmann, and C.S. Suh, *Multi-dimensional time-frequency control of micro-milling instability.* Journal of Vibration and Control, 2012.

149. Moon, F.C. and M.A. Johnson, *Nonlinear techniques to characterize and chatter vibrations in the machining of metals.* International Journal of Bifurcation and Chaos, 2001. **11**(2): p. 449-467.

150. Faassen, R., *Chatter Prediction and Control for High-Speed Milling: Modeling and Experiments.* PhD thesis: Eindhoven University of Technology, Eindhoven, Netherlands, 2007.

151. Merdol, S.D., *Mechanics and dynamics of serrated end mills.* Master of Applied Science - MASc: The university of British Columbia, Turkey, 2003.

152. Kim, I.H. and D.Y. Jang, *Cutting Vibration Monitoring Using a Spindle Displacement Sensor in Turning.* ASME 2003 International Design Engineering Technical Conferences and Computers and Information in Engineering Conference: 19th Biennial Conference on Mechanical Vibration and Noise, Parts A, B, and C. Chicago, Illinois, USA, September 2–6, 2003, 2003. **5**: p. 1529-1535.

153. Chaurasiya, H., *Recent Trends of Measurement and Development of Vibration Sensors.* International Journal of Computer Science Issues, 2012. **9**(4): p. 6 pages.

154. Ning, Y., M. Rahman, and Y.S. Wong, *Monitoring of Chatter in High Speed Endmilling Using Audio Signals Method*, in *Proceedings of the 33rd International MATADOR Conference*, D. Hayhurst, et al., Editors. 2000, Springer London. p. 421-426.

155. Morris, A.S., *Measurement and Instrumentation Principles*. 2001: Elsevier Science.

156. Kuljanic, E., M. Sortino, and G. Totis, *Multisensor approaches for chatter detection in milling.* Journal of Sound and Vibration, 2008. **312**(4–5): p. 672-693.

157. Tansel, I.N., et al., *Transformations in machining. Part 2. Evaluation of machining quality and detection of chatter in turning by using s-transformation.* International Journal of Machine Tools and Manufacture, 2006. **46**(1): p. 43-50.

158. Sutherland, J.W., *A Dynamic Model of the Cutting Force System in the End Milling Process*. 1987: University of Illinois at Urbana-Champaign.

159. Pongsathornwiwat, N. and S. Tangjitsitcharoen. *Intelligent monitoring and detection of chatter in ball-end milling process on CNC machining center*. in *Computers and Industrial Engineering (CIE), 2010 40th International Conference on*. 2010.

160. Oberg, E., et al., *Machinery's Handbook: A Reference Book for the Mechanical Engineer, Designer, Manufacturing Engineer, Draftsman, Toolmaker, and Machinist*. 2004: Industrial Press.

161. Ghani, J.A., I.A. Choudhury, and H.H. Hassan, *Application of Taguchi method in the optimization of end milling parameters.* Journal of Materials Processing Technology, 2004. **145**(1): p. 84-92.

162. Chen, J. and W.-L. Chen, *A tool breakage detection system using an accelerometer sensor.* Journal of Intelligent Manufacturing, 1999. **10**(2): p. 187-197.

163. Sekiya, K., et al., *Detection of chatter by the measurement of acceleration of the spindle head in the axial direction(Monitoring of machining process).* Proceedings of International Conference on Leading Edge Manufacturing in 21st century : LEM21, 2009. **2009**(5): p. 477-482.

164. Matuszak, M., B. Powalka, and P. Kochmanski, *Chatter stability investigation in micro-milling.* Journal of Machine Engineering, 2013. **13**(2): p. 36-45.

165. Moradi, H., M.R. Movahhedy, and G. Vossoughi, *Dynamics of regenerative chatter and internal resonance in milling process with structural and cutting force nonlinearities.* Journal of Sound and Vibration, 2012. **331**(16): p. 3844-3865.

166. Wolfram, S., *A new kind of science*. 2002: Wolfram Media.

167. Kautz, R., *Chaos: The Science of Predictable Random Motion*. 2010: OUP Oxford.

168. Stewart, I., *Does God Play Dice?: The New Mathematics of Chaos*. 1997: Penguin Adult.

169. Mingyao, W., et al. *Topologically Mixing and Chaos of One Class of Bernoulli-Shift Cellular Automata Rules*. in *Chaos-Fractals Theories and Applications, 2009. IWCFTA '09. International Workshop on*. 2009.

170. Boccaletti, S., et al., *The control of chaos: theory and applications.* Physics Reports, 2000. **329**(3): p. 103-197.

171. KOLYADA, S. and L. SNOHA, *Some aspects of topological transitivity—A survey.* Iteration Theory, ECIT 94, Opava, Grazer Math. Ber., Karl Franzens Univ. Graz, 1997. **334**: p. 3-35.

172. Tsonis, A.A., *Chaos: From Theory to Applications*. 1992: Plenum Press.

173. R., S., *Climate chaotic instability: Statistical determination and theoretical background.* Environmetrics, 1997. **8**: p. 517-532.

174. Hanchao, Y. *An Empirical Analysis on Forecasting Stock Price: By Maximum Lyapunov Exponent and Fractal Dimension*. in *Management and Service Science (MASS), 2011 International Conference on*. 2011.

175. Theiler, J., *Estimating fractal dimension.* Journal of Optical Society of America, 1990. **7**(6): p. 1055-1073.

176. Guralnik, Z., C. Pehlevan, and G. Guralnik, *On exact statistics and classification of ergodic systems of integer dimension.* arXiv preprint arXiv:1311.7157, 2013.

177. Greiner, W., *Lyapunov Exponents and Chaos*, in *Classical Mechanics*. 2010, Springer: Heidelberg, Berlin. p. 503-516.

178. Banihasan, M. and F. Bakhtiari-Nejad, *Chaotic vibrations in high-speed milling.* Nonlinear Dynamics, 2011. **66**(4): p. 557-574.

179. Lutzen, J., *Master of Pure and Applied Mathematics, Series: Studies in the History of Mathematics and Physical Sciences.* 1990. **15**: p. 885 pages.

180. Nolte, D.D., *The tangled tale of phase space.* American Institute of Physics, 2010. **63**(4): p. 33-38.

181. Basharat, A. and M. Shah. *Time series prediction by chaotic modeling of nonlinear dynamical systems*. in *Computer Vision, 2009 IEEE 12th International Conference on*. 2009.

182. Karatasou, S. and M. Santamouris, *Detection of low-dimensional chaos in buildings energy consumption time series.* Communications in Nonlinear Science and Numerical Simulation, 2010. **15**(6): p. 1603-1612.

183. S., Y., *Chaos and order in complex modern industrial machines.* Machine Engineering, 2005. **5**(1/2): p. 5-10.

184. Farmer, J.D. and J.J. Sidorowich, *Predicting chaotic time series.* Physical Review Letters, 1987. **59**(8): p. 845-848.

185. Xu, P., *Differential phase space reconstructed for chaotic time series.* Applied Mathematical Modelling, 2009. **33**(2): p. 999-1013.

186. Owens, B.D., *Using phase space attractors to evaluate system safety constraint enforcement : case study in space shuttle mission control procedure rework.* PhD thesis: Massachusetts Institute of Technology. Engineering Systems Division., 2009.

187. Roopaei, M., et al., *Chaotic based reconstructed phase space features for detecting ventricular fibrillation.* Biomedical Signal Processing and Control, 2010. **5**(4): p. 318-327.

188. Xia, D., et al., *Determination of corrosion types from electrochemical noise by phase space reconstruction theory.* Electrochemistry Communications, 2012. **15**(1): p. 88-92.

189. Schreiber, T., *Interdisciplinary Application of Nonlinear Time Series Methods.* Phys. Rep, 1998. **308**: p. 1-64.

190. Wang, L., et al., *Dynamic characteristics of an NC table with phase space reconstruction.* Frontiers of Mechanical Engineering in China, 2009. **4**(2): p. 179-183.

191. Wu, C.L. and K.W. Chau, *Data-driven models for monthly streamflow time series prediction.* Engineering Applications of Artificial Intelligence, 2010. **23**(8): p. 1350-1367.

192. Rusinek, R., *Cutting process of composite materials: An experimental study.* International Journal of Non-Linear Mechanics, 2010. **45**(4): p. 458-462.

193. Shang, P., X. Na, and S. Kamae, *Chaotic analysis of time series in the sediment transport phenomenon.* Chaos, Solitons & Fractals, 2009. **41**(1): p. 368-379.

194. Mizrach, B., *Determining delay times for phase space reconstruction with application to the FFDM exchange rate.* Journal of Economic Behavior & Organization, 1996. **30**(3): p. 369-381.

195. Small, M., *Applied Nonlinear Time Series Analysis: Applications in Physics, Physiology and Finance*. 2005: World Scientific.

196. Ma, H.-g. and C.-z. Han, *Selection of Embedding Dimension and Delay Time in Phase Space Reconstruction.* Frontiers of Electrical and Electronic Engineering in China, 2006. **1**(1): p. 111-114.

197. Shang, P., X. Li, and S. Kamae, *Chaotic analysis of traffic time series.* Chaos, Solitons & Fractals, 2005. **25**(1): p. 121-128.

198. Chou, Y.L., *Chapter 17 – Linear bivariate analysis. Statistical Analysis, .* pub. Holt, Rinehart and Winston, 1975.

199. Pan, B. and K. Li, *A fast digital image correlation method for deformation measurement.* Optics and Lasers in Engineering, 2011. **49**(7): p. 841-847.

200. Kaneko, S.i., Y. Satoh, and S. Igarashi, *Using selective correlation coefficient for robust image registration.* Pattern Recognition, 2003. **36**(5): p. 1165-1173.

201. Greenhalgh, C., et al., *Time and structural cross-correlation image analysis of microscopic volumes, simultaneously recorded with second harmonic generation, third harmonic generation, and multiphoton excitation fluorescence microscopy.* Proceeding of the society of Photo-Optical instrumentation, 2005. **5969**: p. 596-603.

202. Di Lena, P. and L. Margara, *Optimal global alignment of signals by maximization of Pearson correlation.* Information Processing Letters, 2010. **110**(16): p. 679-686.

203. Rodgers, J. and A. Nicewander, *Thirteen Ways to Look at the Correlation Coefficient.* The American Statistician, 1988. **42**(1): p. 59-66.

204. Chauhan, A. and R. Vaish, *Magnetic material selection using multiple attribute decision making approach.* Materials & Design, 2012. **36**(0): p. 1-5.

205. Parker, J.R., *Algorithms for Image Processing and Computer Vision*. 2010: Wiley Publishing. 504.

206. Monedero, I., et al., *Detection of frauds and other non-technical losses in a power utility using Pearson coefficient, Bayesian networks and decision trees.* International Journal of Electrical Power & Energy Systems, 2012. **34**(1): p. 90-98.

207. Patwari, M.A.U., A.K.M.N. Amin, and W.F. Faris, *Influence of Chip Serration Frequency on Chatter Formation During End Milling of Ti6Al4V.* Journal of Manufacturing Science and Engineering, 2011. **133**(1): p. 011013-011013.

208. Harrell, F.E., *Regression Modeling Strategies: With Applications to Linear Models, Logistic Regression, and Survival Analysis.* Springer, 2002. **1st ed.**: p. 571 p.

209. Seber, G.A.F. and A.J. Lee, *Linear Regression Analysis*. 2003: Wiley.

210. Jun, C.-H. and S.-H. Suh, *Statistical tool breakage detection schemes based on vibration signals in NC milling.* International Journal of Machine Tools and Manufacture, 1999. **39**(11): p. 1733-1746.

211. O'Donovan, T.M., *Short Term Forecasting: An Introduction to the Box-Jenkins Approach*. 1983: Wiley.

212. Chatfield, C., *Time-Series Forecasting*. 2000: Taylor & Francis.

213. Cooray, T.M.J.A., *Applied Time Series: Analysis and Forecasting*. 2008: Alpha Science International Limited Oxford UK.

214. Montgomery, D.C., E.A. Peck, and G.G. Vining, *Introduction to linear regression analysis*. 5 ed. 2012: Wiley.

215. Bukkapatnam, S., P. Rao, and R. Komanduri, *Experimental dynamics characterization and monitoring of MRR in oxide chemical mechanical planarization (CMP) process.* International Journal of Machine Tools and Manufacture, 2008. **48**(12–13): p. 1375-1386.

216. İç, Y.T., *An experimental design approach using TOPSIS method for the selection of computer-integrated manufacturing technologies.* Robotics and Computer-Integrated Manufacturing, 2012. **28**(2): p. 245-256.

217. Xue, Y., et al., *Fuzzy regression method for prediction and control the bead width in the robotic arc-welding process.* Journal of Materials Processing Technology, 2005. **164–165**(0): p. 1134-1139.

218. Su, J.L. and J.B. Dingwell, *Dynamic stability of passive dynamic walking on an irregular surface.* J Biomech Eng, 2007. **129**(6): p. 802-10.

219. Kaunda, R.B., *A linear regression framework for predicting subsurface geometries and displacement rates in deep-seated, slow-moving landslides.* Engineering Geology, 2010. **114**(1–2): p. 1-9.

220. Foucart, T., *Stability of the inverse correlation matrix. Partial ridge regression.* Journal of Statistical Planning and Inference, 1999. **77**(1): p. 141-154.

221. P-T, H., C. JC., and C. C-Y, *A statistical approach in detecting tool breakage in end milling operations.* Journal of Industrial Technology, 1999. **15**(3): p. 2-7.

222. C., C.J. and C.J. C., *A multiple-regression model for monitoring tool wear with a dynamometer in milling operations.* Journal of Technology Studies, 2004. **30**(4): p. 71-77.

223. Ihsan, K., A. Adem, and B. Mehmet, *Application of regression and artificial neural network analysis in modelling of tool–chip interface temperature in machining.* Expert Systems with Applications, 2011. **38**(9): p. 11651-11656.

224. Ciurana, J., G. Quintana, and M.L. Garcia-Romeu, *Estimating the cost of vertical high-speed machining centres, a comparison between multiple regression analysis and the neural networks approach.* International Journal of Production Economics, 2008. **115**(1): p. 171-178.